Scaffold Pore Size and Calcium Phosphate Coating Control Chondrogenesis and Endochondral Ossification

by

Melanie J. Gupte

A dissertation submitted in partial fulfillment
of the requirements for the degree of
Doctor of Philosophy
(Biomedical Engineering)
in The University of Michigan
2015

Doctoral Committee:

Professor Peter X. Ma, Chair
Professor Renny T. Franceschi
Professor William V. Giannobile
Associate Professor Andrew J. Putnam

DEDICATION

This dissertation is dedicated to my parents,

Kiran and Janine Gupte

who have always been dedicated to me.

ACKNOWLEDGEMENTS

First I would like to thank my advisor Dr. Peter Ma for his guidance over the last five years. You mentored me to be an independent scientist by giving me ownership of my project and pushing me to explore numerous scientific questions. Your encouragement reassured me when I struggled through failed experiments and seemingly impossible deadlines. Your willingness to discuss science and beyond, even when we went far past our 15 minute meeting time, will always be appreciated. Thank you for sharing your infectious passion for research and setting an example that I will strive to achieve as I move forward in my scientific career. Finally, thanks for patiently helping me reach the top of the exponential trajectory of a PhD that you drew for me five years ago!

Thank you to my committee members Dr. Andy Putnam, Dr. Renny Franceschi, and Dr. Will Giannobile for their insightful input and questions that helped to shape my project and consider new ideas. I would also like to thank my collaborator Dr. Laurie McCauley for her high expectations, direct questions, and attention to detail that pushed me to be a better scientist. I would also like to acknowledge Dr. Eugene Chen for his generously donated rabbits, without which I could not have isolated the highly important stem cells for this dissertation.

I especially want to thank my mentors from day one, Drs. Jiang Hu and Xiaobing Jin, for always dropping whatever they were working on to answer my questions and discuss my project. Jiang, thank you for teaching me the importance of setting up the system, well-designed experiments, asking deep biological questions, and looking at the big picture. Xiaobing, thank you for your excitement to see my newest data and assist with analysis, your top-notch surgical skills, and your constant encouragement. To my collaborators Zhanpeng Zhang and Ming Dang, thanks for supplying me with an endless amount of both scaffolds and laughs. To Jeremy Holzwarth, Yasmine Doleyres, Jae Shin, and Kunal Rambhia, thanks for listening to my frustrations and making lab a fun place to be every day! I would also like to thank Ganjun Feng, Zhongning Liu, and Rong Kuang for teaching me numerous techniques with patience and a smile. I must also

thank my other collaborators Xue Mi and Weiqiao Zhu, as well as the rest of my current and former labmates for their help over the years. I have been truly lucky to work in such a large, collaborative, and diverse lab and have enjoyed getting to know all of you! Finally, thanks to my lab neighbors Janani Ramaswamy, Harsha Ramaraju, and Erin McNerny for sharing your knowledge over the years!

I also want to thank Chris Strayhorn and Theresa Cody in the UM School of Dentistry Histology Core, Michelle Lynch in the MicroCT Core, BME Grad Coordinator Maria Steele, and Dental Procurement Liz Rodriguez for their help over the years. You are all indispensable staff members, and I greatly appreciate your hard work! I would also like to thank the professors of the BME courses I have instructed (Drs. Joan Greve, Joseph Bull, and Luyun Chen) for their excellent mentorship and development of my teaching skills.

To all my friends in Ann Arbor, grad school wouldn't have been nearly as fun without all you! To my best friends Alex Emly, Kevin Jonke, and Cynthia Huang, you have been an amazing support system both near and far! Most importantly, to my family, thanks for all of your love and support, the stress-relieving vacations, the food transported across state lines, and not asking when I would be finished with my PhD too often! I could not have done this without all of you!

TABLE OF CONTENTS

LIST OF FIGURES

CHAPTER 1

INTRODUCTION

SPECIFIC AIMS

In the United States, 30% of adults suffer joint pain, most commonly in the knee. Knee pain can severely limit mobility and can often be attributed to injury to the cartilage and underlying bone in the joint. Unfortunately, a growing population of young athletes is developing osteochondral knee injuries due to repetitive joint stress and sports-related injuries such as meniscus or ligament tears. Microfracture and autografts are currently primary treatments for small osteochondral defects. However, microfracture results in less resilient fibrocartilage with eventual failure, and autografting can cause donor site morbidity and poor integration. To overcome these significant drawbacks, material scientists and bioengineers have collaborated to design tissue-engineered cartilage-bone grafts as an alternate therapy for small osteochondral defects. Recently, we have made significant progress in developing novel nanofibrous, porous polymer scaffolds for tissue regeneration. **The goal of this project is to optimize scaffold pore architecture of a composite scaffold for both cartilage and bone regeneration.** Using a 3D nanofibrous poly(ʟ-lactic acid) (PLLA) scaffold seeded with bone marrow-derived mesenchymal stem cells (BMSCs), the following three specific aims depicted in **Fig. 1.1** will be investigated:
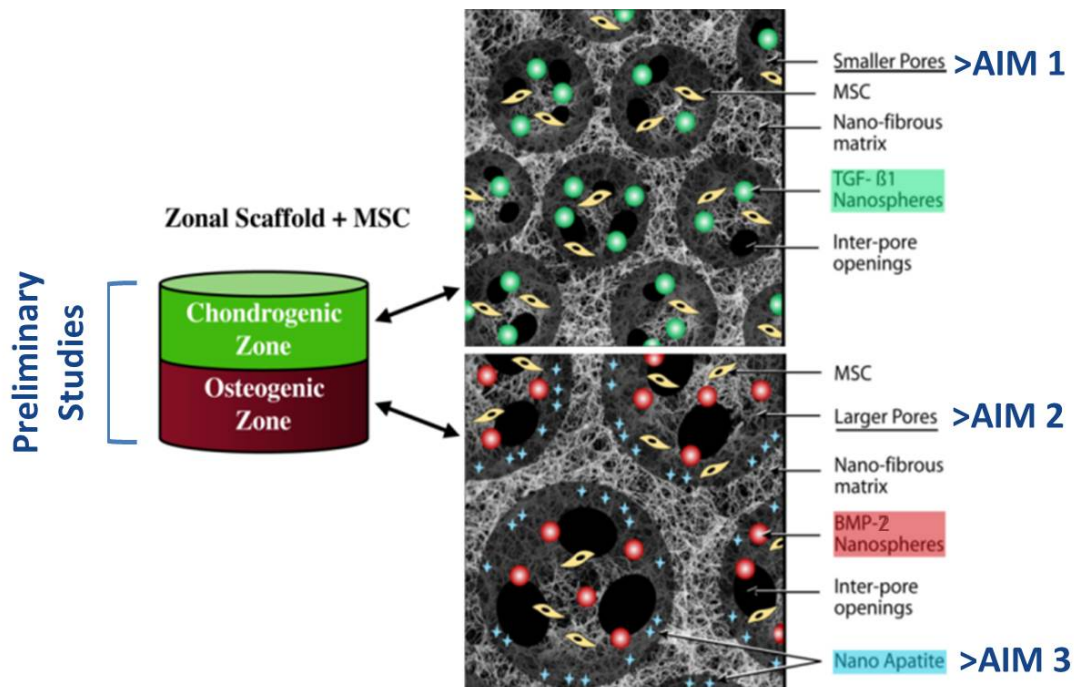
Figure 1.1. Scaffold design investigated for cartilage and bone tissue regeneration.

Aim 1 is to determine the effect of scaffold pore size on chondrogenic differentiation and cartilage formation both *in vitro* and *in vivo*.

Aim 2 seeks to optimize scaffold pore size in an ectopic model to control endochondral ossification for bone regeneration.

Aim 3 is to evaluate how a calcium phosphate electrodeposited on the porous scaffold affects bone formation.

Hypothesis: We hypothesize that chondrogenesis and endochondral ossification can be controlled by scaffold pore size and enhanced by the calcium phosphate coating to direct cartilage and bone regeneration.

In the future, the tissue-engineered cartilage and bone graft materials could be combined into a one biphasic scaffold for an osteochondral knee graft with two unique pore sizes and biphasic

growth factor delivery, as shown by preliminary data. This cell-instructive, biomimetic composite material could even serve as a platform to engineer various complex tissues and organ systems.

SIGNIFICANCE

In a study of 1,000 knee arthroscopies, over 60% of patients had a chondral or osteochondral lesion (1). Osteochondral defects are especially common among the young, active population due to the stresses placed on the joints during high physical activity (2). Injury to the menisci or ligaments in the knee, common in many sports, can also place added stress on the knee (3). This repeated loading causes the cartilage volume to decrease and chondral or osteochondral defects to form (4). Self-repair of these defects is limited because cartilage is avascular (5). If articular cartilage further degenerates and loses its ability to adapt to repetitive stress, osteoarthritis can develop. However, osteoarthritis can be prevented in these individuals with proper, early treatment of the osteochondral defects. There are currently two treatment options for small femoral osteochondral defects - microfracture or autografts (6). While microfracture (drilling through cartilage into bone marrow) can relieve pain, resulting fibrocartilage does not have the same resiliency of articular hyaline cartilage and can fail over time (5). With autografts, it is difficult to exactly match defect geometry, requires multiple surgeries, and can cause donor site morbidity (7).

Due to the significant drawbacks of current treatments, there is a clear need for an alternate therapy. A tissue-engineered osteochondral graft could potentially serve as a better solution for patients. In cartilage and bone tissue engineering, as in nearly all tissue engineering, scaffolds play a pivotal role by serving as an artificial extracellular matrix (ECM) (8). There has been active research using biodegradable synthetic polymer scaffolds for osteochondral regeneration

(9), showing the promise of this approach. However, the scaffolds developed up to this point to construct this complex composite tissue have not been able to replicate the physiological properties of both cartilage and bone. The design of synthetic biodegradable scaffolds remains a key issue in engineering quality osteochondral grafts. Our novel scaffold design features phase-separated nanofibers to mimic ECM, previously shown to enhance cell adhesion, proliferation, and differentiation of multiple stem cell types (10-16). By tailoring this novel material, *we believe that a BMSC-seeded, nanofibrous biphasic scaffold with optimized pore size and electrodeposited calcium phosphate may functionally regenerate cartilage and bone tissue. This approach is innovative because multiple complex technologies never before combined will be used to fabricate a composite scaffold to control dual differentiation of bone marrow-derived stem cells and modulate the intricate endochondral ossification process for cartilage and bone regeneration.*

DISSERTATION OVERVIEW

Chapter 2 provides a literature review on nanofibrous scaffolds and their use in cartilage and bone tissue engineering applications. Three methods for nanofibrous scaffold fabrication are described: electrospinning, self-assembly, and phase separation. The positive effects of nanofibers on cell function are elucidated, including adhesion, proliferation, and differentiation, along with potential mechanisms. Finally, patient-specific nanofibrous scaffolds and controlled release of growth factors on nanofibrous scaffolds are discussed. This work was published as a portion of: Gupte MJ, Ma PX, "Nanofibrous scaffolds for dental and craniofacial applications." J Dent Res (91) 3: 227-234, 2012. [PMCID: PMC3275331]

Chapter 3 focuses on Aim1 and studies the scaffold pore size effect on cartilage formation. We compare the chondrogenic differentiation of hMSCs on three-dimensional nanofibrous (NF) PLLA scaffolds with small pore size (125-250 µm) or large pore size (425-600 µm) both in vitro and in vivo. Following 4 wk chondrogenic culture and 8 wk subcutaneous implantation in nude mice, small-pore scaffolds supported avascular cartilage formation, but large-pore scaffolds contained only fibrous tissue. Therefore, small-pore scaffolds enhanced chondrogenic differentiation in vitro and cartilage formation in vivo compared to large-pore scaffolds.

Chapter 4 investigates Aim 2 and the effect of scaffold pore size on endochondral ossification in an in vivo ectopic model. Three pore sizes, small (125-250µm), medium (250-425µm), and large (425-600µm), all supported endochondral ossification *in vivo* after 4w and 8w. A very small pore size (60-125µm) was required to block blood vessel invasion for cartilage formation.

Chapter 5 explores Aim 3 to determine whether an electrodeposited calcium phosphate (CaP) coating on a medium pore size, nanofibrous PLLA scaffold could promote the scaffold's osteoconductivity. This study showed that the electrodeposited calcium phosphate (CaP) on a nanofibrous PLLA scaffold seeded with rabbit bone marrow-derived mesenchymal stem cells (BMSCs) enhanced mature, mineralized bone formation, compared to a blank scaffold without CaP, by promoting stem cell proliferation. The introduction of this chapter was adapted from a published book chapter: Smith IO, Gupte MJ, Ma PX, "Polymer/ceramic Composite Scaffolds for Tissue Regeneration," Biomaterials and Regenerative Medicine, Cambridge University Press, 2014.

Chapter 6 reveals preliminary work using 1) TGF-β1 delivery for rat knee defect repair and 2) the biphasic scaffold shown in **Figure 1.1** with two different pore sizes and biphasic controlled

release of TGF-β1 and BMP-2 for osteochondral regeneration in an ectopic model. This chapter

also provides a summary of conclusions of the entire dissertation and discusses future work.

CHAPTER 2

LITERATURE REVIEW:

NANOFIBROUS SCAFFOLDS FOR CARTILAGE AND BONE REGENERATION

ABSTRACT

Tissue engineering solutions often harness biomimetic materials to support cells for functional tissue regeneration. Three dimensional scaffolds can create a multi-scale environment capable of stimulating cell adhesion, proliferation, and differentiation. One such multi-scale scaffold incorporates nanofibrous features to mimic the extracellular matrix along with a porous network for the regeneration of a variety of tissues. This chapter will focus on nanofibrous scaffold synthesis/fabrication, biological effects of nanofibers, their tissue engineering applications in bone, cartilage, patient-specific scaffolds, and incorporated growth factor delivery systems. Nanofibrous scaffolds cannot advance technology for tissue engineered replacements in many physiological systems.

INTRODUCTION

Hard tissue regeneration is in high demand due to trauma, post-cancer surgery, skeletal disease, and congenital malformations. Successful regeneration of affected tissues is necessary to reconstruct skeletal support, restore mobility, and protect vital organs. One common approach in the field of tissue engineering aims to restore tissue function by growing cells on a designed scaffold that creates a three-dimensional microenvironment for cell support.

In designing appropriate scaffolding to provide this support, material selection is important. Scaffolds have been fabricated using a variety of natural and synthetic biomaterials such as proteins, ceramics, and polymers (1). Synthetic polymers are gaining popularity because they can be designed to have a high processing capability, mechanical stability, biocompatibility, and biodegradability (2). These features allow a polymer scaffold to be integrated into biological systems and tailored to mimic the natural cell environment of the extracellular matrix (ECM). The ECM is the nanofibrous protein network that surrounds cells in all tissues to support their many functions (1) and can be emulated with a nanofibrous polymer scaffold. The nanofibers can be designed to promote cell functions such as adhesion, proliferation, differentiation, and tissue neogenesis. **In addition to nanofibers, the scaffold should have an internal interconnected porous network, a common scaffold design requirement, to allow cellular integration into the scaffold among other functions** (3). It can even be designed to release growth factors to tailor tissue development (4).

Many cell types have been cultured on nanofibrous materials to regenerate hard tissues. Embryonic stem cells and mesenchymal stem cells, such as bone marrow stromal cells and adipose stem cells, are attractive cell sources due to their ability to differentiate to multiple lineages and self-renew. Differentiated cells have also been utilized to form the single tissue type in which they are found: osteoblasts for bone and chondrocytes for cartilage (5). Each of these cell sources can be successfully implemented to promote desired tissue formation with adequate support of cell function. 3D porous, nanofibrous scaffolds have been used to regenerate many hard and soft tissues with several stem cell and differentiated cell sources. However, this review will focus the use of the nanofibrous scaffold on bone and cartilage regeneration.

NANOFIBROUS SCAFFOLD SYNTHESIS AND FABRICATION

Many methods have been developed to synthesize scaffolds for tissue engineering applications; however, only a limited number of methods can generate the nano-scale features necessary to mimic the extracellular matrix. Nanofibrous scaffolds have been fabricated using three techniques: electrospinning, self assembly, and phase separation.

Electrospinning

The electrospinning process creates polymer nanofibers by applying a high voltage to a syringe needle filled with a polymer solution. The applied voltage creates an electric field, which causes a jet stream of polymer solution by creating a force greater than the surface tension of the solution. The jet then bends and elongates due to electrical instability, causing a spiraling motion and smaller diameter jet. The solvent then evaporates, leaving only a charged polymer nanofiber. The nanofiber is attracted to a grounded collector, where it solidifies into a nonwoven mat. The collector can be rotated to produce a desired fiber orientation (6).

Several parameters of this method must be controlled in order to achieve nanofibers with desired morphology including voltage, motor speed, distance from needle to collector, syringe pump flow rate, external temperature, and polymer solution concentration. For example, increasing temperature can decrease fiber diameter due to reduced viscosity of the polymer solution and increased conductivity. Conversely, increasing polymer solution concentration can greatly increase fiber diameter (7). Therefore, these parameters must be optimized to achieve polymer nanofibers.

Electrospinning can be used for many synthetic and natural polymers and can produce scaffolds to which many cell types can adhere. In the dental field, electrospinning has been used to form a

gelatin membrane for periodontal tissue regeneration. When seeded with periodontal ligament cells, the electrospun gelatin membrane showed good cell attachment and proliferation over 7 days (7). This process also supports creating copolymers such as PLGA (8) or polymer blends such as PVA with collagen (9) by using a copolymer or polymer blend solution at an optimal ratio. In addition, the electrospun scaffold can be composited with biological molecules such as growth factors (10) or minerals (8, 9, 11). Electrospinning is the most commonly used technique to produce synthetic and natural polymer fibers due to its ease; however, it often cannot produce true nanofibers that are at the order of 100 nm or less with frequently used biodegradable polymers. *More importantly, electrospinning cannot produce complex 3D scaffolds with designed pore geometry.*

Self Assembly

Self assembly is the autonomous organization of components into a specific structure. This important process occurs naturally with the self-assembly of nucleic acids and proteins like collagen, a main extracellular matrix protein of many tissues (bone, cartilage, blood vessels, skin, tendons, etc.). Collagen self-assembles when molecular interactions cause three polypeptides to form a triple helix, which organizes into a fibril, and many fibrils bundle together to form a collagen fiber (12). This natural self-assembly process for collagen can be mimicked to form nanofibrous polymer scaffolds from engineered self-assembling peptides. These peptides can be designed to form a stable organized structure through spontaneous organization of molecules due to non-covalent interactions (13).

Many groups have used this approach to fabricate hydrogels, commonly used for cell encapsulation (14). Self assembly can often produce nanofibers of a much smaller diameter than electrospun fibers. They can also be useful in injection applications as the self assembly process

can occur *in vivo* following injection. However, self-assembled *hydrogels do not allow control over internal pore shape* and can have poor mechanical strength, making them unsuitable for many tissue engineering applications. Self-assembly peptides are also susceptible to enzymatic degradation, which can affect scaffold degradation rate in an uncontrolled fashion. These issues need to be addressed, especially when utilizing self-assembling scaffolds for tissue engineering applications.

Phase Separation (Used in this Dissertation)

Phase separation is a process where a single phase homogenous polymer solution is critically quenched, causing separation into a polymer-rich phase and a solvent-rich phase. This separation occurs to lower the system free energy due to the thermodynamically unstable state of the solution (15).

Our laboratory has developed a novel method that uses thermally induced phase separation to produce a synthetic biodegradable polymer scaffold with nanofiber features. This is done by combining poly(L-lactic acid) (PLLA) with a solvent (tetrahydrofuran, THF) and freezing at a low temperature. Freezing causes the material to separate into two distinct phases of PLLA nanofibers and THF. The THF can then be extracted using another solvent and sublimated, leaving only the PLLA nanofibers (16). We have also applied this method to create a nanofibrous gelatin scaffold using different solvents (17).

In biological applications, it is advantageous for nanofibrous scaffolds to have interconnected, internal pore structures in order to aid in cell migration, nutrient/waste exchange, and uniform cell and nutrient distribution (18). Porous scaffolds can be manufactured using this method because a porogen such as sugar or paraffin can be used to form

pores within a bulk material and then leached out following phase separation, leaving open pores as well as nanofibers. Therefore, the entire process to make a nanofibrous, macroporous scaffold shown in **Figure 2.1** is as follows: spherical porogen template formation, heat treatment to interconnect individual porogen spheres, polymer casting, phase separation, solvent exchange, porogen leaching, and freeze drying (19). Using this method, nanofibers that have an average diameter on the order of 100 nm can be formed, which can be difficult using other techniques. **Phase separation also beneficially allows for the incorporation of internal macro-pores and complex scaffold geometries.** Therefore, phase separation is a valuable method for nanofibrous scaffold preparation for tissue engineering applications.

EFFECTS OF NANOFIBERS ON CELL FUNCTION

The natural extracellular matrix (ECM) consists of nano-scale proteins such as collagen, fibronectin, and vitronectin. Cell-ECM interactions affect many signaling pathways that alter cell responses such as adhesion, proliferation, differentiation, and tissue neogenesis (20). Similarly, nanofibers affect these cell behaviors as seen in numerous cell types cultured on nanofibrous materials.

Adhesion and Proliferation

During initial attachment, cells lightly adhere to a substrate. Cells then spread and form adhesion structures to create stronger adhesion and increase interaction with the substrate. Without sufficient adhesion to surroundings, cell death can occur. Nanofibrous materials have been shown to promote adhesion so cells can take on morphology similar to that *in vivo* as compared to smooth materials. This has been demonstrated by human embryonic stem cell derived osteo progenitor cells cultured on thin nanofibrous matrix, solid non-nanofibrous films, and gelatin-

coated tissue plastic (21). On nanofibrous matrix, cells beneficially maintain 3D morphology and form adhesions with nanofibers. However, on both solid films and tissue culture plastic, cells spread into a non-physiological 2D morphology which is not conducive to tissue development (**Fig. 2.2**). Oppositely, mouse embryonic stem cells lack interaction with solid films and take on a rounded morphology, another undesirable result (22).

Following adhesion, cells must proliferate for successful tissue formation. This has been reported with many cell types cultured on nanofibrous scaffolds including human dental pulp stem cells (23) and pre-osteoblasts (24).

Differentiation and Tissue Formation

Nanofibrous scaffolds have been shown to improve differentiation of numerous stem cell populations (18, 23, 25-27). With human mesenchymal stem cells, the nanofibrous scaffold supported both osteogenic and chondrogenic differentiation with chemical stimulation (18, 28). Chondrogenic differentiation was marked by increased Sox-9 gene expression on nanofibrous matrix compared to solid films (18). Further examples of differentiation will be detailed with respect to specific tissues later in the review.

While most studies support that nanofibers promote differentiation better than other materials, it has been shown that nanofibers can aid in maintaining pluripotency of proliferating mouse embryonic stem cells (29). This suggests that nanofiber effects may be dependent on culture conditions and that nanofibers may affect several complex signaling pathways. Further work is required to elucidate the role of nanofibrous features in stem cell differentiation.

Potential Mechanisms

There are a few proposed mechanisms that may explain why nanofibers induced these positive biological effects: increased protein adsorption, increased integrin expression, and altered signaling pathways. It is suggested that initial attachment of cells may be due to increased adsorption of ECM proteins such as fibronectin, vitronectin, and laminin (30). While nanofibers do increase surface area, varying amounts of these proteins indicate that selective adsorption of important proteins may occur. Increased protein adsorption may in turn increase expression of integrins, transmembrane proteins that mediate cell-ECM attachment. Mouse embryonic stem cells have shown increased expression of α2, α5, and β1 integrins when cultured on nanofibrous matrix versus smooth films. Increased integrins were furthermore linked to increased mesodermal and osteogenic differentiation in this study (22). It has been proposed that integrins may aid in differentiation by activating paxillin and focal adhesion kinase, which are involved in differentiation pathways (31). Morphology, adhesion, and differentiation responses have also been attributed to RhoA (32) and Rac (29) expression, which regulate cytoskeletal organization and other cell behaviors. While these are possible underlying mechanisms of nanofiber effects, more work is required to fully investigate complex cell signaling pathways that may be involved. However, the effects of nanofibers on the regeneration of bone and cartilage will be further discussed.

BONE TISSUE ENGINEERING

Bone tissue forms the entire axial and appendicular skeleton, including the skull, ribs, vertebral column, pelvic and pectoral girdles, and upper and lower limbs. Regenerating bone tissue in following injury or genetic defects, for example, can be vital to allow for mobility, performance of everyday tasks, and pain relief.

While tissue engineered bone grafts have been researched for years, challenges still lie in achieving *in vivo* mechanical properties and vascularization. Necessary mechanical properties must be reached because the bone formed following scaffold degradation must withstand significant stresses over many years. Vascularization is essential for tissue survival and function because blood vessels supply oxygen and other nutrients and remove waste. The solution to overcoming these challenges to produce tissue engineered bone may lie in combining the right cell source with a nanofibrous scaffold.

Nanofibrous (NF) scaffolds may be an advantageous microenvironment for bone tissue formation by mimicking the Type I collagen fibers that are a major component of bone. **The large macro-pores that are also a component of our NF scaffolds allow for necessary blood vessel in-growth for bone tissue regeneration and survival.** Even without cells, the osteoconductive NF scaffold has shown promising results *in vivo* following scaffold implantation in a rat calvarial defect model likely due to host MSC migration and subsequent osteogenic differentiation (33). Several cell types and composite scaffold materials have been successfully utilized by our laboratory and others to successfully produce bone tissue, such as embryonic stem cells, embryonic stem cell-derived mesenchymal stem cells, mesenchymal stem cells, and amniotic fluid-derived stem cells.

Embryonic stem cells (ESCs) are explored in a vast range of tissue engineering applications due to their pluripotency. Our laboratory has directed them to an osteogenic lineage for bone formation by seeding them on nanofibrous thin matrix. Mouse ESCs were also seeded on solid, flat films without the NF features for comparison. After 12 hours, the nanofibers promoted cell adhesion seen by protrusion formation by ESCs on nanofibers. In contrast, mouse ESCs had a rounded morphology on the solid films, which is not conducive to osteogenic differentiation.

Differentiation was also enhanced by nanofibers as shown by increased gene expression of osteogenic markers and calcium content with the NF matrix compared to solid films (22). This study reveals that nanofibers improve osteogenic differentiation of ESCs by providing a synthetic extracellular matrix environment.

This positive nanofiber effect was also seen on the differentiation of human embryonic stem cell-derived mesenchymal stem cell (hESC-MSC) into osteoblasts. This recently derived stem cell source is attractive because they are more homogenous than ESCs and more proliferative than mesenchymal stem cells (MSCs) (34). Hu *et al.* (2010) further supported the NF architecture effects shown above with ES cells for hESC-MSCs through increased alkaline phosphate activity and calcium mineralization extent on NF thin matrix versus solid films. Secondly, by synergistically using dexamethasone and bone morphogenetic protein (BMP)-7 with 3D NF scaffold, osteogenic differentiation of hESC-MSC significantly improved during culture on nanofibrous scaffolds (25). Thus, another bone forming system was developed utilizing the NF PLLA scaffold with hESC-MSCs and osteogenic factors.

Thirdly, human amniotic fluid-derived stem cells (hAFSCs) can be supported by NF scaffold for bone formation. Human AFSCs are multipotent but more investigation is required regarding their response to biomaterials and soluble factors (35). Along with ES cells and hESC-MSCs, hAFSCs can be directed to an osteogenic lineage when facilitated by NF features and BMP-7, simulating their *in vivo* environment (27).

A mineral phase such as hydroxyapatite (HAP) can also been incorporated into the nanofibrous scaffolds to form a composite bone matrix-mimicking scaffold (36). This mineral addition was hypothesized to be beneficial in bone tissue engineering because it is the

main inorganic components in natural bone. The NF PLLA scaffold has been modified by HAP crystals using simulated body fluid incubation previously (37, 38). Most recently, Liu *et al.* (2009) incorporated nano-HAP into a 3D nanofibrous gelatin scaffold. Nanofibers allow adequate adhesion of HAP crystals (**Fig. 2.3a**) while preventing blockage of pore interconnections (**Fig. 2.3b**). When seeded with MC3T3 pre-osteoblasts, the NF gelatin/HAP scaffold supported differentiation, shown by bone sialoprotein (BSP) and osteocalcin (OCN) expression in **Fig. 2.3c** and **2.3d**, and was mechanically superior to commercially available Gelfoam® (24). Other groups have shown successful bone formation using nanofibrous synthetic and natural polymer scaffolds such as electrospun PLGA (8), PVA/Type I Collagen (9), and many others (39).

Nanofibrous scaffolds provide a cellular platform for bone formation. However, challenges still remain in repairing bone defects with sufficient vascularization that is capable of both short term and long term mechanical stability and is capable of native remodeling during aging. Therefore, additional long term studies are needed to improve restoration of this important tissue.

CARTILAGE TISSUE ENGINEERING

Cartilage regeneration is often in demand for arthritic knees, hips, or shoulders, often due to high activity placing increased stress on joints. These articulating joints and the nasal septum are composed of hyaline cartilage, while the annulus fibrous in the intervertebral disc and mandibular condyles in the temporomandibular joint (TMJ) are covered with fibrocartilage, which when diminished can cause back pain or TMJ disorder, respectively (40). Lastly, the outer ear, nasal tip, and epiglottis consist of elastic cartilage. While each type of cartilage differs in cell and matrix arrangement and proportion, the constituents of cartilage remain the same: namely,

chondrocytes, collagen type II, and proteoglycans (41). Therefore, successful cartilage formation can be widely applied within the articulating joints and the craniofacial region.

Cartilage tissue development is similar to bone in many ways; however, it has different environmental requirements for support of tissue growth. **In regards to scaffold pore structure, small pores may be needed to prevent vascular ingrowth *in vivo* in order to maintain its avascularity**. Nanofiber dimensions are similar due to the abundant Type I collagen in bone ECM and Type II collagen in cartilage ECM that are physically very similar. Mechanical properties, porosity, and pore interconnection size may also need to differ but this has not yet been studied. These complex architectural features of the nanofibrous scaffold may control the cell microenvironment better than hydrogels, commonly used in cartilage tissue engineering for stem cell encapsulation (42).

When seeded with mesenchymal stem cells (hMSCs), the 3D NF scaffold supported chondrogenic differentiation, shown by gene expression of chondrogenic markers. After 6 weeks of culture, GAG accumulation and Type II collagen deposition occurred in the presence of TGF-β1 (18). In addition to ECM deposition, scaffold's pore architecture favorably forced hMSC aggregation which may have improved stem cell condensation for chondrogenic commitment. This study shows that nanofibers can not only support bone formation but also cartilage formation, with the inclusion of appropriate growth factor(s), to create a tissue-specific synthetic environment. Therefore, with the ability to form both cartilage and bone, the entire osteochondral interface found in most joints like the temporomandibular joint, knee, hip, and shoulder can potentially be restored following injury or disease.

PATIENT-SPECIFIC SCAFFOLDS

Due to the unique and widely varied skeletal sizes and complex shapes, there is a need for patient-specific tissue regeneration, currently a hot topic in the popular media. To serve this need, our laboratory has developed technology to create patient-specific, anatomically-shaped scaffolds. A scaffold unique to each patient can be helpful in regenerating the mandible shape, for example, as it has complex geometry and can highly vary between individuals. This can be done by creating a wax mold of one mandible section following 3D printing of the entire mandible from computed tomography (CT) scans of the patient (**Fig. 2.4a**). The mold is then used to form the NF scaffold (**Fig. 2.4b,c**) with macroporous structure (**Fig. 2.4d**) and patient-specific geometry. The scaffold of one section of patient's mandible successfully showed bone formation when seeded with MC3T3-E1 preosteoblasts (43). Similar results have been shown for an anatomical ear (43) and section of a hand digit (44). This technique holds great potential for tissue replacements that are specific to each patient in order to best restore natural appearance and function.

DRUG DELIVERY USING IMMOBILIZED NANOSPHERES

As shown for each tissue described previously, growth factors can have a large influence on stem cell differentiation. *In vivo,* growth factors lose bioactivity very rapidly due to several protein degradation pathways (45). Therefore, controlled release of bioactive molecules is highly necessary *in vivo* to sustain their activity over an extended time period. Drug delivery vehicles must also be designed to release the drug at the correct dosage due to cell sensitivity and to preserve drug bioactivity by maintaining molecular stability (46). Not only can drug delivery aid in tissue formation but could also deliver therapeutic drugs following implantation such as anti-inflammatories or antibiotics.

Previous drug delivery techniques used with porous scaffold systems include incorporating the drug into the polymer solution, coating the scaffolds, or entrapping drug-filled microspheres within the scaffold (1). Although these methods allow for slower release, true release kinetics and spatial delivery control is not achieved. Hydrogels such as polyethylene glycol (PEG) are often used as drug carriers because drugs can be easily incorporated into the hydrogel solution (46, 47). However, biodegradable polyesters such as PLGA can be made into spheres to more precisely control release kinetics for significantly longer release compared to hydrogels.

We have recently developed drug-encapsulating PLGA nanospheres that can be immobilized on the nanofibrous scaffold (4). These nanospheres, fabricated using a double emulsion technique, allow both spatial and temporal control of one or more growth factors. Immobilization of the nanospheres on nanofibers prevents nanosphere coalescence and migration to promote uniform spatial delivery. Release kinetics of PLGA nanospheres can be fine-tuned by varying the polymer molecular weight or copolymer composition (LA:GA ratio). For further control, nanosphere size can also be altered during the double emulsion process through amount of surfactant or emulsion strength. Using these novel PLGA nanospheres, sustained growth factor release at a high dosage has been achieved.

In a study by Wei *et al.* (2007), PLGA nanospheres were used to deliver BMP-7 to induce ectopic bone formation. Nanospheres were immobilized on the nanofibers (**Fig. 2.5a**) without blocking interpore connections (**Fig. 2.5b**). Scaffolds with BMP-7 nanospheres (NS) without seeded cells were implanted into rats and evaluated after 3 weeks using H&E staining. Scaffolds soaked with BMP-7 (**Fig. 2.5c**) or with blank NS (not shown) contained only fibrous tissue, but scaffolds with BMP-7 NS revealed initial bone formation (**Fig. 2.5d**) (4). Results were similar after 6 wk implantation with even more significant bone formation in BMP-7 NS scaffolds.

Thus, sustained release of BMP-7 using PLGA nanospheres spurred bone formation better than BMP-7 soaked scaffolds with no delivery system.

Similarly, another study determined the effect of PDGF using the PLGA nanosphere vehicle to promote angiogenesis. Following *in vitro* studies that demonstrated the bioactivity of PDGF, NF scaffolds with immobilized NS were implanted in rats (48). Results indicated significant angiogenesis when NS were present but negligible blood vessel formation in scaffolds lacking NS (48). Therefore, controlled release of PDGF can improve vascular ingrowth more effectively than endogenous signaling alone.

These drug-delivering PLGA nanospheres with tunable release kinetics can be beneficially applied to several tissues in need of sustained growth factor(s) release. The temporal and spatial control achieved on the nanofibrous scaffold is a significant improvement over previous techniques used for controlled release.

CONCLUSION

The fields of biomaterials and tissue regeneration have recently advanced to create a suitable microenvironment for cell development to form a variety of tissues. Nanofibrous scaffolds are one such biomaterial approach shown to enhance bone and cartilage regeneration. Growth factor delivery on the scaffold has further improved tissue formation through controlled release for sustained bioactivity. However, challenges in precise material and biological control still exist that can be overcome to produce tissues closer to their native state. This will push the future of the field toward cell-based therapies to achieve functional tissue replacements.

FIGURES
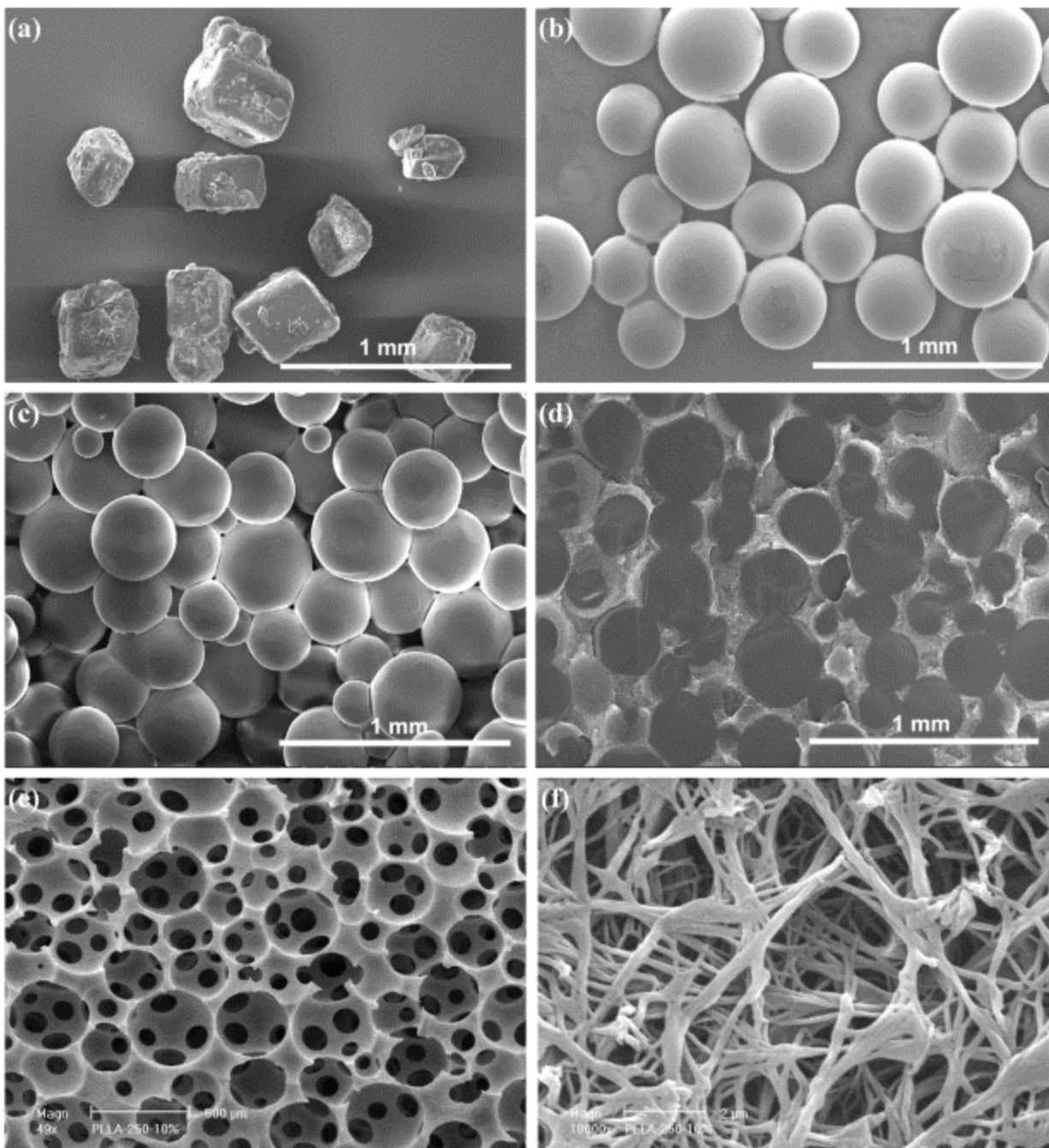
Figure 2.1. SEM micrographs of nanofibrous, macroporous PLLA scaffold with sugar sphere template leaching and thermally induced phase separation method. (a) sugar crystals; (b) sugar spheres (250-425µm diameter); (c) interconnected sugar sphere template after heat treatment at 37°C for 15 min; (d) polymer/sugar composite following polymer casting, phase separation at -20°C, solvent exchange, prior to sugar template leaching; (d,e) final 3D nanofibrous, macroporous scaffold after sugar template leaching and freeze drying at low (50x) and high (10,000x) magnifications. From (37). Copyright © 2006 by John Wiley & Sons.

Nano   Solid   Control
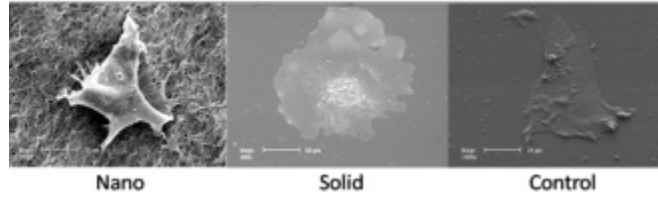
Figure 2.2. SEM micrographs of hESC-derived bone progenitor cells after 48 hr of culture in osteogenic supplemented media on a thin nanofibrous film (Nano), a solid film with no nanofibrous features (Solid), and gelatin-coated tissue plastic (Control). Cells maintain 3D morphology on nanofibers but spread into an undesirable 2D morphology on solid film and control tissue plastic. Scale bars = 20µm for Nano & Control, 50µm for Solid. From (21). Copyright © 2010 by Elsevier.
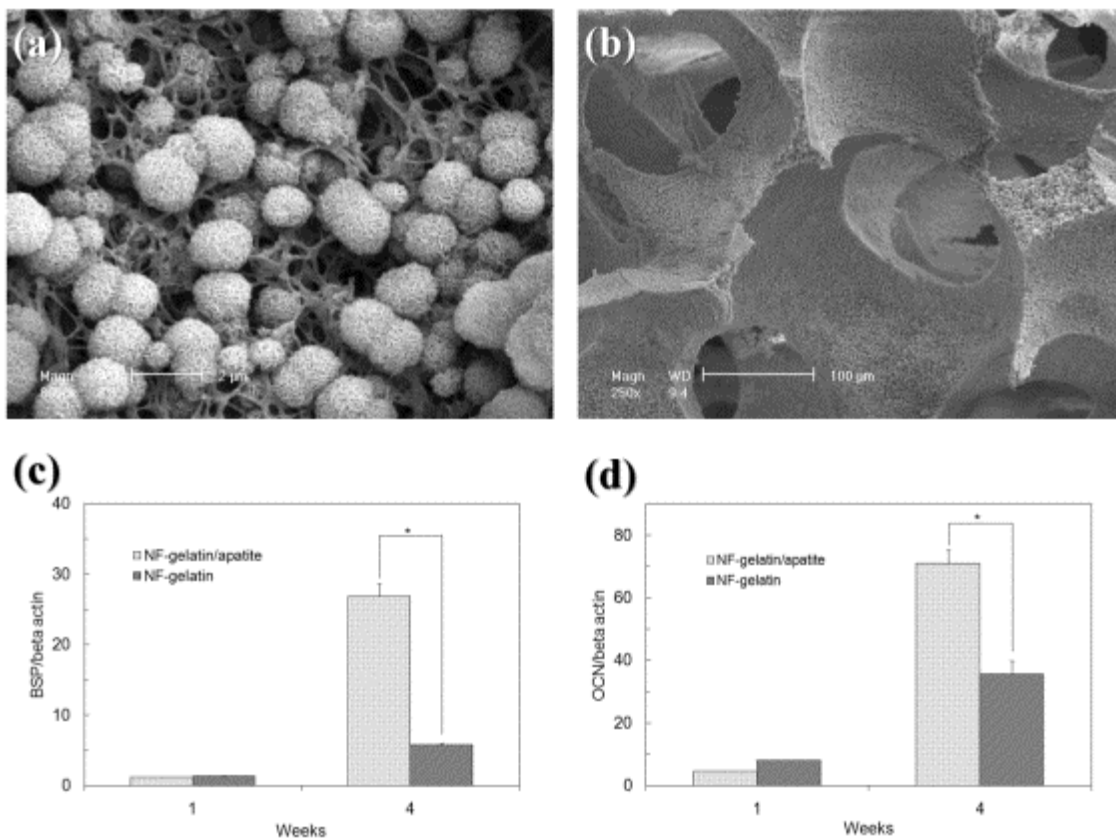
Figure 2.3. Effect of nano-hydroxyapatite/gelatin nanofibrous scaffold on MC3T3-E1 pre-osteoblast differentiation. SEM micrographs of scaffolds incubated in 1.5x SBF for 7 days. (a) high magnification shows significant apatite deposition on nanofibers. (b) low magnification shows apatite crystals line pore walls without blocking pore interconnections. Real time PCR results of (c) bone sialoprotein (BSP) and (d) osteocalcein (OCN) after 1 and 4 weeks of culture on gelatin or gelatin/apatite scaffold, normalized to beta-actin expression. Gene expression of both bone markers is significantly higher at 4 weeks for gelatin/apatite composite scaffold than gelatin scaffold alone. (*) represents statistically significant difference, $p > 0.05$. From (24). Copyright © 2009 by Elsevier.

23
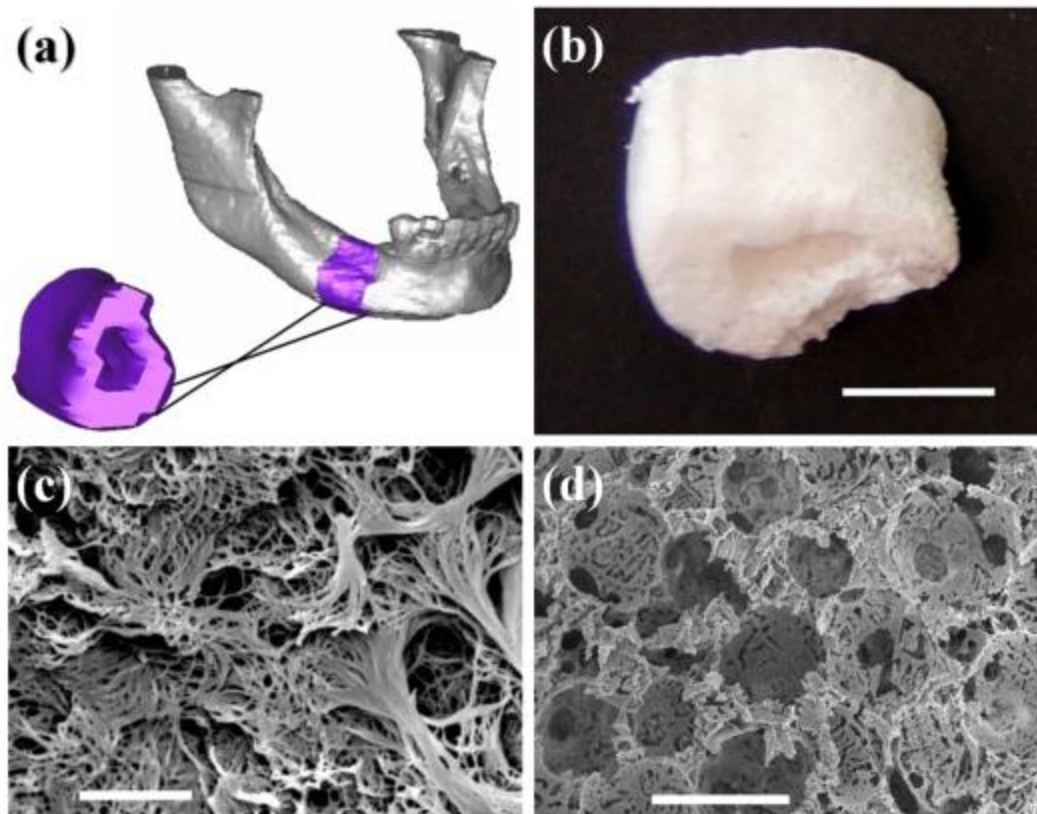
Figure 2.4. Patient-specific nanofibrous (NF) scaffold for mandible section from CT-scan. (a) 3D reconstruction of entire human mandible with highlighted section molded for scaffold fabrication. (b) Resulting bulk NF scaffold. Scale bar = 10mm. SEM micrographs of (c) nanofibers (Scale bar = 5 μm) and (d) interconnected pore structure of scaffold (Scale bar = 500 μm). From (43). Copyright © 2006 by Elsevier.
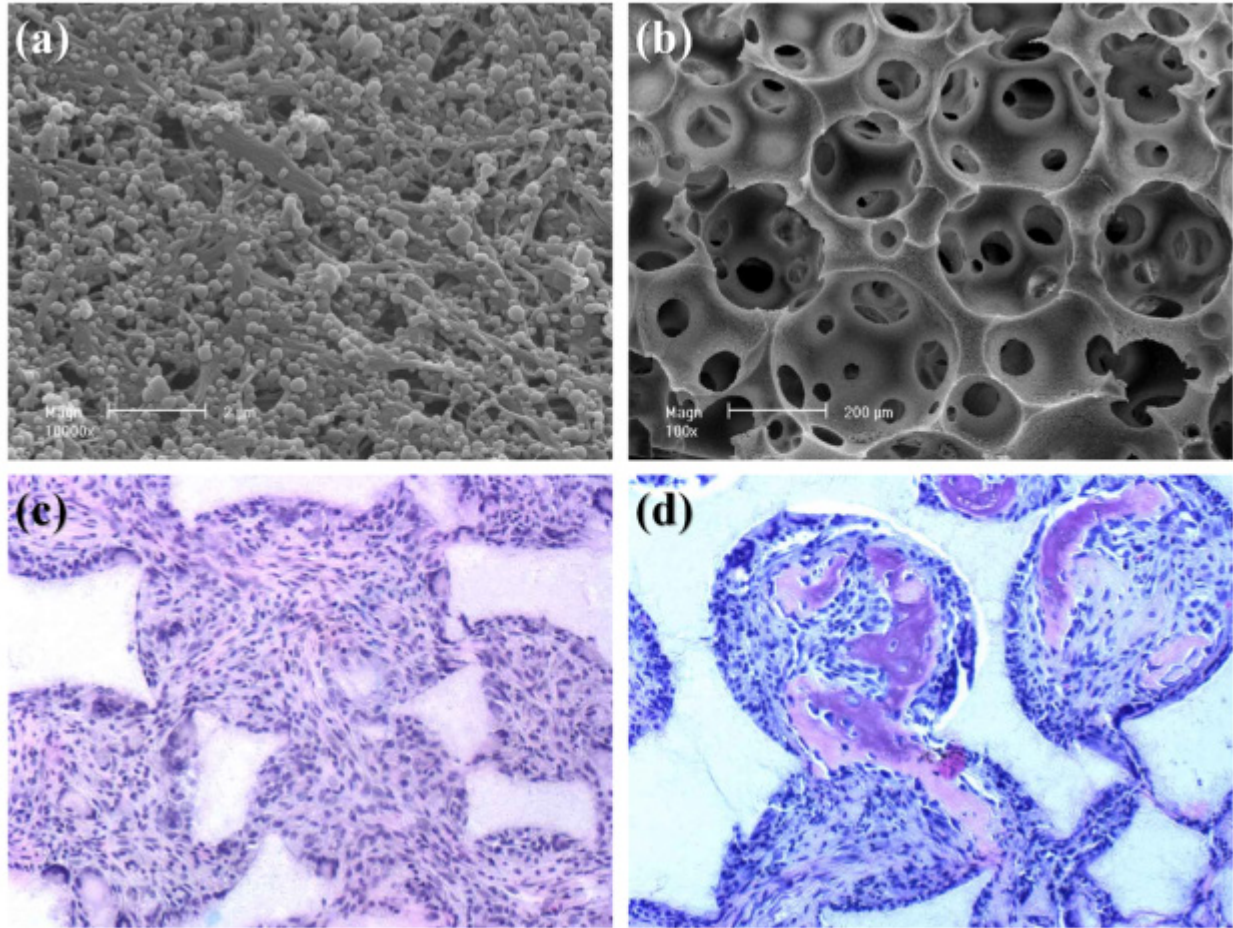
Figure 2.5. BMP-7 releasing nanospheres (NS) immobilized on nanofibrous scaffold and *in vivo* histological analysis. SEM micrographs of (a) NS immobilized on nanofibers with (b) undisturbed porous structure. H-E staining following 3 wk rat implantation *in vivo* for (c) BMP-7 absorbed scaffold and (d) BMP-7 NS scaffold at 200x magnification. Bone formation is observed in BMP-7 NS scaffold only shown by matrix formation within pores. From (4). Copyright © 2007 by Elsevier.

REFERENCES

1.   Ma PX. Biomimetic materials for tissue engineering. Advanced Drug Delivery Reviews. 2008;60(2):184-98.
2.   Liu XH, Ma PX. Polymeric scaffolds for bone tissue engineering. Annals of Biomedical Engineering. 2004;32(3):477-86.
3.   Ma PX. Scaffolds for tissue fabrication. Materials Today. 2004;7(5):30-40.
4.   Wei G, Jin Q, Giannobile W, Ma P. The enhancement of osteogenesis by nano-fibrous scaffolds incorporating rhBMP-7 nanospheres. Biomaterials. 2007;28(12):2087-96.
5.   Zaky S, Cancedda R. Engineering Craniofacial Structures: Facing the Challenge. Journal of dental research. 2009;88(12):1077-91.
6.   Yang T, Yao Y, Lin Y, Wang B, Xiang R, Wu Y. Electrospinning of polyacrylonitrile fibers from ionic liquid solution. Applied physics A, Materials science & processing. 2010;98(3):517-23.
7.   Zhang S, Huang Y, Yang X, Mei F, Ma Q, Chen G. Gelatin nanofibrous membrane fabricated by electrospinning of aqueous gelatin solution for guided tissue regeneration. Journal of biomedical materials research. 2009;90A(3):671-9.
8.   Jose M, Thomas V, Xu Y, Bellis S, Nyairo E, Dean D. Aligned Bioactive Multi-Component Nanofibrous Nanocomposite Scaffolds for Bone Tissue Engineering. Macromolecular bioscience. 2010;10(4):433-44.
9.   Asran A, Henning S, Michler G. Polyvinyl alcohol-collagen-hydroxyapatite biocomposite nanofibrous scaffold: Mimicking the key features of natural bone at the nanoscale level. Polymer. 2010;51(4):868-76.
10.   Binulal N, Deepthy M, Selvamurugan N, Shalumon K, Suja S, Mony U. Role of Nanofibrous Poly(Caprolactone) Scaffolds in Human Mesenchymal Stem Cell Attachment and Spreading for In Vitro Bone Tissue Engineering-Response to Osteogenic Regulators. Tissue Engineering: Part A. 2010;16(2):393-404.
11.   Deng XL, Xu MM, Li D, Sui G, Hu XY, Yang XP. Electrospun PLLA/MWNTs/HA hybrid nanofiber scaffolds and their potential in dental tissue engineering. Key Engineering Materials Bioceramics. 2007;19(330-332):393-6.
12.   Lewin B, Cassimeris L, Lingappa VR, Plopper G, editors. Cells. 1 ed. Sudbury, MA: Jones and Bartlett Publishers; 2007.
13.   Huang Z, Newcomb CJ, Bringas Jr P, Stupp SI, Snead ML. Biological synthesis of tooth enamel instructed by an artificial matrix. Biomaterials. 2010;31(35):9202-11.
14.   Sun J, Zheng Q, Wu Y, Liu Y, Guo X, Wu W. Culture of nucleus pulposus cells from intervertebral disc on self-assembling KLD-12 peptide hydrogel scaffold. Materials science & engineering C, Biomimetic materials, sensors and systems. 2010;30(7):975-80.
15.   Ma PX. Tissue Engineering. In: Kroschwitz JI, editor. Encyclopedia of Polymer Science and Technology. 3 ed. Hoboken NJ: John Wiley & Sons, Inc.; 2005. p. 261-91.
16.   Ma P, Zhang R. Synthetic nano-scale fibrous extracellular matrix. Journal of biomedical materials research. 1999;46(1):60-72.
17.   Liu X, Ma P. Phase separation, pore structure, and properties of nanofibrous gelatin scaffolds. Biomaterials. 2009;30(25):4094-103.
18.   Hu J, Feng K, Liu X, Ma P. Chondrogenic and osteogenic differentiations of human bone marrow-derived mesenchymal stem cells on a nanofibrous scaffold with designed pore network. Biomaterials. 2009;30(28):5061-7.
19.   Wei G, Ma P. Partially nanofibrous architecture of 3D tissue engineering scaffolds. Biomaterials. 2009;30(32):6426-34.
20.   Wei GB, Ma PX. Nanostructured Biomaterials for Regeneration. Adv Funct Mater. 2008;18(22):3568-82.

21. Smith LA, Liu XH, Hu JA, Ma PX. The Enhancement of human embryonic stem cell osteogenic differentiation with nano-fibrous scaffolding. Biomaterials. 2010;31(21):5526-35.

22. Smith L, Liu X, Hu J, Wang P, Ma P. Enhancing Osteogenic Differentiation of Mouse Embryonic Stem Cells by Nanofibers. Tissue Engineering: Part A. 2009;15(7):1855-64.

23. Wang J, Liu X, Jin X, Ma H, Hu J, Ni L, et al. The odontogenic differentiation of human dental pulp stem cells on nanofibrous poly(L-lactic acid) scaffolds in vitro and in vivo. Acta Biomaterialia. 2010;6(10):3856-63.

24. Liu X, Smith L, Hu J, Ma P. Biomimetic nanofibrous gelatin/apatite composite scaffolds for bone tissue engineering. Biomaterials. 2009;30(12):2252-8.

25. Hu J, Smith LA, Feng K, Liu X, Sun H, Ma PX. Response of human embryonic stem cell-derived mesenchymal stem cells to osteogenic factors and architectures of materials during in vitro osteogenesis. Tissue Engineering: Part A. 2010;16(11):3507-14.

26. Smith L, Liu X, Hu J, Ma P. The influence of three-dimensional nanofibrous scaffolds on the osteogenic differentiation of embryonic stem cells. Biomaterials. 2009;30(13):2516-22.

27. Sun H, Feng K, Hu J, Soker S, Atala A, Ma P. Osteogenic differentiation of human amniotic fluid-derived stem cells induced by bone morphogenetic protein-7 and enhanced by nanofibrous scaffolds. Biomaterials. 2010;31(6):1133-9.

28. Li W, Tuli R, Huang X, Laquerriere P, Tuan R. Multilineage differentiation of human mesenchymal stem cells in a three-dimensional nanofibrous scaffold. Biomaterials. 2005;26(25):5158-66.

29. Nur-E-Kamal A, Ahmed I, Kamal J, Schindler M, Meiners S. Three-dimensional nanofibrillar surfaces promote self-renewal in mouse embryonic stem cells. Stem cells. 2006;24(2):426-33.

30. Woo KM, Chen VJ, Ma PX. Nano-fibrous scaffolding architecture selectively enhances protein adsorption contributing to cell attachment. J Biomed Mater Res Part A. 2003;67A(2):531-7.

31. Woo K, Jun J, Chen V, Seo J, Baek J, Ryoo H, et al. Nano-fibrous scaffolding promotes osteoblast differentiation and biomineralization. Biomaterials. 2007;28(2):335-43.

32. Hu J, Liu X, Ma P. Induction of osteoblast differentiation phenotype on poly(L-lactic acid) nanofibrous matrix. Biomaterials. 2008;29(28):3815-21.

33. Woo K, Chen V, Jung H, Kim T, Shin H, Baek J, et al. Comparative Evaluation of Nanofibrous Scaffolding for Bone Regeneration in Critical-Size Calvarial Defects. Tissue Engineering: Part A. 2009;15(8):2155-62.

34. Brown S, Tong W, Krebsbach P. The Derivation of Mesenchymal Stem Cells from Human Embryonic Stem Cells. Cells tissues organs. 2009;189(1-4):256-60.

35. De Coppi P, Bartsch G, Siddiqui MM, Xu T, Santos CC, Perin L, et al. Isolation of amniotic stem cell lines with potential for therapy. Nat Biotechnol. [Article]. 2007 Jan;25(1):100-6.

36. Woo K, Seo J, Zhang R, Ma P. Suppression of apoptosis by enhanced protein adsorption on polymer/hydroxyapatite composite scaffolds. Biomaterials. 2007;28(16):2622-30.

37. Wei GB, Ma PX. Macroporous and nanofibrous polymer scaffolds and polymer/bone-like apatite composite scaffolds generated by sugar spheres. J Biomed Mater Res Part A. [Article]. 2006 Aug;78A(2):306-15.

38. Zhang R, Ma P. Poly(alpha-hydroxyl acids) hydroxyapatite porous composites for bone-tissue engineering. I. Preparation and morphology. Journal of biomedical materials research. 1999;44(4):446-55.

39. Venugopal J, Prabhakaran M, Zhang Y, Low S, Choon A, Ramakrishna S. Biomimetic hydroxyapatite-containing composite nanofibrous substrates for bone tissue engineering. Philosophical transactions - Royal Society Mathematical, Physical and engineering sciences. 2010;368(1917):2065-81.

40. Girdler N. Repair of articular defects with autologous mandibular condylar cartilage. Journal of bone and joint surgery British volume. 1993;75(5):710-4.

41. Wachsmuth L, Soder S, Fan Z, Finger F, Aigner T. Immunolocalization of matrix proteins in different human cartilage subtypes. Histology and histopathology. 2006;21(4-6):477-85.

42. Salinas CN, Anseth KS. The enhancement of chondrogenic differentiation of human mesenchymal stem cells by enzymatically regulated RGD functionalities. Biomaterials. 2008;29(15):2370-7.
43. Chen VJ, Smith LA, Ma PX. Bone regeneration on computer-designed nano-fibrous scaffolds. Biomaterials. 2006;27(21):3973-9.
44. Wang P, Hu J, Ma PX. The engineering of patient-specific, anatomically shaped, digits. Biomaterials. 2009;30(14):2735-40.
45. Krishnamurthy R, Manning M. The stability factor: Importance in formulation development. Current pharmaceutical biotechnology. 2002;3(4):361-71.
46. Lin C, Anseth K. PEG Hydrogels for the Controlled Release of Biomolecules in Regenerative Medicine. Pharmaceutical research. 2009;26(3):631-43.
47. Elisseeff J, McIntosh W, Fu K, Blunk T, Langer R. Controlled-release of IGF-I and TGF-β1 in a photopolymerizing hydrogel for cartilage tissue engineering. Journal of Orthopaedic Research. 2001;19(6):1098-104.
48. Jin Q, Wei G, Lin Z, Sugai J, Lynch S, Ma P. Nanofibrous Scaffolds Incorporating PDGF-BB Microspheres Induce Chemokine Expression and Tissue Neogenesis In Vivo. PloS one. 2008;3(3):e1729.

CHAPTER 3

SCAFFOLD PORE SIZE CONTROLS CHONDROGENESIS OF HUMAN MESENCHYMAL STEM CELLS ON NANOFIBROUS, POROUS PLLA SCAFFOLD

ABSTRACT

Proper scaffold design is of great importance to guide chondrocytes and their progenitors to reconstruct both the morphology and function of reparative cartilage tissue. Previously, we demonstrated that poly-L-lactide (PLLA) two-dimensional nanofibrous (NF) matrices promoted human bone marrow-derived mesenchymal stem cell (hMSC) commitment along the chondrogenic route, compared to non-NF matrices. While porosity and pore size of scaffolds are receiving increasing attention, the existing scaffolds fabricated using various techniques are not standardized and their pore shape and size are not well defined, lacking comparability between them. It remains unclear how pore size independently affects chondrogenic differentiation of stem cells in a scaffold. In this study, we compare the chondrogenic differentiation of hMSCs on three-dimensional NF PLLA scaffolds with small pore size (125-250 μm) or large pore size (425-600 μm) both *in vitro* and *in vivo*. Small-pore scaffolds were better in supporting chondrogenic differentiation *in vitro* with TGF-β1 stimulation. This was shown by higher marker gene expression levels at 2 wk and cartilage-specific extra-cellular matrix deposition at 2 and 4 wk. Following 4 wk chondrogenic culture and 8 wk subcutaneous implantation in nude mice,

small-pore scaffolds supported avascular cartilage formation, but large-pore scaffolds contained only fibrous tissue. Therefore, small-pore scaffolds enhanced chondrogenic differentiation *in vitro* and cartilage formation *in vivo* compared to large-pore scaffolds. This study provides a strategy to control the cartilage regeneration process with designed pore architecture of porous NF scaffolds.

INTRODUCTION

The regenerative capacity of damaged or osteoarthritic articular cartilage is limited due to the avascularity of cartilage and low mitotic activity of chondrocytes (1). Unlike chondrocytes, bone-marrow derived mesenchymal stem cells (MSCs) are a suitable cell source for cartilage regeneration because a large number of cells can easily be isolated from a patient's bone marrow. Furthermore, MSCs can quickly proliferate and undergo chondrogenic differentiation for robust cartilage tissue formation.

Chondrogenesis of MSCs is a complex, highly controlled developmental process involving four important steps: mesenchymal condensation, chondrogenic commitment, differentiation into chondrocytes, and secretion of cartilaginous ECM. Mesenchymal condensation is the aggregation of pre-cartilage MSCs, mediated by cell-cell interactions, cell-matrix interactions, and several intracellular signaling pathways. It is the integral step that initiates the cartilage development process and must be controlled using advanced technology to use MSCs to regenerate functional cartilage.

Tissue engineering techniques show great promise in regenerating damaged cartilage tissue. These techniques require proper scaffold design to guide chondrocytes and their progenitors to reconstruct both the morphology and function of reparative cartilage tissue (2). Hydrogels are one category of common scaffold materials used in cartilage tissue engineering (3-6). For example, a photopolymerizing hydrogel system was used to encapsulate chondrocytes and revealed extra-cellular matrix (ECM) deposition with collagen and proteoglycan contents that increased with time of *in vitro* culture (7). However, hydrogels are typically unable to mimic the multi-scale architectural structure required for cartilage formation and achieve poor osteochondral integration when implanted (8). Porous synthetic polymer scaffolds, on the other hand, were reported to allow proper integration with subchondral bone tissue (9, 10). Importantly, the high processability of porous polymer scaffolds allows architectural features to be designed on the nano- to macro- scales that can be tailored to enhance tissue regeneration (11). Both the nano- and macro- scales are important because chondrogenic differentiation of chondrocytes and stem cells is promoted by the interaction with nanofibrous (NF) architecture (12, 13) and affected by the macro-pore size of the scaffold (14-19). However, the existing scaffolds fabricated using various techniques are not standardized and do not have well-defined pore shape and pore size, or do not have the desired ECM-mimicking features.

The electrospun fibrous scaffolds have been used for cartilage regeneration. However, the issue with electrospinning is that the two variables of fiber size and pore size cannot be independently controlled. Pore size is increased by increasing fiber diameter, often from nano- to micro-fibers.

31

Thus, it remains unclear how pore size independently affects chondrogenic differentiation.

To solve this issue, NF polymer scaffolds can be fabricated using a thermally-induced

phase-separation (TIPS) technique instead of electrospinning. To generate macro-pores in a 3D

NF scaffold, the polymer can be cast onto an interconnected porogen template consisting of

heat-treated sugar spheres, prior to TIPS for NF formation (20). The diameter of the sugar

spheres can then control the scaffold pore size. Following sugar leaching, the resulting scaffold is

highly uniform with interconnected spherical pore structure of desired pore size, unlike the

irregular pore geometry commonly obtained through salt leaching. In addition, the pore walls

uniformly consist of phase-separated nanofibers, which by themselves can promote

chondrogenic differentiation of human mesenchymal stem cells (hMSCs) (12). Therefore, our

high-porosity, phase-separated NF polymer scaffold with highly uniform, spherical pore

structure is a good model to examine the effect of pore size on cartilage formation. In this study,

we compare the chondrogenic differentiation of hMSCs on 3D NF scaffolds with two distinct

pore sizes both *in vitro* and *in vivo* in a mouse subcutaneous implantation model.

MATERIALS AND METHODS

Fabrication of NF PLLA scaffolds with different pore sizeS

Fabrication of 3D NF scaffolds has been described in detail previously (20). Briefly, 10%

PLLA/tetrahydrofuran (THF) solution was cast into an assembled sugar template (formed from

bound sugar spheres, 125–250 µm or 425–600 µm in diameter respectively) under mild vacuum.

The polymer-sugar composite was phase separated at -20°C overnight and then immersed into

cyclohexane to exchange THF for 2 d. The composites were then freeze-dried, and the sugar

spheres were leached out in distilled water and freeze-dried again to obtain highly porous

scaffolds. Scaffolds were cut into circular disks with dimensions of 3.6 mm in diameter and 1

mm in thickness. For cell culture study, the scaffolds were sterilized with ethylene oxide.

Characterization of scaffolds

The scaffolds were sputter-coated with gold and observed under a scanning electron microscope

(Philips XL30 FEG) at 10 kV. The quantification of interconnection opening size and ratio was

according to a previous report (20) based on scanning electron microscopy (SEM) micrographs

and using ImageJ software (NIH, Bethesda, MD). At least 10 pores for each type of scaffold

were selected for analysis.

Cell seeding and culture on scaffolds

Human bone marrow-derived mesenchymal stem cells (hMSCs) were obtained from Lonza

Walkersville, Inc. (Walkersville, MD). The cells were cultured according to the manual provided

by the supplier. Scaffolds were soaked in 70% ethanol for 30 min, washed three times with PBS

for 30 min each, and twice in Lonza's MSC Growth Medium for 2 hr each on an orbital shaker at

75 rpm. 2.5×10^5 cells were seeded onto each scaffold (3.6 mm in diameter and 1 mm in

thickness). After 2 hr of initial seeding, cell-seeded scaffolds were further cultured for 22 hr

under static condition to enhance cell adhesion on scaffolds. To induce chondrogenesis,

cell-seeded scaffolds were transferred to 15 ml polypropylene culture tubes and maintained in

0.5 mL chondrogenic medium (DMEM, 1% insulin-transferrin-selenium, 100µg/ml sodium

pyruvate, 40µg/ml proline, 10^{-7} M dexamethasone, 50µg/ml ascorbic acid) supplemented with 10

ng/ml TGF-β1 (Peprotech, Rocky Hill, NJ). The medium was changed twice a week.

Immunofluorescent staining of constructs

After 24h, constructs were washed in PBS and fixed in 4% formaldehyde for 1 hour. Cell

membranes were then permeabilized in 0.1% Triton-X for 5 mins. After washing in PBS 3x, the

actin cytoskeleton was stained using Alexa-Fluor® 555 phalloidin (Life Technologies #A34055)

at a 1:35 dilution in 1% bovine serum albumin as specified by the manufacturer. Constructs were

mounted on slides in mounting media containing DAPI (Vector Laboratories, Burlingame, CA)

to stain nuclei and observed using confocal microscopy (Nikon Eclipse C1).

Quantification of total DNA amount

After 24 hr of initial seeding and culture, the constructs were washed with PBS for 5 min,

homogenized with a Tissue-Tearor (BioSpec Products, Inc., Bartlesville, OK), and the DNA

content was determined with the DNA Quantification Fluorescence Assay Kit from Sigma (St.

Louis, MO).

Gene expression analysis

Samples were homogenized with a Tissue-Tearor. Total RNA was isolated using RNeasy Mini

Kit (Qiagen, Valencia, CA) according to the manufacturer's protocol. The cDNA was

reverse-transcribed with TaqMan reverse transcription reagents (Applied Biosystems, Foster City,

CA).

Real time PCR was carried out with at least 3 samples per group using TaqMan Universal PCR

Master Mix (Applied Biosystems) and pre-designed primers and probes (Applied Biosystems) for collagen type I (Hs00164004_m1), collagen type II (Hs01064869_m1) on a ViiA 7 Real time PCR system (Applied Biosystems). The gene expression level was normalized against glyceraldehyde 3-phosphate dehydrogenase (GAPDH, Hs99999905_m1) expression.

Glycosaminoglycan (GAG) assay

GAG amount was quantified as previously published (21). Briefly, constructs were harvested after 2 wk and 4 wk of culture, washed with PBS, and digested with 100 μl papain solution (280 μg/mL in 50 mM sodium phosphate, pH 6.5, containing 5 mM *N*-acetyl cystein and 50 mM EDTA) for 24 hr at 65°C. GAG content was measured by reaction with dimethylmethylene blue. Optical density was determined at 525 nm and GAG content of each construct was calculated using shark chondroitin 4-sulfate as the standard.

Subcutaneous implantation

Following 4 wk of chondrogenic induction *in vitro* with 10 ng/ml TGF-β1, cell-scaffold constructs with small or large pore size were implanted subcutaneously into nude mice for 8 wk. Male nude mice that were 6-8 wk old (Charles River, Wilmington, MA) were used. Surgery was performed under general anesthesia by inhalation of isoflurane. To implant four constructs per mouse, two midsagittal incisions were made on the dorsa, and one subcutaneous pocket was created on each side of each incision. One cell-scaffold construct was implanted into each pocket at random. Four samples were implanted for each group (small or large pore size). Incisions were closed with suture clips. Following 8 wk implantation period, mice were euthanized and implants

35

harvested. These animal procedures were performed according to the protocol approved by the

Univeristy Committee on Use and Care of Animals (UCUCA) at the University of Michigan.

Histological analysis

Constructs were washed in PBS, fixed with 3.7% formaldehyde in PBS overnight, dehydrated

through a graded series of ethanol, embedded in paraffin, and sectioned at a thickness of 5 μm.

For histological analysis, sections were deparaffinized, rehydrated, and stained with H&E, Alcian

blue or Safranin-O. For immunohistochemical staining, rehydrated sections were pre-treated with

pepsin solution for 15 min, incubated with Collagen type II antibody (Thermo Fisher Scientific

Inc., Fremont, CA) at a 1:100 dilution for 1 hr and detected by a Cell & Tissue Staining Kit

(R&D systems Inc., Minneapolis, MN) according to the manual. All sections were counterstained

with hematoxylin.

Statistical analysis

For cell culture studies, numerical values were reported as mean ± standard deviation ($n = 3$). To

test the significance of observed differences between the study groups, the Student's *t*-test was

applied. A value of $p < 0.05$ was considered to be statistically significant.

RESULTS

Two types of scaffolds with a pore size of 125-250 μm or 425-600 μm were fabricated

(**Fig.3.1A-E**). Both of the scaffolds have similar NF matrix structures except the different pore

sizes. After 24 hr of initial seeding and culture, the cells formed aggregates inside the small-pore

and large-pore scaffolds (**Figs.3.2A-B**). The size of aggregates was confined by the pore size

with fewer cells in the aggregates within small pores compared to large pores. There was no significant difference in total DNA amount after 24 hr of cell seeding, showing comparable seeding efficiency on small- and large-pore scaffolds (**Fig. 3.2C**).

GAG content was quantified for constructs cultured for 2 wk and 4 wk. A much higher amount of GAG was secreted by cells cultured on small-pore scaffolds than cells cultured on large-pore scaffolds during the two culture periods. Although, GAG deposition into scaffolds increased with time for both pore sizes (**Fig. 3.3A**). Total RNA was extracted from constructs and subjected to gene expression analysis. Collagen type II gene expression level was substantially higher for small-pore constructs than large-pore constructs (**Fig. 3.3B**); conversely, collagen type I gene expression level was lower in small-pore constructs than large-pore constructs (**Fig. 3.3C**). After 4 wk of culture, the constructs were subjected to histological analysis. The cells grew throughout both the small-pore scaffolds (**Fig.3.4A**) and large-pore scaffolds (**Fig. 3.4B**) during the culture period, shown by H-E stain. Consistent with GAG quantification data, denser GAG-containing ECM was deposited in small-pore scaffolds (**Fig. 3.4C**) compared to large-pore scaffolds (**Fig. 3.4D**), shown by Alcian blue staining. Immunohistological stain of Collagen type II further showed more Collagen type II was deposited into ECM by cells cultured in small-pore scaffolds (**Fig.3.4E**) compared to large-pore scaffolds (**Fig.3.4F**).

Following 4 wk in vitro chondrogenic culture and 8 wk mouse subcutaneous implantation, small-pore constructs supported cartilage formation with typical cartilage morphology (**Fig. 3.5A**). However, large-pore constructs succumbed to fibrous tissue invasion with obvious

hypercellularity (**Fig. 3.5B**). Furthermore, the cartilage tissue in the small-pore constructs were positively stained by Safranin-O for GAG (**Fig. 3.5C**), while large-pore constructs had negative Safranin-O staining (**Fig. 3.5D**). IHC staining of endothelial cell marker CD31 for blood vessel visualization showed that small pore implants were mostly avascular cartilage tissue (**Fig. 3.5E**), while large pore implants contained rich microvessels, indicative of fibrous tissue (**Fig. 3.5F**).

DISCUSSION

Chondrogenesis is a tightly controlled developmental process, involving multiple steps including condensation of MSCs, chondrogenic commitment, differentiation into chondrocytes, and secretion of cartilaginous ECM (22). Importantly, the phenotype of differentiated chondrocytes is dependent on the cell morphology. Chondrocytes often de-differentiate when cultured on a 2D surface as a monolayer and can re-differentiate to rounded cell morphology after pellet culture (23, 24), transwell culture (25), culture in 3D hydrogel (7), or culture on porous scaffolds (12, 26, 27). All of these chondrogenic culture models involve cell aggregation to mimic the mesenchymal condensation process. We hypothesized that the pore size of scaffolds can be used to control MSCs aggregation and subsequent chondrogenic commitment and differentiation processes. Our highly porous, well-interconnected scaffold served as a good model to study this effect of pore size. This study showed that the small pores (125-250 μm) promoted chondrogenesis *in vitro*, with higher marker gene expression levels, more GAG deposition, and more typical cartilage morphology. Following mouse subcutaneous implantation, small-pore scaffold enhanced cartilage formation with GAG matrix deposition. The cartilage formation also

served as a sufficient template for endochondral ossification in this ectopic model, allowing bone formation on the easily vascularized edges of the scaffolds. However, in the orthotopic model of cartilage defect repair, endochondral ossification would likely be prevented, resulting in stable cartilage formation. Due to poor *in vitro* cartilage formation and rigorous vascular invasion, large-pore construct contained only fibrous tissue following *in vivo* implantation.

In some studies, pore size effect could be attributed to varied cell seeding efficiencies because it was previously reported that the chondrogenic differentiation is related to cell densities (28). However, in the current study, the cell seeding efficiency was similar for small-pore and large-pore scaffolds, so the difference in extent of cartilage differentiation was not caused by different initial cell seeding densities. Rather, the cell aggregates were confined by the pore size, and the difference in cell aggregation may have led to the consequent difference in chondrogenic differentiation in this study.

It should also be noted that the small-pore and large-pore scaffolds additionally had different pore interconnection properties, with comparable interconnection opening to pore surface ratio (27.58 ± 7.38% for small-pore and 28.63 ± 8.27% for large-pore scaffolds, with no significance) but different interconnection opening size (55.7 ± 14.41 μm for small-pore scaffolds and 140.59 ± 26.60 μm for large-pore scaffolds, $p < 0.001$). The pore interconnection size may affect mass transfer such as diffusion of nutrient and waste and cell migration (29, 30). Limitation in mass transfer will cause limited cell growth inside the scaffolds. However, we did not find significant difference in cell distribution inside the different pore size scaffolds during the culture period

from the observation of histology results, showing that mass transfer is not a limiting factor in our study. This is likely because our phase-separated NF scaffold advantageously has greater than 95% porosity with well-interconnected pore structure, so as not to negatively affect cell seeding or mass transfer even in the small-pore scaffolds. Therefore, the difference in pore interconnectivity between the two different pore-sized scaffolds did not significantly affect chondrogenesis of hMSCs in this study.

Overall, this study showed that pore size can be used to control MSC aggregation and subsequent chondrogenic differentiation, providing a useful method for controlling the cartilage regeneration process and constructing functional cartilage tissues.

CONCLUSION

In this study, scaffold pore size was used to control the highly-regulated process of cartilage regeneration. A phase-separated nanofibrous, macro-porous PLLA scaffold provided a good model for this study due to: 1) a uniform, spherical, and well-interconnected pore structure, and 2) nanofibers that promote chondrogenic differentiation. Using this model, nanofibrous PLLA scaffolds with small pore size (125-250 µm) significantly enhanced chondrogenic differentiation of human MSCs and cartilage formation compared to a large pore size (425-600 µm) both *in vitro* and *in vivo*. Based on these positive results, we believe that tailoring the highly-designed pore architecture of nanofibrous polymer scaffolds may also improve the regeneration of many other tissues.

FIGURES
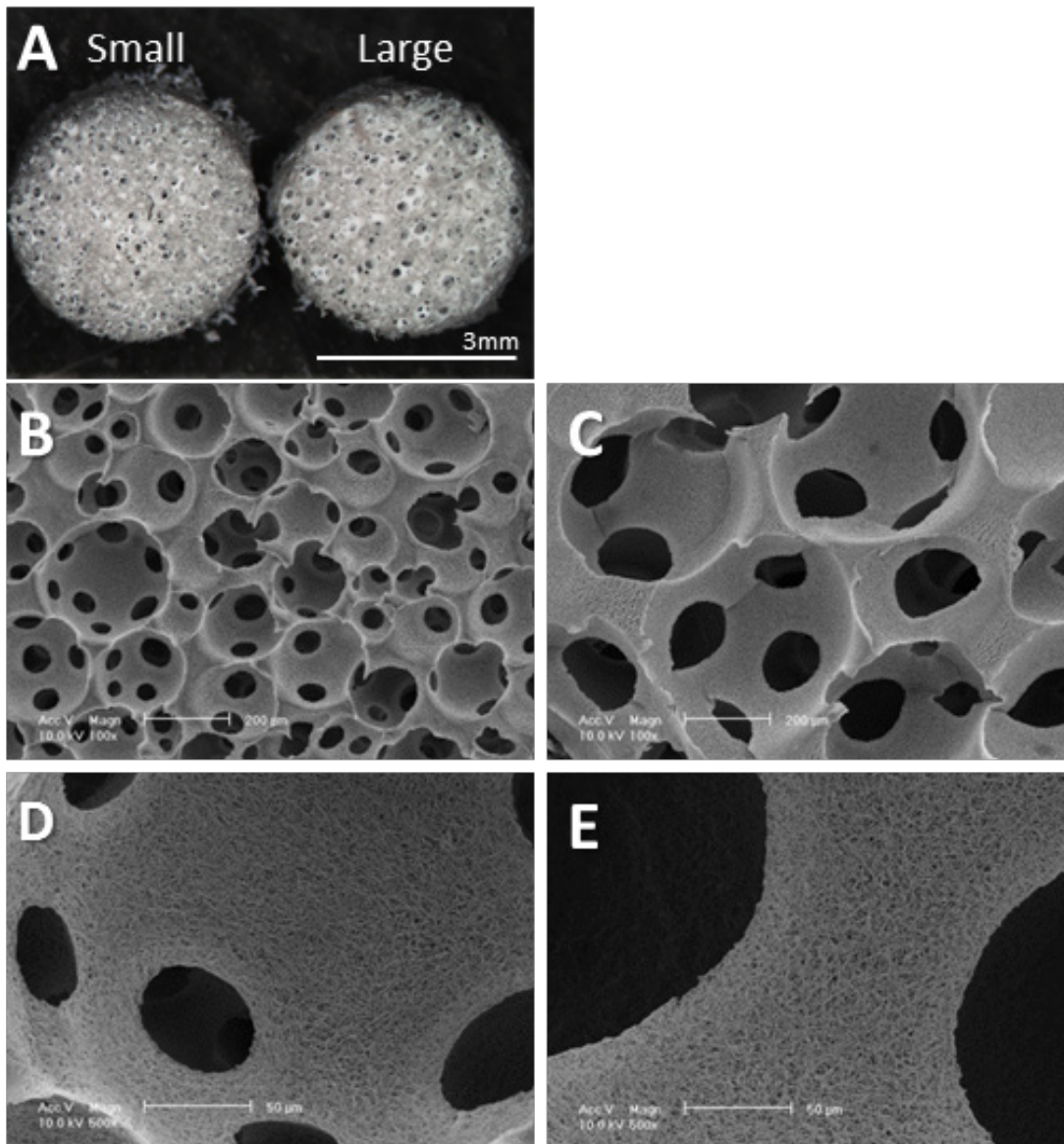
Figure 3.1 Morphologies of small (125-250 µm) and large (425-600 µm) pore scaffolds. A) Overall morphology. Scale bar: 3 mm. SEM micrographs of B) Small pore scaffold and C) large pore scaffold at low magnification, showing interconnected macro-pores; D) small pore scaffold and E) large pore scaffold at high magnification, showing identical nanofibrous structure of the pore walls.
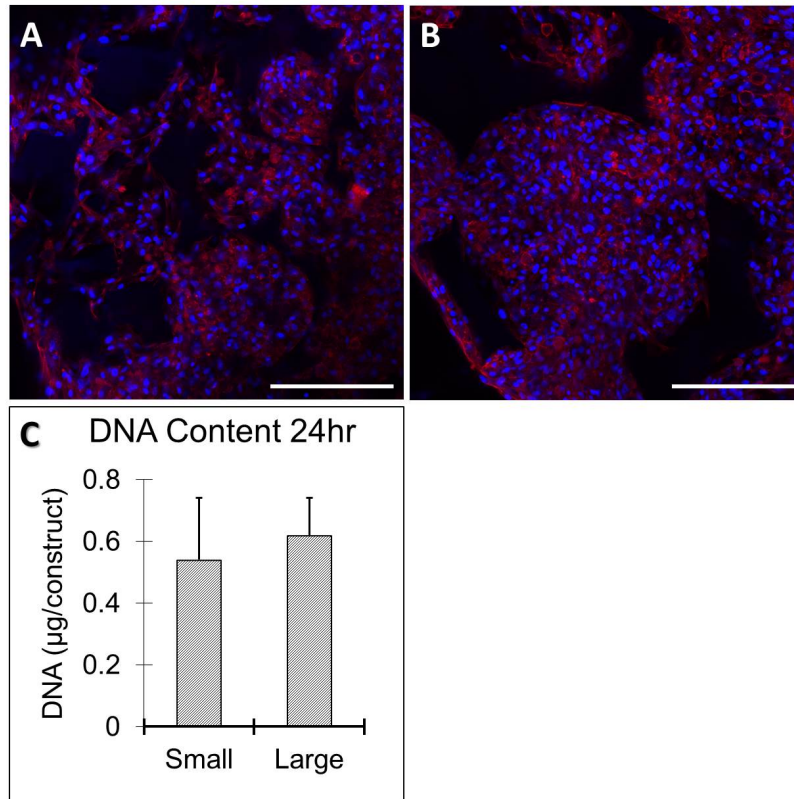
Figure 3.2 Human bone marrow-derived mesenchymal stem cells (hMSCs) adhered to and aggregated within A) small pore and B) large pore scaffold 24 hr after seeding, shown by immunofluorescent staining of F-actin (red) and nuclei (blue). There was no significant difference in cell seeding efficiency between small-pore and large-pore scaffolds (C), demonstrated by quantification of total DNA amount. Scale bar: 200 μm.
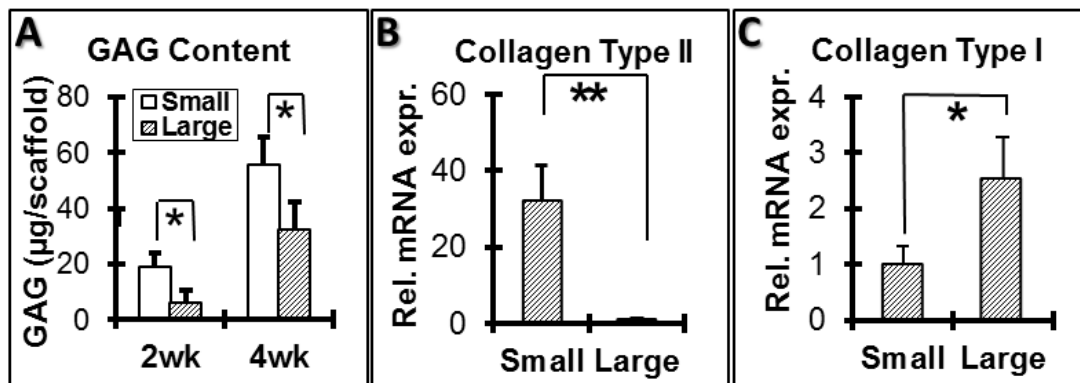
Figure 3.3 Glycosaminoglycan (GAG) quantification and gene expression of hMSCs seeded on small and large pore scaffolds during *in vitro* chondrogenic culture with 10 ng/ml TGF-β1. A) Small pore scaffolds had significantly higher GAG content per scaffold at 2 wk and 4 wk compared to large pore scaffolds. Small pore scaffolds also had B) significantly higher collagen type II gene expression and C) significantly lower collagen type I gene expression after 2 wk chondrogenic culture. *p< 0.05. **p<0.01.
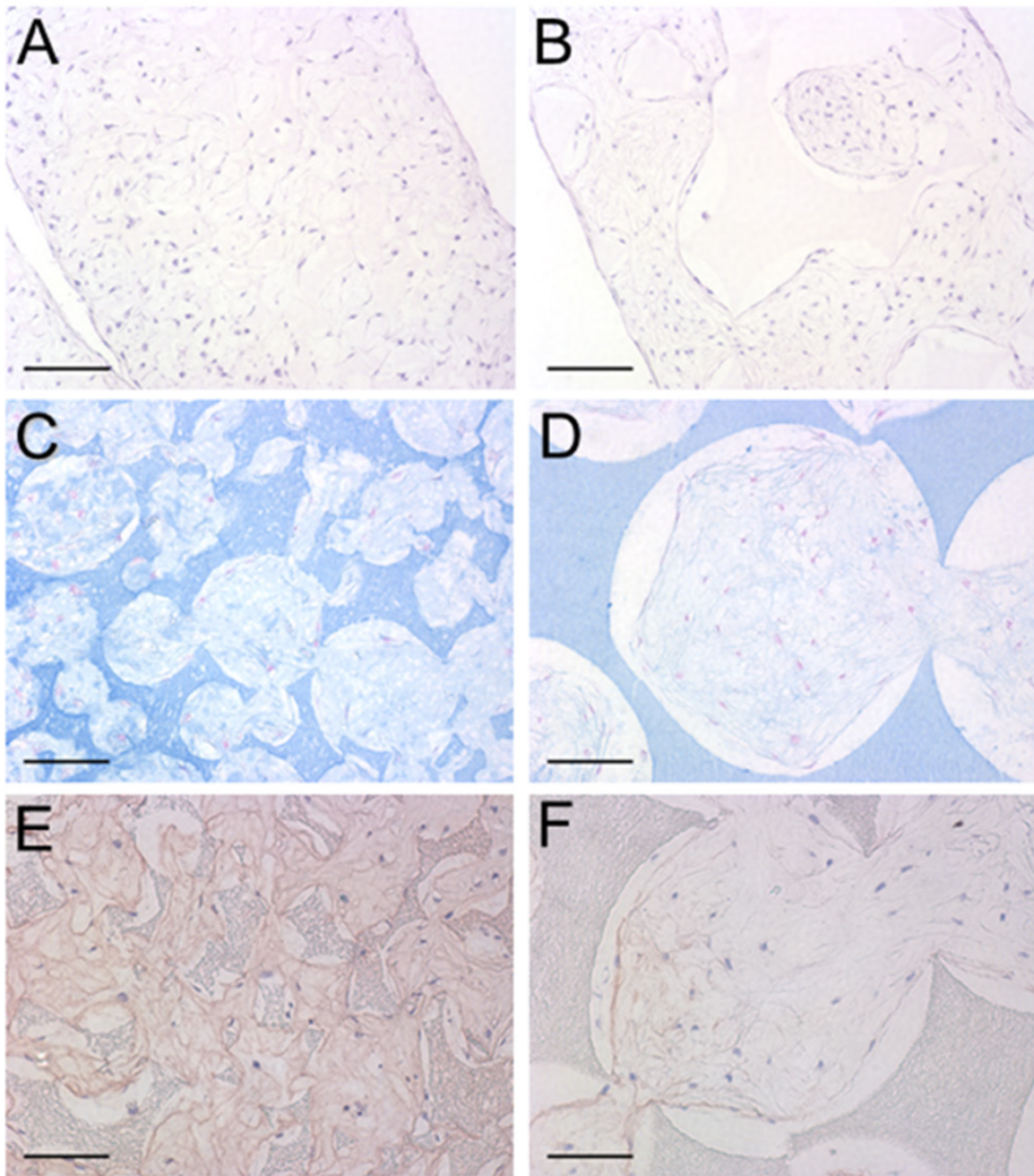
Figure 3.4 Histological analysis at 4 wk *in vitro* chondrogenic culture of hMSCs on small and large pore scaffolds. H&E staining showed the cells grew throughout the whole scaffolds both for A) small-pore and B) large-pore scaffolds. Scale bar: 200 µm. Alcian blue staining showed denser glycosaminoglycan matrix deposition in C) small pore scaffolds compared to D) large pore scaffolds. Similarly, collagen type II immunohistochemical staining revealed more collagen type II matrix deposition in E) small pore than in F) large pore scaffolds. Scale bar: 100 µm.
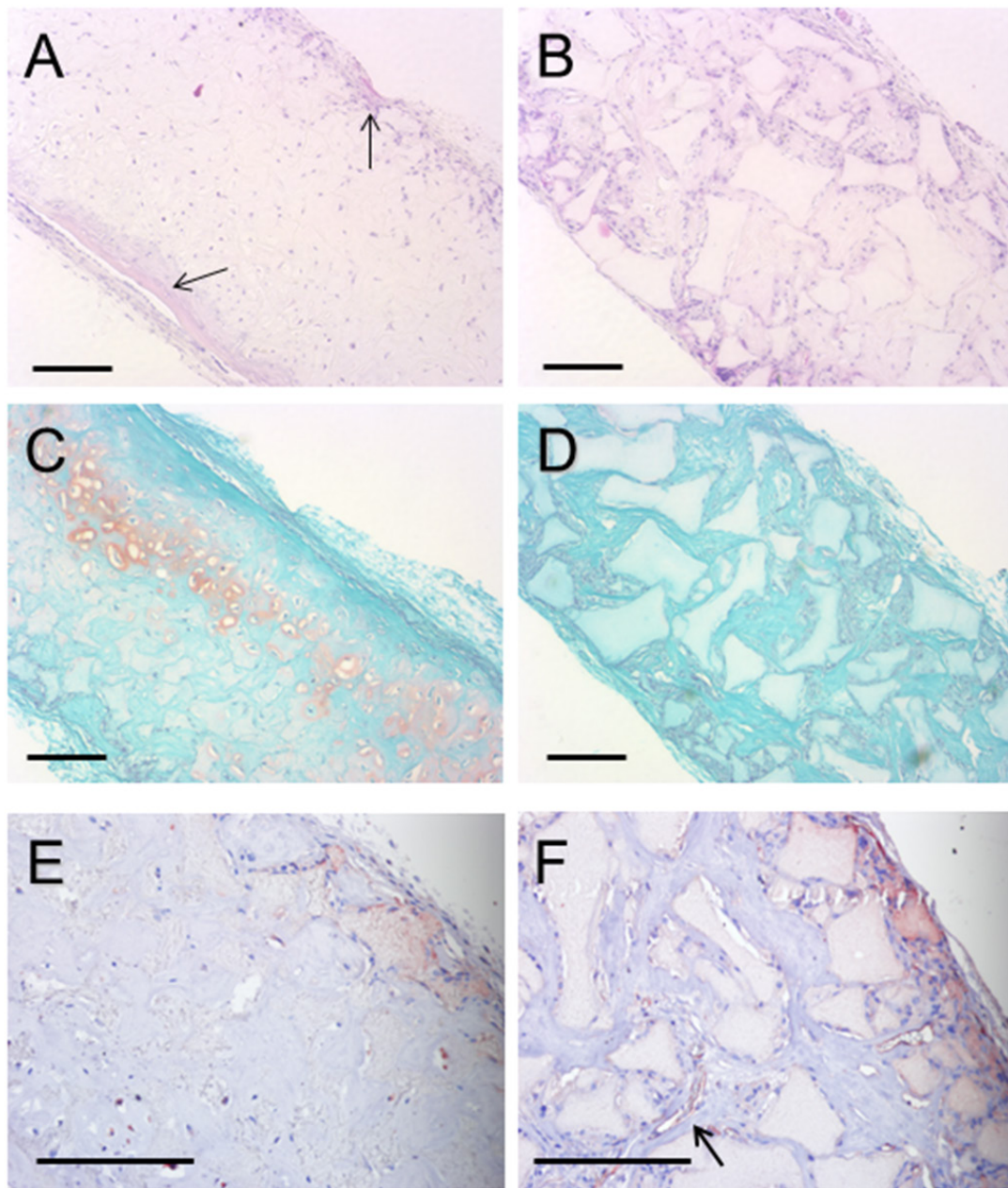
Figure 3.5 H&E, Safranin O, and CD31 staining following 4 wk *in vitro* chondrogenic culture and 8 wk subcutaneous implantation in nude mice. H&E staining revealed that A) small pore scaffold had typical cartilage morphology with moderate ectopic bone formation (arrows) on scaffold surface; B) large pore scaffold had fibrous tissue invasion and blood vessel ingrowth, preventing chondrogenic phenotype maintenance. C) Safranin O staining showed that small pore scaffold was positive for GAG-containing matrix, whereas D) large pore scaffold was negative. CD31 immunohistochemical staining for endothelial cells showed that E) small pore construct was mostly avascular but F) large pore scaffold contained rich microvessels (arrow indicates a typical microvessel). Scale bar: 200 μm.

REFERENCES

1. Mano JF, Reis RL. Osteochondral defects: present situation and tissue engineering approaches. Journal of Tissue Engineering and Regenerative Medicine. 2007 Jul-Aug;1(4):261-73.
2. Klein TJ, Malda J, Sah RL, Hutmacher DW. Tissue Engineering of Articular Cartilage with Biomimetic Zones. Tissue Engineering Part B-Reviews. 2009 Jun;15(2):143-57.
3. Bryant SJ, Anseth KS. Hydrogel properties influence ECM production by chondrocytes photoencapsulated in poly(ethylene glycol) hydrogels. Journal of Biomedical Materials Research. [Article]. 2002 Jan;59(1):63-72.
4. Kim M, Kim SE, Kang SS, Kim YH, Tae G. The use of de-differentiated chondrocytes delivered by a heparin-based hydrogel to regenerate cartilage in partial-thickness defects. Biomaterials. 2011;32(31):7883-96.
5. Park JS, Shim M-S, Shim SH, Yang HN, Jeon SY, Woo DG, et al. Chondrogenic potential of stem cells derived from amniotic fluid, adipose tissue, or bone marrow encapsulated in fibrin gels containing TGF-β3. Biomaterials. 2011;32(32):8139-49.
6. Toh WS, Lim TC, Kurisawa M, Spector M. Modulation of mesenchymal stem cell chondrogenesis in a tunable hyaluronic acid hydrogel microenvironment. Biomaterials. 2012;33(15):3835-45.
7. Elisseeff J, McIntosh W, Anseth K, Riley S, Ragan P, Langer R. Photoencapsulation of chondrocytes in poly(ethylene oxide)-based semi-interpenetrating networks. Journal of Biomedical Materials Research. 2000;51(2):164-71.
8. Wang DA, Varghese S, Sharma B, Strehin I, Fermanian S, Gorham J, et al. Multifunctional chondroitin sulphate for cartilage tissue-biomaterial integration. Nature Materials. 2007 May;6(5):385-92.
9. Emans PJ, Jansen EJ, van Iersel D, Welting TJ, Woodfield TB, Bulstra SK, et al. Tissue-engineered constructs: the effect of scaffold architecture in osteochondral repair. J Tissue Eng Regen Med. 2012 Mar 21.
10. Galperin A, Oldinski RA, Florczyk SJ, Bryers JD, Zhang M, Ratner BD. Integrated bi-layered scaffold for osteochondral tissue engineering. Adv Healthc Mater. 2013 Jun;2(6):872-83.
11. Ma PX. Biomimetic materials for tissue engineering. Advanced Drug Delivery Reviews. 2008 Jan 14;60(2):184-98.
12. Hu J, Feng K, Liu XH, Ma PX. Chondrogenic and osteogenic differentiations of human bone marrow-derived mesenchymal stem cells on a nanofibrous scaffold with designed pore network. Biomaterials. 2009;30(28):5061-7.
13. Shanmugasundaram S, Chaudhry H, Arinzeh TL. Microscale versus nanoscale scaffold architecture for mesenchymal stem cell chondrogenesis. Tissue Eng Part A. 2011 Mar;17(5-6):831-40.
14. Chia SL, Gorna K, Gogolewski S, Alini M. Biodegradable elastomeric polyurethane membranes as chondrocyte carriers for cartilage repair. Tissue Engineering.

2006;12(7):1945-53.

15. Griffon DJ, Sedighi MR, Schaeffer DV, Eurell JA, Johnson AL. Chitosan scaffolds: Interconnective pore size and cartilage engineering. Acta Biomaterialia. 2006;2(3):313-20.

16. Yamane S, Iwasaki N, Kasahara Y, Harada K, Majima T, Monde K, et al. Effect of pore size on in vitro cartilage formation using chitosan-based hyaluronic acid hybrid polymer fibers. Journal of Biomedical Materials Research Part A. 2007;81A(3):586-93.

17. Mukherjee DP, Smith DF, Rogers SH, Emmanual JE, Jadin KD, Hayes BK. Effect of 3D-Microstructure of Bioabsorbable PGA:TMC Scaffolds on the Growth of Chondrogenic Cells. Journal of Biomedical Materials Research Part B-Applied Biomaterials. 2009;88B(1):92-102.

18. Stenhamre H, Nannmark U, Lindahl A, Gatenholm P, Brittberg M. Influence of pore size on the redifferentiation potential of human articular chondrocytes in poly(urethane urea) scaffolds. J Tissue Eng Regen Med. 2011 Jul;5(7):578-88.

19. Jeong CG, Hollister SJ. Mechanical and biochemical assessments of three-dimensional poly(1,8-octanediol-co-citrate) scaffold pore shape and permeability effects on in vitro chondrogenesis using primary chondrocytes. Tissue Eng Part A. 2010 Dec;16(12):3759-68.

20. Wei GB, Ma PX. Macroporous and nanofibrous polymer scaffolds and polymer/bone-like apatite composite scaffolds generated by sugar spheres. Journal of Biomedical Materials Research Part A. 2006;78A(2):306-15.

21. Farndale RW, Sayers CA, Barrett AJ. A Direct Spectrophotometric Micro-Assay for Sulfated Glycosaminoglycans in Cartilage Cultures. Connective Tissue Research. 1982;9(4):247-8.

22. Goldring MB, Tsuchimochi K, Ijiri K. The control of chondrogenesis. Journal of Cellular Biochemistry. 2006 Jan 1;97(1):33-44.

23. Mackay AM, Beck SC, Murphy JM, Barry FP, Chichester CO, Pittenger MF. Chondrogenic differentiation of cultured human mesenchymal stem cells from marrow. Tissue Engineering. 1998;4(4):415-28.

24. Pittenger MF, Mackay AM, Beck SC, Jaiswal RK, Douglas R, Mosca JD, et al. Multilineage potential of adult human mesenchymal stem cells. Science. 1999 Apr 2;284(5411):143-7.

25. Murdoch AD, Grady LM, Ablett MP, Katopodi T, Meadows RS, Hardingham TE. Chondrogenic differentiation of human bone marrow stem cells in transwell cultures: Generation of Scaffold-free cartilage. Stem Cells. 2007 Nov;25(11):2786-96.

26. Freed LE, Marquis JC, Nohria A, Emmanual J, Mikos AG, Langer R. Neocartilage formation in vitro and in vivo using cells cultured on synthetic biodegradable polymers. J Biomed Mater Res. 1993 Jan;27(1):11-23.

27. Li WJ, Tuli R, Okafor C, Derfoul A, Danielson KG, Hall DJ, et al. A three-dimensional nanofibrous scaffold for cartilage tissue engineering using human mesenchymal stem cells. Biomaterials. 2005;26(6):599-609.

28. Vunjak-Novakovic G, Obradovic B, Martin I, Bursac PM, Langer R, Freed LE. Dynamic cell seeding of polymer scaffolds for cartilage tissue engineering. Biotechnology Progress. 1998 Mar-Apr;14(2):193-202.

29. Nam J, Huang Y, Agarwal S, Lannutti J. Improved cellular infiltration in electrospun fiber

via engineered porosity. Tissue Engineering. 2007;13:2249-57.

30. Baker BM, Gee AO, Metter RB, Nathan AS, Marklein RA, Burdick JA, et al. The potential to improve cell infiltration in composite fiber-aligned electrospun scaffolds by the selective removal of sacrificial fibers. Biomaterials. 2008;29(15):2348-58.

CHAPTER 4

SCAFFOLD PORE SIZE CONTROLS ENDOCHONDRAL OSSIFICATION IN VIVO

INTRODUCTION

Bone is a highly vascularized tissue comprised of a collagen type I-rich matrix that is mineralized with hydroxyapatite. During long bone development and bone healing, bone is formed via endochondral ossification. This process begins when chondrocytes (cartilage cells) from the periosteum (bone outer membrane) form collagen type II and proteoglycan-rich matrix cartilage template. Chondrocytes then become hypertrophic or enlarged, calcify the cartilage matrix, and then die due to nutrient limitations (1). Blood vessels can then invade the open, enlarged lacunae of the cartilage template, carrying osteoprogenitor cells that differentiate into osteoblasts and osteoclasts. Osteoclasts break down the calcified cartilage, allowing osteoblasts to secrete bone matrix of collagen type I. This bone matrix then calcifies, finally resulting in new bone tissue (2). However, this native bone healing process of endochondral ossification may not be sufficient to repair large critical-sized bone defects. Thus, a tissue-engineered bone graft that supports endochondral ossification could serve as solution for bone defect repair.

For bone tissue engineering, scaffolds play a pivotal role by serving as an artificial extracellular matrix (ECM) to support endochondral ossification (3). Importantly, scaffolds must exhibit an internal porous network because well-interconnected pores are critical for uniform cell distribution, cell migration, nutrient/waste diffusion, blood vessel ingrowth, and tissue ingrowth

into the scaffold, especially as scaffold thickness increases (4). Bone tissue-engineered scaffolds are often made of ceramic-like hydroxyapatite or β-tricalcium phosphate due to their osteoconductivity (5-7) similar to native bone minerals. However, ceramics are brittle, and incorporation of an internal porous network is difficult, resulting in a limited pore size and pore interconnection size (8-11). Therefore, instead of using ceramic scaffolds, biodegradable synthetic polymer scaffolds are actively employed for tissue engineering applications due to their high processability and easily tailored multi-scale design features, including a porous network (12, 13).

Porous polymer scaffolds have two critical pore design parameters: pore size and pore interconnection size. Pore size can control cell attachment, migration, and differentiation (14), and is therefore highly important for bone regeneration. In a seminal review, Karageorgiou and Kaplan establish that bone formation requires a pore size greater than 300 μm for capillary ingrowth (14). However, pore architecture varies greatly between scaffold systems. Porous scaffolds fabricated by salt leaching (15) or gas foaming (16) do have control over pore size but typically have non-uniform, irregularly-shaped pores with minimal pore interconnectivity, making them a poor model for investigating the effect of pore size or interconnection size on endochondral ossification. Due to the lack of control over pore interconnection size, research of interconnection size is limited (11, 17) and has not been systemically studied on polymer scaffolds to our knowledge. Advantageously, Wei et al. has shown that using a sugar porogen template followed by polymer/solvent casting can achieve uniform, spherical, well-interconnected pores with intricate control over both pore size and interconnection size (18). In addition, this pore fabrication method can be combined with thermally-induced phase separation to induce nanofiber formation. By mimicking the nano-structure of collagen of the native ECM

(19), the nanofibrous scaffold has previously been shown to enhance cell adhesion, proliferation, and differentiation of multiple stem cell types (20-26). Therefore, this macroporous, nanofibrous polymer scaffold may serve as a good model for investigating how scaffold pore size controls endochondral ossification.

In this study, we investigated four pore size ranges: 60-125μm, 125-250um, 250-425μm, and 425-600μm of nanofibrous PLLA scaffold. Scaffolds were seeded with rabbit bone marrow derived mesenchymal stem cells (BMSCs) because they are a plentiful, easily harvested cell source, and can differentiate into both chondrocytes and osteoblasts (27). We hypothesized that in a highly interconnected porous scaffold, a small pore size of 125-250μm, even less than 300 μm, could still promote capillary ingrowth for mature bone formation, while the very small pore size scaffold (60-125 μm) may prevent endochondral ossification for cartilage formation.

METHODS

Scaffold Fabrication

The nanofibrous PLLA scaffolds were prepared as previously described (18). Sugar spheres with different sizes were first prepared by an emulsion technique. Typically, 50 g of d-fructose were melted at 120°C for 90 min until clear yellowish liquid was obtained. The liquefied sugar was emulsified into 50 mL mineral oil with 1.3 mL Span 80 at 120°C under stirring. The resulting mixture was cooled down using an ice-bath to solidify sugar spheres. After discarding the mineral oil, the sugar spheres were washed with hexane three times and sieved to select desired sizes (60-125, 125–250, 250–425, and 425– 600 μm size ranges). The sieved sugar spheres were packed in a Teflon vial with hexane and heat treated at 37 °C for 30 min to achieve a highly

interconnected sugar sphere template. After bonding the sugar spheres, hexane was removed, and the sugar template was dried under vacuum.

Then, about 0.6–0.8 mL 10 % (w/v) PLLA/THF solution was cast into the assembled sugar template. Mild vacuum was applied during casting in order to fully fill the interspaces of the bonded sugar template with polymer solution. The polymer solution/sugar template was phase separated at -20 °C overnight and then immersed into cyclohexane to extract solvent (THF) for 2 days. The resulting composites were freeze-dried. The sugar template was then leached away in distilled water, and the porous nano-fibrous scaffold was freeze-dried.

Scanning Electron Microscope (SEM) Observation

Scaffolds were coated with gold for 120 s using a sputter coater (DeskII, Denton vacuum Inc) and observed using SEM (Philips XL30 FEG).

Bone Marrow Stem Cell Isolation and Culture

Bone marrow-derived mesenchymal stem cells (BMSCs) were obtained from the New Zealand White rabbits by aspiration of the femoral and tibial bone marrow using an 18-gauge syringe needle. A total of 10 ml of marrow was collected into 1000 U of heparin-containing maintenance media (high-glucose alpha-MEM (Gibco) containing 10% fetal bovine serum (FBS) (Gibco) and antibiotics (penicillin G, 100 U/ml; streptomycin, 0.1 mg/ml)). The marrow was washed with PBS once and fresh media twice, and centrifuged at 2000 rpm for 3 min after each wash. Rabbit BMSCs were collected and cultured in 60-cm^2 culture dishes in maintenance media at 37 C under 5% CO_2, changing media every 2-3 days. Cells were used at passage 3.

Cell Seeding on Scaffold

Scaffolds were soaked in 70% ethanol for 30 min, washed three times with PBS for 30 min each, and twice in alpha MEM with 10% fetal bovine serum for 30 min each. Scaffolds (5 mm in diameter and 1.5 mm in thickness) were seeded such that 200,000 cells were adhered onto each scaffold after 24h. After 2 hr of initial seeding, cell-seeded scaffolds were further cultured for 22 hr under static condition to enhance cell adhesion on scaffolds.

Subcutaneous Implantation

Cell-scaffold constructs with sample size of at least 3 were implanted subcutaneously into nude mice for 4 or 8 weeks. Male nude mice that were 6-8 wk old (Charles River, Wilmington, MA) were used. Surgery was performed under general anesthesia by inhalation of isoflurane with balanced oxygen. To implant four constructs per mouse, two midsagittal incisions were made on the dorsa, and one subcutaneous pocket was created on each side of each incision. One cell-scaffold construct was implanted into each pocket at random, and incisions were closed with suture clips. Following 4 or 8 wk implantation period, mice were euthanized with CO_2, and implants were harvested. These animal procedures were performed according to the protocol approved by the University Committee on Use and Care of Animals (UCUCA) at the University of Michigan.

MicroCT Analysis

Samples were embedded in 1% agarose and placed in a 14 mm diameter tube and scanned over the entire length of the scaffold using a microCT system (μCT100 Scanco Medical, Bassersdorf, Switzerland). Scan settings were: voxel size 12 μm, 70 kVp, 114 μA, 0.5 mm AL filter, and integration time 500 ms. Analysis was performed using the manufacturer's evaluation software,

and a fixed global threshold of 18% (180 on a grayscale of 0–1000) was used to segment bone from non-bone to in order to quantify bone volume and create 3D reconstructions.

Histological Analysis

Constructs were washed in PBS, fixed with 3.7% formaldehyde in PBS overnight, and decalcified in 10% EDTA (pH=7.4) for two weeks. Decalcified constructs were then dehydrated through a graded series of ethanol, embedded in paraffin, and sectioned at a thickness of 5 μm. For histological analysis, sections were deparaffinized, rehydrated, and stained with H&E. For immunohistochemical staining, rehydrated sections were heated to 99C for 10 min in citrate buffer for heat-induced antigen retrieval, blocked using the Cell & Tissue Staining Kit (R&D systems Inc., Minneapolis, MN) according to the manual. Slides were then incubated with CD31 antibody (Abcam) at a 1:50 dilution overnight, detected by the kit's AEC chromogen, and counterstained with hematoxylin.

Statistical Analysis

Analysis of bone volume results were performed using ANOVA followed by a post-hoc Tukey test in JMP Pro 11 (by SAS) with $p < 0.05$.

RESULTS

In this study, four scaffold pore size ranges (60-125, 125–250, 250–425, and 425–600 µm) were used to study the effect of pore size on endochondral ossification *in vivo*. Unlike most porous polymer scaffolds, the pores were highly uniform, spherical, and well-interconnected (**Figure 4.1**). Scaffolds of each pore size were seeded with rabbit BMSCs and implanted subcutaneously into nude mice to induce endochondral ossification in an ectopic model. Following 4w and 8w in vivo, bone volume of the construct were quantified using MicroCT. After 4w, bone volume increased with pore size, as expected, but the increase was not statistically significant. After 8w subcutaneous implantation, the large pore scaffold (425-600 µm) had significantly higher bone volume than the very small pore scaffold (60-125 µm), with a clear trend that bone volume increases with pore size (**Figure 4.2**).

MicroCT was also used to create 3D reconstruction of the 8w explanted constructs from the top and side cross-section views (**Figure 4.3**). From the top view, robust bone formation occurred on the outside of all four pore size scaffolds, as expected, because the edges of the scaffolds are easily vascularized in the subcutaneous space. Additionally, all constructs held their original, disc-like shape because cartilage tissue quickly filled the porous scaffold, providing enough mechanical integrity to withstand the force placed on the scaffold in vivo. From the side cross-sectional view of the constructs, the small, medium, and large pore scaffolds contained uniform bone formation throughout the entire cross section with bone porosity increasing with pore size. Interesting, the very small pore scaffold (60-125µm) did not accommodate bone formation throughout the entire cross-section but mainly only on the outer shell of the construct.

From histological analysis of 8w constructs with H&E staining (**Figure 4.4**), the very small pore scaffold contained cartilage tissue in the center of the scaffold with typical low cellularity and rounded hollow lacunae formation. The very small pore scaffold underwent endochondral ossification mainly on the easily-vascularized edges of the scaffold only (noting pink bone matrix), thus resulting in significantly less bone volume shown in **Figure 4.2**. The small and medium pore scaffolds contained a similar amount of bone formation on the pore walls, while the large pore scaffold had thicker layer bone matrix on the pore walls, though not significantly higher bone volume than small or medium pore scaffolds ($p>0.05$). Interestingly, the small, medium, and large pore scaffolds all contained bone marrow-like tissue within the pores surrounded by bone tissue, consisting of immune cells with darkly-stained nuclei, adipocytes (round, white spaces), and blood vessels filled with pink-stained red blood cells. Impressively, the well-interconnected, spherical pores maintained their structure even after 8w in vivo, allowing pore size to remain consistent throughout the entire study, which is often challenging for porous, polymer scaffolds.

Furthermore, in order to visualize the blood vessels within the constructs, CD31 in the endothelial layer of blood vessels was immunohistochemically stained red-brown in the 8w ectopic constructs (**Figure 4.5**). The cartilage in the very small pore scaffold remained avascular, while the blood vessel diameter increased along with pore size in the small, medium, and large pore scaffolds. The larger blood vessels in the large pore scaffold likely contributed to deposition of highest bone volume by carrying more oxygen, growth factors, other nutrients, and osteoprogenitor cells to enhance bone formation and endochondral ossification.

DISCUSSION

Endochondral ossification is the process by which a cartilaginous matrix is gradually replaced by bone and is important for both skeletal development and bone healing. To support bone healing and regeneration, scaffolds play an important role by serving as an artificial extracellular matrix when self-repair is limited. Porous polymer scaffolds have been widely studied for bone tissue engineering and must contain an internal porous network that is critical for uniform cell distribution, cell migration, nutrient/waste diffusion, blood vessel ingrowth, and tissue ingrowth.

One of the most important design parameters of porous polymer scaffolds is pore size. Most scaffold systems require a pore size of 300 µm in order to allow capillary invasion for bone formation. Impressively, this study showed that if the scaffold pores were well-interconnected, an even smaller pore size (125-250um) could still support mature bone formation. A pore size even less than 125 µm was required to prevent endochondral ossification and inhibit blood vessel ingrowth. Importantly, the very small pore scaffold (60-125µm) still facilitated cell penetration for cell seeding due the high pore interconnectivity, promoting cartilage formation in the center of the 1.5mm thick scaffold. Therefore, scaffold pore size can control the endochondral ossification process by promoting or preventing host vasculature invasion.

We believe that our porous, nanofibrous scaffold with uniform, spherical, highly interconnected pores provided a superior model for studying the effect of well-controlled pore size on endochondral ossification. Not only is the porous architecture advantageous, but the ECM-mimicking nanofibers may have enhanced adhesion, proliferation, and chondrogenic differentiation of BMSCs, which has been shown previously (21).

Importantly, unlike many previous studies, cell-seeded scaffolds were implanted subcutaneously into nude mice the next day for immediate interaction with host vasculature *without any in vitro induction* that may alter the pore architecture effect. This was possible because the early passage 3 rabbit BMSCs were highly proliferative and could form a good cartilage template in less than 3 weeks (data not shown), quickly laying the groundwork for successful endochondral ossification. Therefore, by using a combination of a superior scaffold and cells, robust, mature bone filled with bone-marrow like tissue without any in vitro pre-culture was formed after only 4 weeks of subcutaneous implantation, which is faster and more robust than most bone tissue-engineered material systems.

It is important to note that in the previous pore size study in chapter 3, there was in vitro chondrogenic induction prior to subcutaneous implantation, resulting in the different pore size effect from this study. In chapter 3, the small pore scaffold seeded with human BMSCs formed a strong, hard cartilage template after 4w in vitro, blocking blood vessel invasion in vivo and preventing endochondral ossification. Furthermore, in chapter 3, after 4w in vitro, the large pore scaffold contained a poor cartilage template that allowed blood vessel penetration but could not support endochondral ossification, resulting in fibrous tissue invasion. In contrast, in this study, the small and large pore scaffolds were not cultured in vitro first, allowing a good cartilage template to form in vivo from highly proliferative rabbit BMSCs. Blood vessels could then penetrate the cartilage template, resulting in successful endochondral ossification.

CONCLUSION

In a highly interconnected porous, nanofibrous PLLA scaffold seeded with rabbit BMSCs and implanted subcutaneously for 8 weeks, a small pore size of 125-250μm, even less than 300 μm, could still promote capillary ingrowth for mature bone formation, while the very small pore size

scaffold (60-125 µm) prevented endochondral ossification for cartilage formation. Furthermore, a large pore scaffold (425-600µm) supported the highest bone volume likely due to ingrowth of larger blood vessels through the larger pore network. Using this superior scaffolding model with uniform, spherical, highly interconnected pores, the effect of pore interconnection size on blood vessel ingrowth and ectopic endochondral ossification will be studied.

FIGURES WITH CAPTIONS
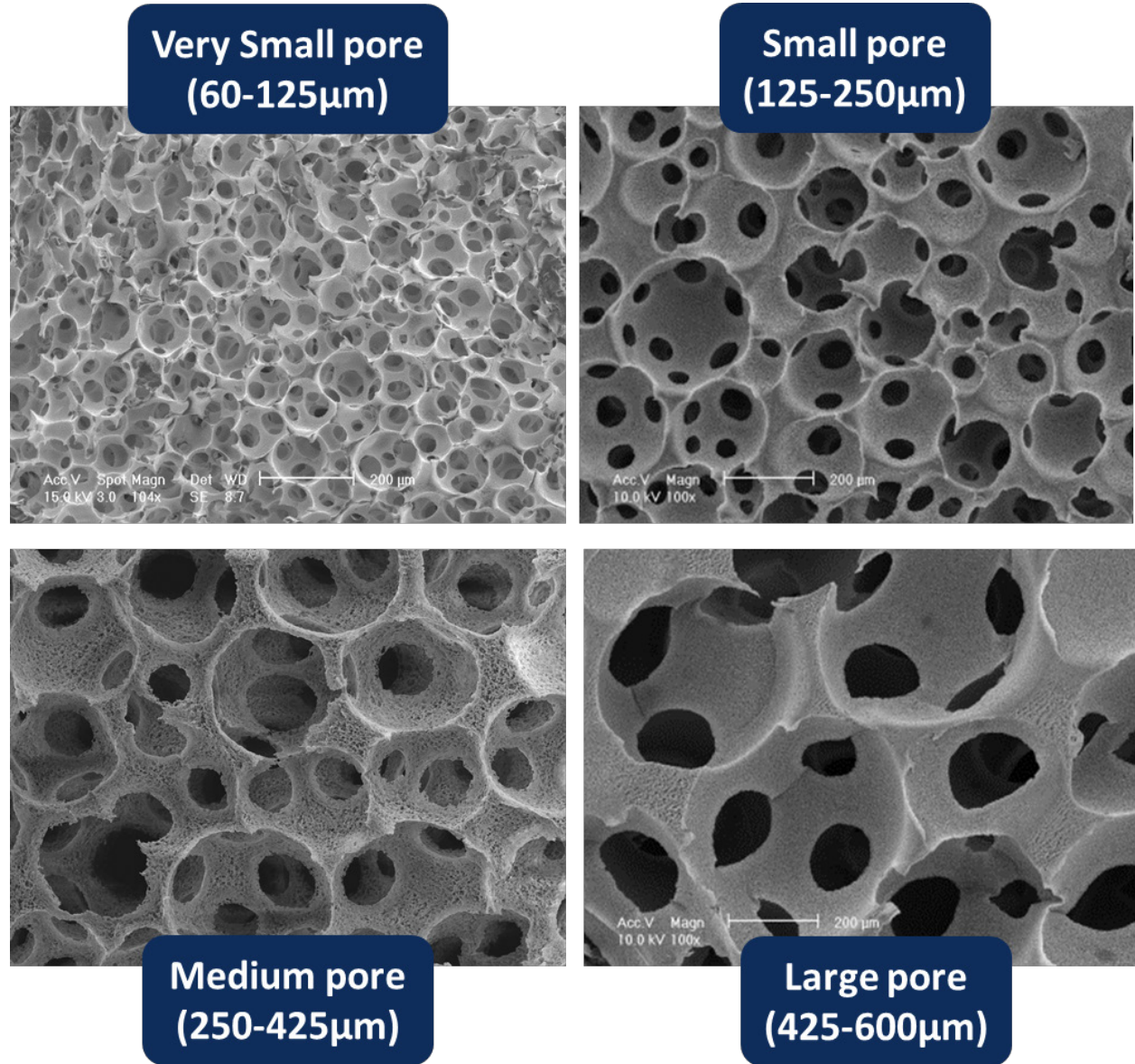
Figure 4.1 SEM Micrographs of nanofibrous PLLA scaffolds of four distinct pore size ranges with uniform, spherical, well-interconnected pores.
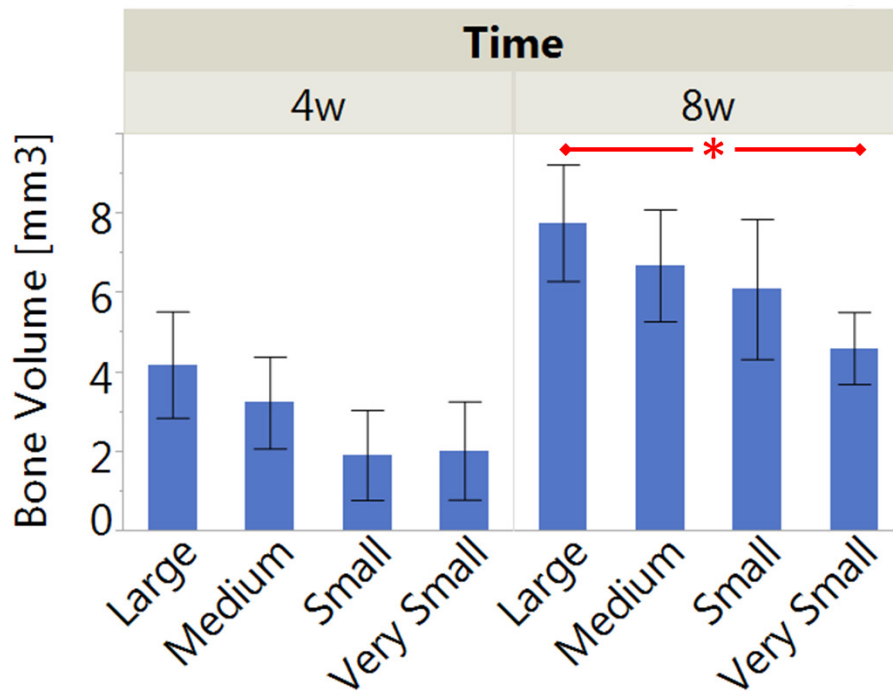
Figure 4.2 Bone volume quantification from MicroCT analysis after 4 or 8w subcutaneous implantation of large, medium, small, and very small pore size scaffolds. Small, medium, and large pore scaffolds supported robust bone formation after 8w. Very small scaffolds inhibited bone formation and had significantly less bone volume than large pore scaffold, *p<0.05.
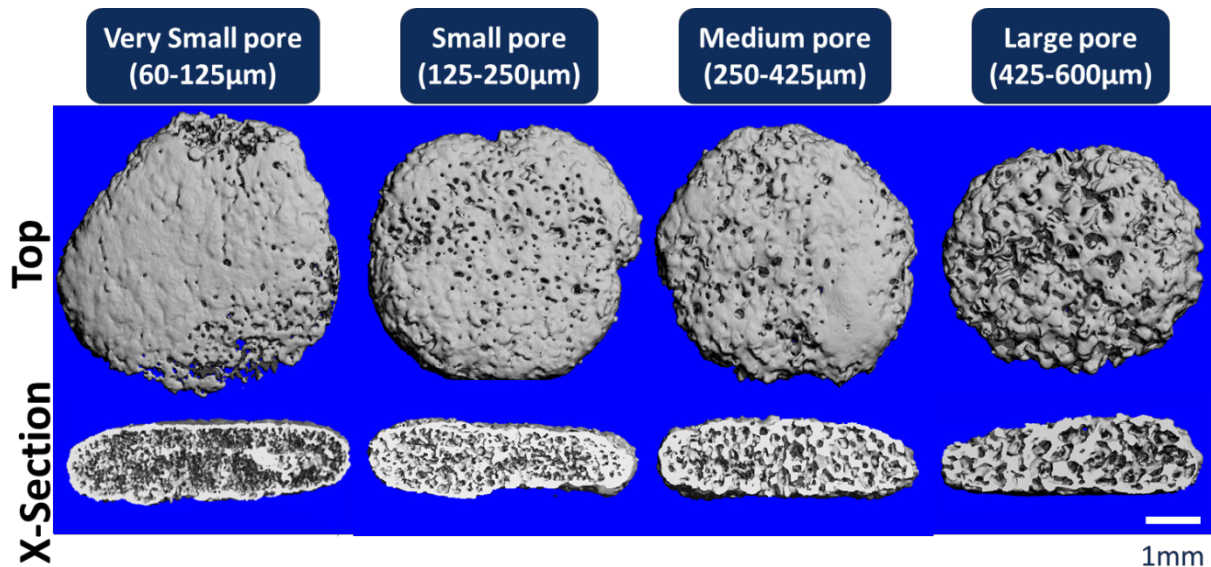
Figure 4.3. MicroCT 3D Reconstructions of four different pore size scaffolds after 8w mouse subcutaneous implantation from top view and side cross-section. Very small pore scaffold (60-125μm) exhibited bone formation mainly on the outer surface of the scaffold. Small, medium, and large pore scaffolds supported robust, uniform bone formation throughout cross section.
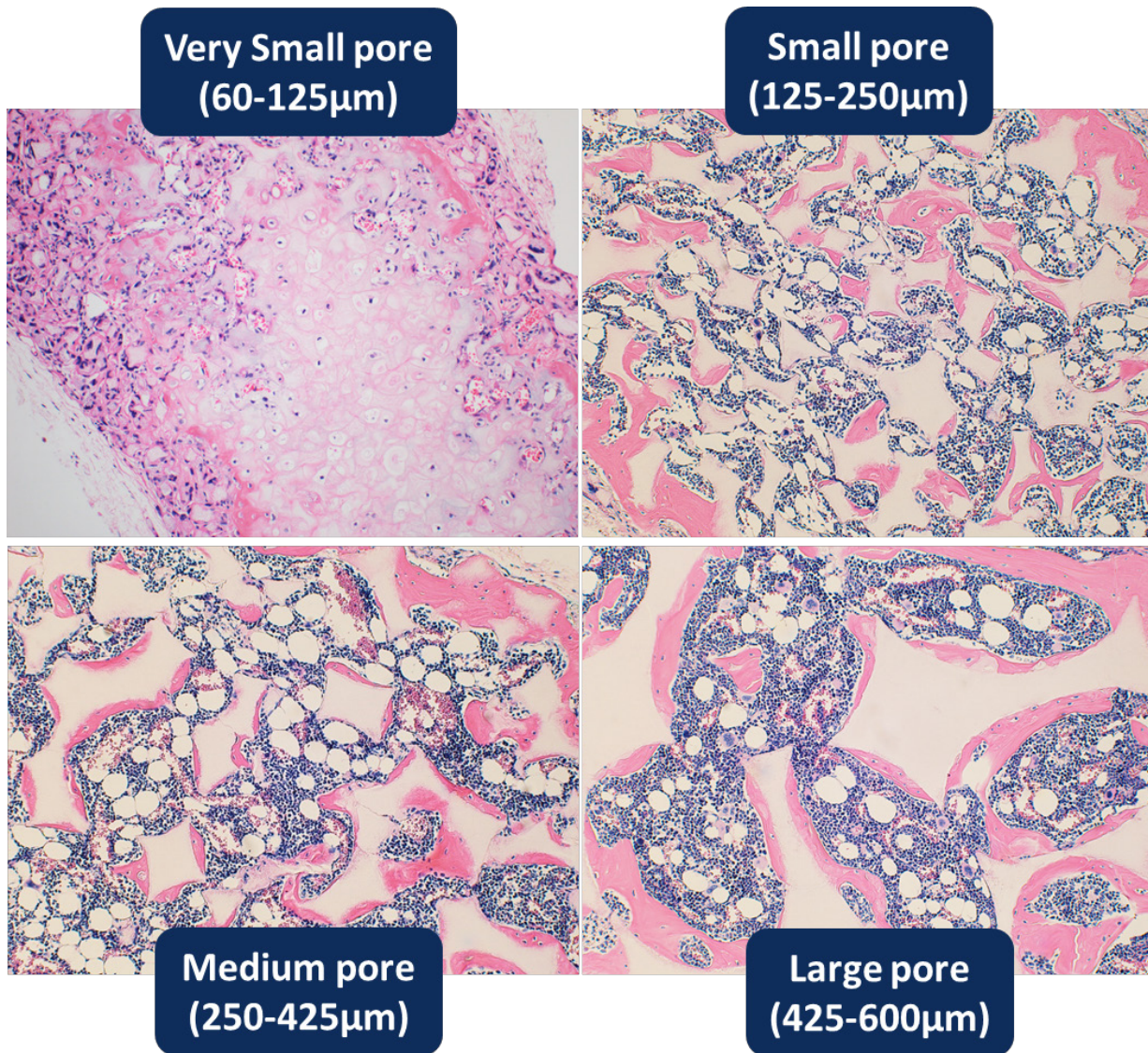
Figure 4.4 H&E histological analysis after 8w subcutaneous implantation at 100x magnification. Very small pore scaffold (60-125μm) contained cartilage with typical morphology in the center of the scaffold. Small, medium, and large pore scaffolds supported bone formation on pore walls, shown by pink staining of bone matrix, with bone marrow-like tissue within the pores.
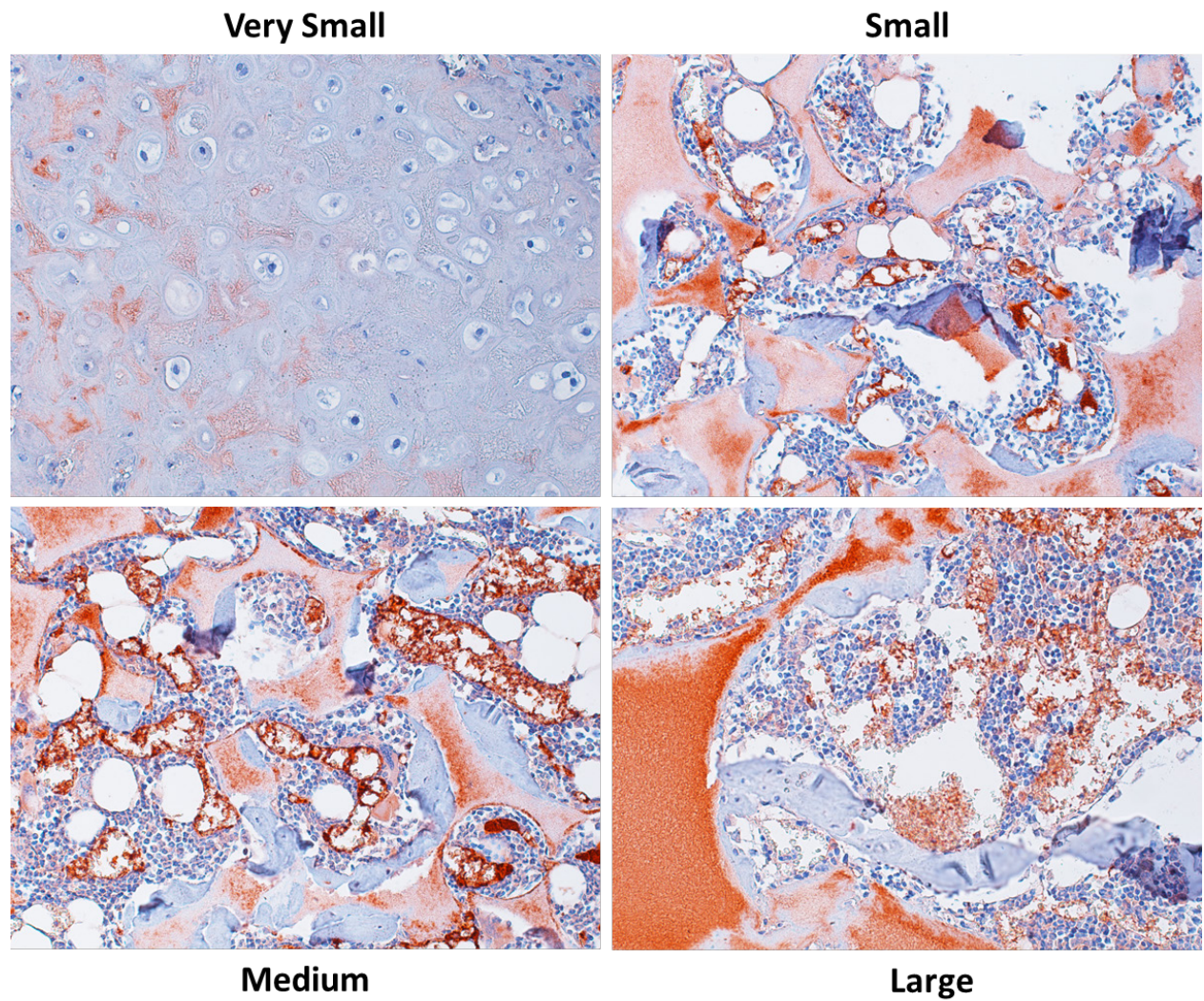
Figure 4.5 CD31 immunohistochemical staining of endothelial layer of blood cells at 200x magnification as red-brown. Cartilage in very small pore scaffold is avascular. Blood vessels within small, medium, and large pore scaffold increase in size within increasing pore size. Note that the scaffold also stains red due to the high surface area of the nanofibers.

REFERENCES

1.   Gerber HP, Vu TH, Ryan AM, Kowalski J, Werb Z, Ferrara N. VEGF couples hypertrophic cartilage remodeling, ossification and angiogenesis during endochondral bone formation. Nature Medicine. 1999 Jun;5(6):623-8.

2.   Mackie EJ, Ahmed YA, Tatarczuch L, Chen KS, Mirams M. Endochondral ossification: How cartilage is converted into bone in the developing skeleton. International Journal of Biochemistry & Cell Biology. 2008 2008;40(1):46-62.

3.   Langer R, Vacanti JP. Tissue Engineering. Science. 1993;260(5110):920-6.

4.   Ma PX. Biomimetic materials for tissue engineering. Advanced Drug Delivery Reviews. 2008;60(2):184-98.

5.   Boyde A, Corsi A, Quarto R, Cancedda R, Bianco P. Osteoconduction in large macroporous hydroxyapatite ceramic implants: Evidence for a complementary integration and disintegration mechanism. Bone. 1999 Jun;24(6):579-89.

6.   Dong JA, Uemura T, Shirasaki Y, Tateishi T. Promotion of bone formation using highly pure porous beta-TCP combined with bone marrow-derived osteoprogenitor cells. Biomaterials. 2002 Dec;23(23):4493-502.

7.   Gauthier O, Bouler JM, Aguado E, Pilet P, Daculsi G. Macroporous biphasic calcium phosphate ceramics: influence of macropore diameter and macroporosity percentage on bone ingrowth. Biomaterials. 1998 Jan-Feb;19(1-3):133-9.

8.   Chang BS, Lee CK, Hong KS, Youn HJ, Ryu HS, Chung SS, et al. Osteoconduction at porous hydroxyapatite with various pore configurations. Biomaterials. 2000 Jun;21(12):1291-8.

9.   De Oliveira JF, De Aguiar PF, Rossi AM, Soares GA. Effect of process parameters on the characteristics of porous calcium phosphate ceramics for bone tissue scaffolds. Artificial Organs. 2003 May;27(5):406-11.

10.   Kon E, Muraglia A, Corsi A, Bianco P, Marcacci M, Martin I, et al. Autologous bone marrow stromal cells loaded onto porous hydroxyapatite ceramic accelerate bone repair in critical-size defects of sheep long bones. Journal of Biomedical Materials Research. 2000 Mar 5;49(3):328-37.

11.   Mastrogiacomo M, Scaglione S, Martinetti R, Dolcini L, Beltrame F, Cancedda R, et al. Role of scaffold internal structure on in vivo bone formation in macroporous calcium phosphate bioceramics. Biomaterials. 2006 Jun;27(17):3230-7.

12.   Liu XH, Ma PX. Polymeric scaffolds for bone tissue engineering. Annals of Biomedical Engineering. 2004 Mar;32(3):477-86.

13.   Wu LB, Ding JD. Effects of porosity and pore size on in vitro degradation of three-dimensional porous poly(D,L-lactide-co-glycolide) scaffolds for tissue engineering. Journal of Biomedical Materials Research Part A. 2005 Dec 15;75A(4):767-77.

14.   Karageorgiou V, Kaplan D. Porosity of 3D biornaterial scaffolds and osteogenesis. Biomaterials. 2005 Sep;26(27):5474-91.

15.   Ma PX, Choi JW. Biodegradable polymer scaffolds with well-defined interconnected spherical pore network. Tissue Engineering. 2001 Feb;7(1):23-33.

16.   Ikada Y. Scope of Tissue Engineering. Tissue Engineering: Fundamentals and Applications2006. p. 1-89.

17.   Lu JX, Flautre B, Anselme K, Hardouin P, Gallur A, Descamps M, et al. Role of interconnections in porous bioceramics on bone recolonization in vitro and in vivo. Journal of Materials Science-Materials in Medicine. 1999 Feb;10(2):111-20.

18.   Wei GB, Ma PX. Macroporous and nanofibrous polymer scaffolds and polymer/bone-like apatite composite scaffolds generated by sugar spheres. Journal of Biomedical Materials Research Part A. [Article]. 2006 Aug;78A(2):306-15.

19.   Zhang RY, Ma PX. Synthetic nano-fibrillar extracellular matrices with predesigned macroporous architectures. Journal of Biomedical Materials Research. 2000;52(2):430-8.

20.   Feng G, Jin X, Hu J, Ma H, Gupte MJ, Liu H, et al. Effects of hypoxias and scaffold architecture on rabbit mesenchymal stem cell differentiation towards a nucleus pulposus-like phenotype. Biomaterials. 2011 Nov;32(32):8182-9.

21.   Hu J, Feng K, Liu X, Ma P. Chondrogenic and osteogenic differentiations of human bone marrow-derived mesenchymal stem cells on a nanofibrous scaffold with designed pore network. Biomaterials. 2009;30(28):5061-7.

22.   Hu J, Xie C, Ma H, Yang B, Ma PX, Chen YE. Construction of Vascular Tissues with Macro-Porous Nano-Fibrous Scaffolds and Smooth Muscle Cells Enriched from Differentiated Embryonic Stem Cells. PloS one. 2012 Apr 24;7(4).

23.   Smith LA, Liu XH, Hu JA, Ma PX. The Enhancement of human embryonic stem cell osteogenic differentiation with nano-fibrous scaffolding. Biomaterials. 2010;31(21):5526-35.

24.   Sun H, Feng K, Hu J, Soker S, Atala A, Ma P. Osteogenic differentiation of human amniotic fluid-derived stem cells induced by bone morphogenetic protein-7 and enhanced by nanofibrous scaffolds. Biomaterials. 2010;31(6):1133-9.

25.   Wang J, Ma H, Jin X, Hu J, Liu X, Ni L, et al. The effect of scaffold architecture on odontogenic differentiation of human dental pulp stem cells. Biomaterials. 2011(in press).

26.   Xie C, Hu J, Ma H, Zhang J, Chang L-J, Chen YE, et al. Three-dimensional growth of iPS cell-derived smooth muscle cells on nanofibrous scaffolds. Biomaterials. 2011 Jul;32(19):4369-75.

27.   Pittenger MF, Mackay AM, Beck SC, Jaiswal RK, Douglas R, Mosca JD, et al. Multilineage potential of adult human mesenchymal stem cells. Science. 1999 Apr 2;284(5411):143-7.

CHAPTER 5

ELECTRODEPOSITED CALCIUM PHOSPHATE ON NANOFIBROUS PLLA SCAFFOLD ENHANCES ECTOPIC BONE FORMATION

INTRODUCTION

Through an understanding of the extracellular matrix (ECM) and associated tissues, engineers have derived a design for tissue engineering scaffolds composed of polymers combined with ceramic crystals. One of the most widely used models for an artificial ECM is the polymer/ceramic composite system. Crystalline ceramics and amorphous materials have long been studied as potential candidates for bone tissue engineering applications (1-9). For example, calcium phosphate (CaP) ceramics, including hydroxyapatite (HA), have drawn interest due to their similarity to bone mineral, their inherent biocompatibility and their exceptional osteoconductivity. HA exhibits a strong propensity for attracting osteoblasts but possesses a low resorption rate in vivo and is not mechanically strong, especially in highly porous forms. This is a disadvantage because porosity is a necessity for tissue ingrowth/regeneration (10).

Polymer scaffolds have also been investigated at length as candidates for artificial ECM because of their mechanical properties, resorbability, and ability to be fabricated with desired nanofibrous structures using techniques like thermally induced phase separation and electrospinning. Polymers including poly (L-lactic acid) (PLLA) (6) and poly(lactic-co-glycolic acid) (PLGA), along with polyamide, polycaprolactone, polyethylene, gelatin, chitosan and collagen have been

fabricated into composite scaffold structures, which incorporate HA (11-21). These combinations allow the scaffold system to maintain many of the positive aspects of HA, while alleviating some of the negative features. Advantages of pairing HA with natural and/or synthetic polymers include improved control of design parameters such as porosity, degradability and mechanical properties when compared to pure HA scaffolds. Porosities greater than 90% are possible, where pure HA scaffold porosity is usually less than 70%. On a different scale, the addition of HA crystals to natural polymer scaffolds has been shown to improve mechanical properties compared to polymer control scaffolds and the presence of an HA component reduces adverse effects associated with the degradation of some synthetic polymers, including pH imbalance (21).

Polymer/ceramic scaffolds can be fabricated by simply mixing a ceramic component into a polymer solution (21), but the HA crystals become trapped within the bulk of the scaffold instead of interacting with cells at the surface, resulting in a low osteoconductivity. Rather than mixing the HA component into the polymer solution prior to scaffold fabrication, HA can be "grown" on the surface of polymer scaffolds, through a biomimetic process involving submersion in simulated body fluid (SBF) (22). SBF incubation results in apatite crystals similar to those present in bone were found along the surfaces of scaffold pores.

While SBF incubation is well-established to deposit HA on polymer scaffolds, a faster method would be more desirable. Recently, a method has been developed that uses electrodeposition to grow HA crystals in just 30 minutes onto 2D films (23) or 3D scaffolds (24), prepared by electrospinning or TIPS. This method was initially used to coat titanium dental implants (25). For electrodeposition, polymer substrates are adhered to a voltage-supplied electrode and submerged in an electrolyte containing both calcium and phosphate. After 30 minutes, much faster than the 1-2 week SBF method, flower-shaped crystals are formed on the substrate. The

deposited crystals consist of a combination of hydroxyapatite, dicalcium phosphate dihydrate (DCPD), and octacalcium phosphate (OCT), as it is common to obtain multiple mineral phases with any mineralization method. While the mechanism behind electrodeposition still requires some investigation, the process is tunable using temperature, pH, voltage, deposition time, and electrolyte composition to alter crystal topography, calcium to phosphate ratio, size, and amount (23). For example, increasing polymer concentration (i.e. fiber diameter) or deposition time increases the amount of minerals. Morphology also changes from flower-like to flake-like when deposition time is increased from 15 mins to 60 mins.

When HA is added to a scaffold, first it can encourage cell adhesion and proliferation. Cell adhesion to the scaffold is important in preventing cell death and creating cell morphology similar to that in vivo. Calcium phosphate, of which HA is one type, may improve cell attachment with each granule serving as a cell attachment point (26). Nanofibers then allow pre-osteoblasts to achieve a preferred 3D elongated shape on nanofiber films compared to an overly spread morphology achieved on flat films (27). This suggests that a composite scaffold with nanofibers and HA may synergistically improve the cell microenvironment. Following adhesion, cell proliferation is essential for tissue formation and may also be enhanced by HA (26, 28).

Once stem cells greatly proliferate, they must differentiate into the desired mature cell type. It has been widely shown that HA improves osteogenic differentiation of numerous stem cell types including embryonic stem cells (29), iPS cells (30), and bone marrow-derived mesenchymal stem cells (31, 32). HA has also been shown to facilitate the differentiation of pre-osteoblasts (33) and enhance osteoblast function (34). The positive effect of HA on osteogenic differentiation is marked by increased bone marker gene expression, collagen type I deposition, mineralization, and alkaline phosphatase activity. Due to these effects, biomaterials containing

HA can successfully support bone tissue formation. For example, Liu et al. showed that HA on a nanofibrous gelatin scaffold adheres to the nanofibers without blocking the interconnected porous structure. When seeded with MC3T3-E1 pre-osteoblasts, HA significantly enhanced gene expression of bone sialoprotein and osteocalcein at four weeks (33). Therefore, this composite scaffold improves osteogenic differentiation of pre-osteoblasts using both apatite minerals and nanofiber architecture.

Nanofibers enhance several stem cell behaviors: adhesion, proliferation, and differentiation. The suggested mechanisms behind these positive nanofiber effects include increased integrin expression (35), increased protein adsorption (36), and modified signaling pathways through paxillin, focal adhesion kinase, RhoA, and Rac (27, 37, 38). While the mechanisms behind the cellular response to hydroxyapatite still require further investigation, a few mechanisms have been proposed. One suggested mechanism is that hydroxyapatite increases protein absorption, most significantly fibronectin and vitronectin absorption, through the integrin-FAK-Akt pathway, which then suppresses apoptosis (39). This hypothesis was established through observation of MC3T3-E1 pre-osteoblasts on 3D PLLA/hydroxyapatite composite scaffold in comparison to those on pure PLLA scaffold. Because this study used pre-osteoblasts, the mechanism for stem cell differentiation must still be elucidated. Another study also implicates an FAK pathway using MC3T3-E1 pre-osteoblasts by showing activation of ERK in response to 2D hydroxyapatite discs (40). 3D studies are warranted to better simulate the in vivo environment.

The hydroxyapatite/polymer composite scaffold model reveals that composite scaffolds can be highly useful in promoting cell adhesion and proliferation and more importantly stem cell differentiation. To date, however, no study to our knowledge has determined the combined effect of: 1) electrodeposited calcium phosphate and 2) TIPS polymer nanofibers seeded with 3) stem

cells in a 4) 3D scaffold 5) in vivo for bone formation. Therefore, this study will determine the effect of electrodeposited calcium phosphate (CaP) on a 3D nanofibrous, polymer scaffold seeded with rabbit bone-marrow derived mesenchymal stem cells (BMSCs) in an ectopic bone model, compared to a blank, nanofibrous scaffold without CaP.

MATERIALS AND METHODS

Scaffold Fabrication

The nanofibrous PLLA scaffolds were prepared as previously described (41). Sugar spheres with different sizes were first prepared by an emulsion technique. Typically, 50 g of d-fructose were melted at 120°C for 90 min until clear yellowish liquid was obtained. The liquefied sugar was emulsified into 50 mL mineral oil with 1.3 mL Span 80 at 120°C under stirring. The resulting mixture was cooled down using an ice-bath to solidify sugar spheres. After discarding the mineral oil, the sugar spheres were washed with hexane three times and sieved to select desired sizes (250–425 µm size range). The sieved sugar spheres were packed in a Teflon vial with hexane and heat treated at 37 °C for 30 min to achieve a highly interconnected sugar sphere template. After bonding the sugar spheres, hexane was removed, and the sugar template was dried under vacuum.

Then, about 0.6–0.8 mL 10 % (w/v) PLLA/THF solution was cast into the assembled sugar template. Mild vacuum was applied during casting in order to fully fill the interspaces of the bonded sugar template with polymer solution. The polymer solution/sugar template was phase separated at -20 °C overnight and then immersed into cyclohexane to extract solvent (THF) for 2 days. The resulting composites were freeze-dried. The sugar template was then leached away in distilled water, and the porous nano-fibrous scaffold was freeze-dried.

Calcium Phosphate Electrodeposition on Scaffolds

Calcium phosphate electrodeposition was adapted from the method previously described for deposition on 2D films (23, 42). The setup for electrodeposition contained two electrodes: a platinum plate electrode (20 × 20 × 0.2 mm) served as the counter electrode and the scaffold-covered, stainless-steel electrode as the working electrode. Six scaffolds (5mm diameter, 1.5mm thick) were adhered onto the surface of the stainless-steel electrode using copper foil conductive adhesive. The scaffold-covered electrode (cathode) was immersed into ethanol for 1–2 min prior to electrodeposition in order to reduce the amount of hydrogen gas evolution at the deposition electrode. Due to the high porosity and surface area of the scaffold, vacuum at 27 psi was applied during the immersion to fully wet the surface of the scaffolds. The distance between the two electrodes was fixed at 2.5 cm. The setup was placed in a beaker filled with a calcium and phosphate-containing electrolyte, which was placed in a water bath to maintain the desired temperature of 60C. The electrolyte was a solution of 0.042 mol L^{-1} $Ca(NO_3)_2 \cdot 4H_2O$ and 0.025 mol L^{-1} $NH_4H_2PO_4$, with a pH of 4.70.

A voltage of 3V was applied to the electrodes and deposition was performed for 1 hour at 60C. Scaffolds were then turned over, and the opposite side of the scaffolds was deposited for another hour to achieve uniform crystal deposition throughout the entire scaffold. Scaffolds were then removed from the electrode and heated at 60C for 30 mins to improve adhesion of crystals to the scaffold. CaP coating on each sample was verified under inverted microscrope.

Scanning Electron Microscope (SEM) Observation

Calcium phosphate-deposited and blank scaffolds were coated with gold for 120 s using a sputter

coater (DeskII, Denton vacuum Inc) and observed using SEM (Philips XL30 FEG) at 50x and 400x.

Bone Marrow Stem Cell Isolation and Culture

Bone marrow-derived mesenchymal stem cells (BMSCs) were obtained from the New Zealand White rabbits by aspiration of the femoral and tibial bone marrow using an 18-gauge syringe needle. A total of 10 ml of marrow was collected into 1000 U of heparin-containing maintenance media (high-glucose alpha-MEM (Gibco) containing 10% fetal bovine serum (FBS) (Gibco) and antibiotics (penicillin G, 100 U/ml; streptomycin, 0.1 mg/ml)). The marrow was washed with PBS once and fresh media twice, and centrifuged at 2000 rpm for 3 min after each wash. Rabbit BMSCs were collected and cultured in 60-cm^2 culture dishes in maintenance media at 37 C under 5% CO_2, changing media every 2-3 days. Cells were used at passage 3.

Cell Seeding on Scaffold

Scaffolds were soaked in 70% ethanol for 30 min, washed three times with PBS for 30 min each, and twice in alpha MEM with 10% fetal bovine serum for 30 min each. CaP and blank scaffolds (5 mm in diameter and 1.5 mm in thickness) were seeded with 250,000 cells in 13 µl of medium. After 2 hr of initial seeding, enough media was added to cover scaffolds, and cell-seeded scaffolds were further cultured for 22 hr under static condition to enhance cell adhesion on scaffolds.

Subcutaneous Implantation

Cell-scaffold constructs (n=8) were implanted subcutaneously into nude mice for 4 or 8 weeks. Male nude mice that were 6-8 wk old (Charles River, Wilmington, MA) were used. Surgery was

71

performed under general anesthesia by inhalation of isoflurane with balanced oxygen. To implant four constructs per mouse, two midsagittal incisions were made on the dorsa, and one subcutaneous pocket was created on each side of each incision. One cell-scaffold construct was implanted into each pocket at random. Eight samples were implanted for each group, and incisions were closed with suture clips. Following 4 or 8 wk implantation period, mice were euthanized with CO_2, and implants were harvested. These animal procedures were performed according to the protocol approved by the Univeristy Committee on Use and Care of Animals (UCUCA) at the University of Michigan.

MicroCT Analysis

Samples were embedded in 1% agarose and placed in a 14 mm diameter tube and scanned over the entire length of the scaffold using a microCT system (μCT100 Scanco Medical, Bassersdorf, Switzerland). Scan settings were: voxel size 12 μm, 70 kVp, 114 μA, 0.5 mm AL filter, and integration time 500 ms. Analysis was performed using the manufacturer's evaluation software, and a fixed global threshold of 18% (180 on a grayscale of 0–1000) was used to segment bone from non-bone in order to quantify bone volume and create 3D reconstructions. It is important to note that this fixed threshold at 18% is significantly higher than the threshold that the CaP coating is visible (15%), and therefore the initial CaP coating is considered non-bone in this analysis.

Histological Analysis

Constructs were washed in PBS, fixed with 3.7% formaldehyde in PBS overnight, and decalcified in 10% EDTA (pH=7.4) for two weeks. Decalcified constructs were then dehydrated through a graded series of ethanol, embedded in paraffin, and sectioned at a thickness of 5 μm. For histological analysis, sections were deparaffinized, rehydrated, and stained with H&E.

72

In Vitro Cell Proliferation

Rabbit BMSCs at passage 3 were plated in a 48 well plate with 9,000 cells per well (n=3). Cells were cultured in 4 different growth media conditions with 1) calcium-free DMEM (#21068, Gibco) plus 2 mM glutamine (GlutaMAX, Gibco) or alpha MEM with 2) 70 µg/ml calcium, 3) 140 µg/ml calcium or 4) 280 µg/ml calcium. To achieve 140 µg/ml and 280 µg/ml calcium concentration, sterile 1M calcium chloride was added to the base alpha MEM formulation which already includes 70 µg/ml calcium. The following supplements were also added to all media conditions: 10% fetal bovine serum (FBS) (Gibco), 100U/ml penicillin, and 100µg/ml streptomycin (Gibco). Osteogenic differentiation media was the growth media above, plus 100nm dexamethasone, 10mM β-glycerophosphate, and 50µg/ml ascorbic acid. Media was changed 3 times per week.

Cell number was determined using CCK-8 cell counting kit (Dojingo, Japan) according to the manual. Briefly, at each time point, 15 µl of CCK-8 reagent plus 150 µl of fresh media was added to each well and incubated for 1 hour to induce color change. 40µl of reagent/media from each well was transferred in triplicate to a 96 well plate, and absorbance was read at 450nm. Culture plate was washed with PBS, fresh media was added, and culture was continued until 14 days.

Quantitative Real-time PCR for Osteopontin and Bone sialoprotein Gene Expression

Rabbit BMSCs at passage 3 were plated in a 24 well plate with 45,000 cells per well with n=3. Cells were cultured in the same osteogenic differentiation media described in the proliferation study for 14 days with the same 4 groups of 0, 70, 140, and 280 µg/ml calcium. Media was changed three times per week.

RNA was extracted using Trizol (Invitrogen) according to the manual by adding 1 ml Trizol directly to each well. Reverse transcription-PCR was then performed to form cDNA using Superscript II RT kit (Invitrogen) according to the manual. Quantitative real-time PCR was performed using TaqMan Universal PCR Master Mix (Applied Biosystems) and primers for osteopontin and bone sialoprotein (Applied Biosystems) on a ViiA 7 Real time PCR system (Applied Biosystems). Gene expression level was normalized against GAPDH expression (Applied Biosystems).

Statistical Analysis

Analysis of bone volume to compare CaP versus blank scaffolds were performed using a t-test in Microsoft Excel with $p < 0.05$.

RESULTS AND DISCUSSION

When NF PLLA scaffolds are electrodeposited at 3V and 60C for 2 hours in a calcium and phosphate-containing electrolyte, flower-like crystals of calcium phosphate uniformly form on the scaffold without blocking pore interconnections (**Figure 5.1**). CaP coating consists of hydroxyapatite and amorphous CaP, and the amorphous CaP slowly releases from the scaffold over three weeks (data not shown). In order to the determine the effect of electrodeposited calcium phosphate (CaP), scaffolds with and without CaP were seeded with rabbit BMSCs and implanted subcutaneously into nude mice for 4w or 8w. Using MicroCT analysis to quantify mineralized tissue, CaP-deposited scaffold significantly enhanced bone volume formed within the scaffold after both 4w and 8w, compared to the blank scaffold without CaP ($p<0.05$) (**Figure 5.2**). It is important to note that the quantified bone volume is only new bone tissue and does not include the initial CaP coating, which was below the threshold used for analysis. This clear CaP effect can be also visualized using 3D MicroCT reconstructions of the newly formed ectopic bone issues, viewed from the top of the scaffold (**Figure 5.3**). The CaP scaffold induced significant mineralized bone formation after only 4w, with robust bone formation throughout the scaffold at 8w, while the blank scaffold contained minimal bone after 4w and supported less ectopic bone formation at 8w (**Figure 5.3**).

This positive CaP effect can further been seen by histological analysis with H&E staining. After 4w in vivo, more bone formation (pink) formed on the pore walls throughout the entire cross-section of the CaP scaffold, compared to the blank scaffold (**Figures 5.4**). From 4w to 8w, bone matrix deposition increased in both CaP and blank scaffolds (**Figure 5.5**). After 8w, while the blank scaffold did support some osteogenesis, the neo-bone was still found only in part of the scaffold, with fibrous tissue (light pink) invading the remainder of the scaffold at 8w (**Figure**

75

5.5D). This lack of bone tissue also caused the blank scaffold to slightly flatten or collapse in response to external forces, causing it to have a thinner cross-section (**Figure 5.5C**) than the CaP scaffold (**Figure 5.5A**). In contrast, at 8w, the CaP scaffold contained uniform, mature bone formation through the scaffold filled with bone marrow-like tissue of darkly-stained immune cells, adipocytes (round white areas), and large blood vessels, such as the one marked with an arrow extending through a pore interconnection (**Figure 5.5A**). Therefore, the electrodeposited CaP on a nanofibrous, PLLA scaffold enhanced ectopic osteogenesis compared to an identical blank scaffold without CaP.

In order to determine why CaP promoted osteogenesis, rabbit BMSCs were cultured on tissue culture plastic in growth or osteogenic differentiation media containing 0, 70 (base media concentration), 140, or 280 µg/ml calcium (**Figure 5.6**). Proliferation was measured over 14 days. In growth media, cells proliferated similarly independent of calcium concentration; though without any calcium, proliferation was slightly inhibited at day 14. In contrast, in differentiation media, proliferation varied significantly in response to exogenous calcium concentration. Without any calcium, cells only proliferated minimally and never reached confluency. All other groups with calcium-containing differentiation media achieved confluency by 7 days. Maximum proliferation was attained with 280 µg/ml calcium, while cells proliferation plateaued with 70 µg/ml calcium, likely indicating that differentiation was underway.

In order to test this hypothesis, differentiation was measured at 14 days using real-time PCR for two osteogenic differentiation markers: osteopontin (OPN), a middle marker, and bone sialoprotein (BSP), a late marker (**Figure 5.7**). Just as in the proliferation study, rabbit BMSCs were cultured on tissue culture plastic in osteogenic differentiation media containing 0, 70 (base media concentration), 140, or 280 µg/ml calcium. At 14 days, there was no significant difference

in OPN expression between groups because the 14 day time point may be too late for upregulation of OPN. Interestingly, BSP expression was 4 fold higher with 70 µg/ml calcium, compared to 140 or 280 µg/ml calcium. Therefore, as hypothesized, in the 70 µg/ml calcium group, cells likely proliferated until 7 days, then began to differentiate, causing the plateau in proliferation from 7 to 14 days. Based on the proliferation and differentiation responses to an increased calcium concentration of 280 µg/ml, the electrodeposited CaP likely enhanced proliferation but not differentiation.

CONCLUSION

In an ectopic in vivo model, electrodeposited calcium phosphate (CaP) on a nanofibrous PLLA scaffold seeded with rabbit bone marrow-derived mesenchymal stem cells (BMSCs) enhanced mature, mineralized bone formation compared to a blank scaffold without CaP, shown by MicroCT and histological analysis. Furthermore, the calcium in the beneficial CaP crystal coating likely promoted rabbit BMSC proliferation, shown by an in vitro model. In the future, this promising CaP/polymer composite scaffold could be used to enhance femoral bone defect repair without any implanted cells by encouraging host stem cell proliferation.
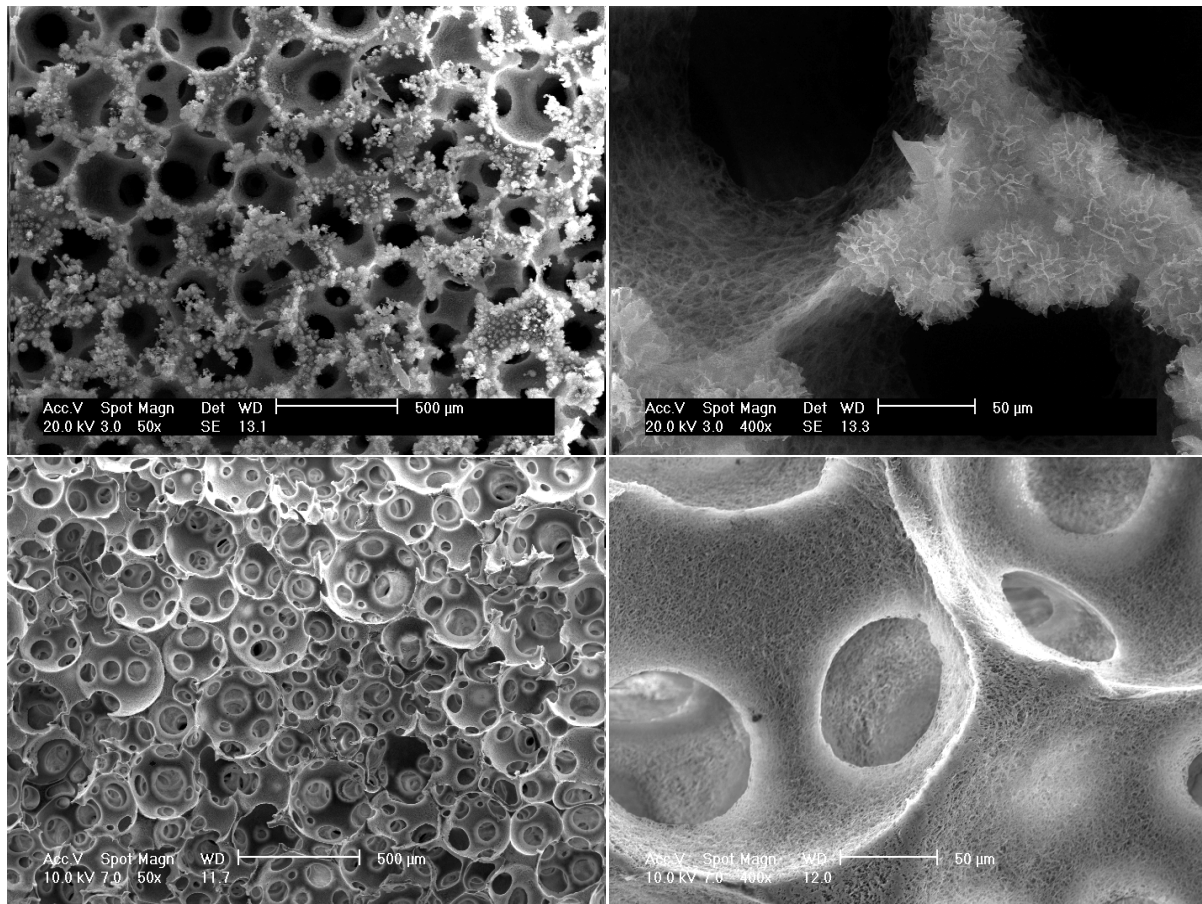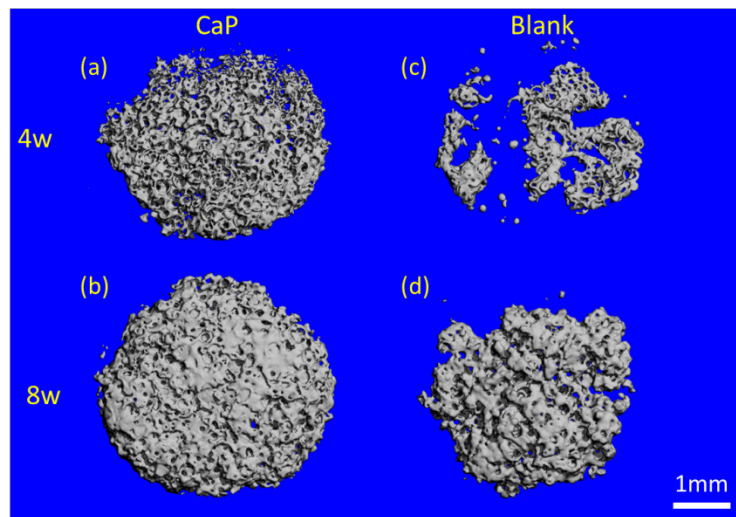
Figure 5.1. SEM micrographs of Top: CaP-deposited (3V, 60C, 60min) nanofibrous PLLA scaffold and Bottom: Blank scaffold at 50x and 400x magnifications.
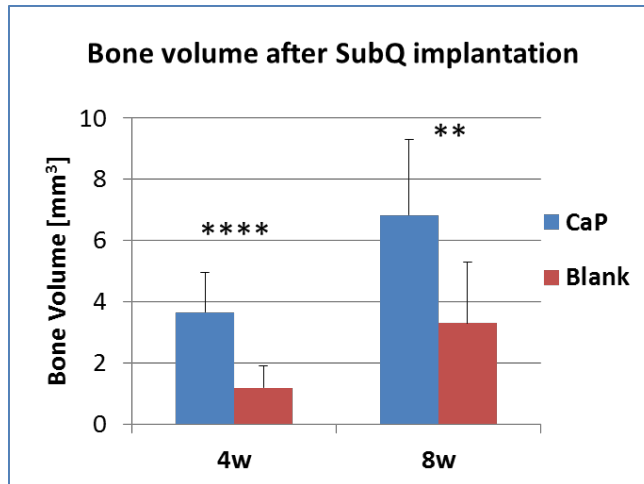
Figure 5.2. Bone volume quantification from microCT analysis of calcium phosphate-electrodeposited scaffold versus blank scaffold after 4w and 8w subcutaneous implantation. **p<0.01, ****p<0.0001


Figure 5.3. 3D MicroCT reconstruction of (a, b) calcium phosphate-electrodeposited scaffold and (c, d) blank scaffold after 4w and 8w mouse subcutaneous implantation, from top view.
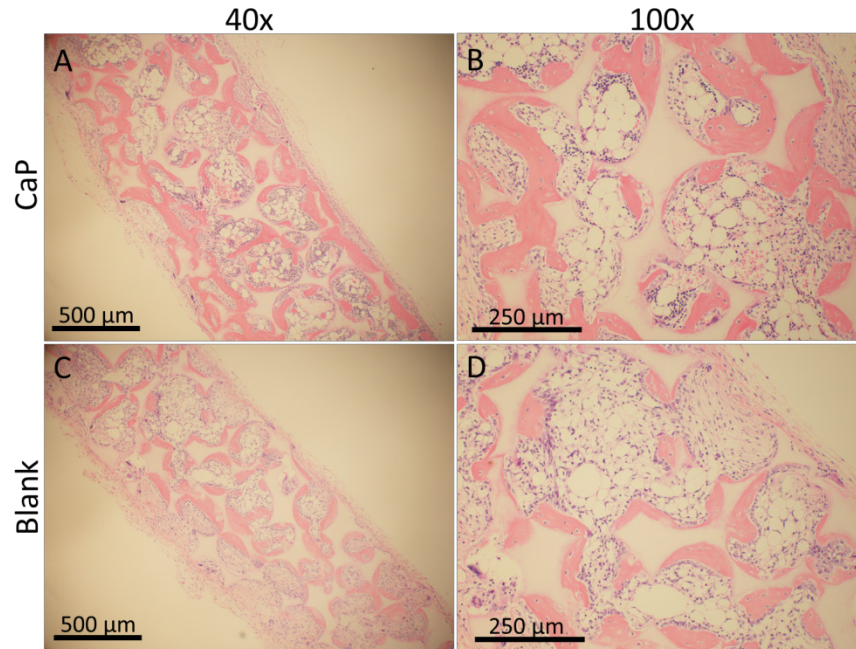
Figure 5.4. H&E staining after 4w subcutaneous implantation. Calcium phosphate (CaP) deposited scaffold at A) 40x magnification and B) 100x magnification. Blank scaffold at C) 40x magnification and D) 100x magnification.
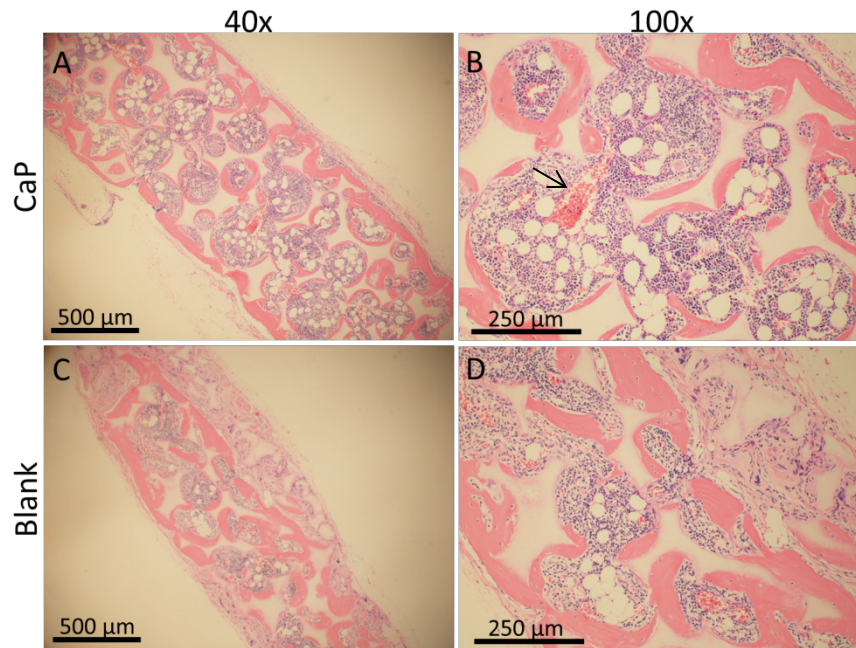

Figure 5.5. H&E staining after 8w subcutaneous implantation. Calcium phosphate (CaP) deposited scaffold at A) 40x magnification and B) 100x magnification. Blank scaffold at C) 40x magnification and D) 100x magnification. Arrow: blood vessel filled with pink-stained red blood cells.
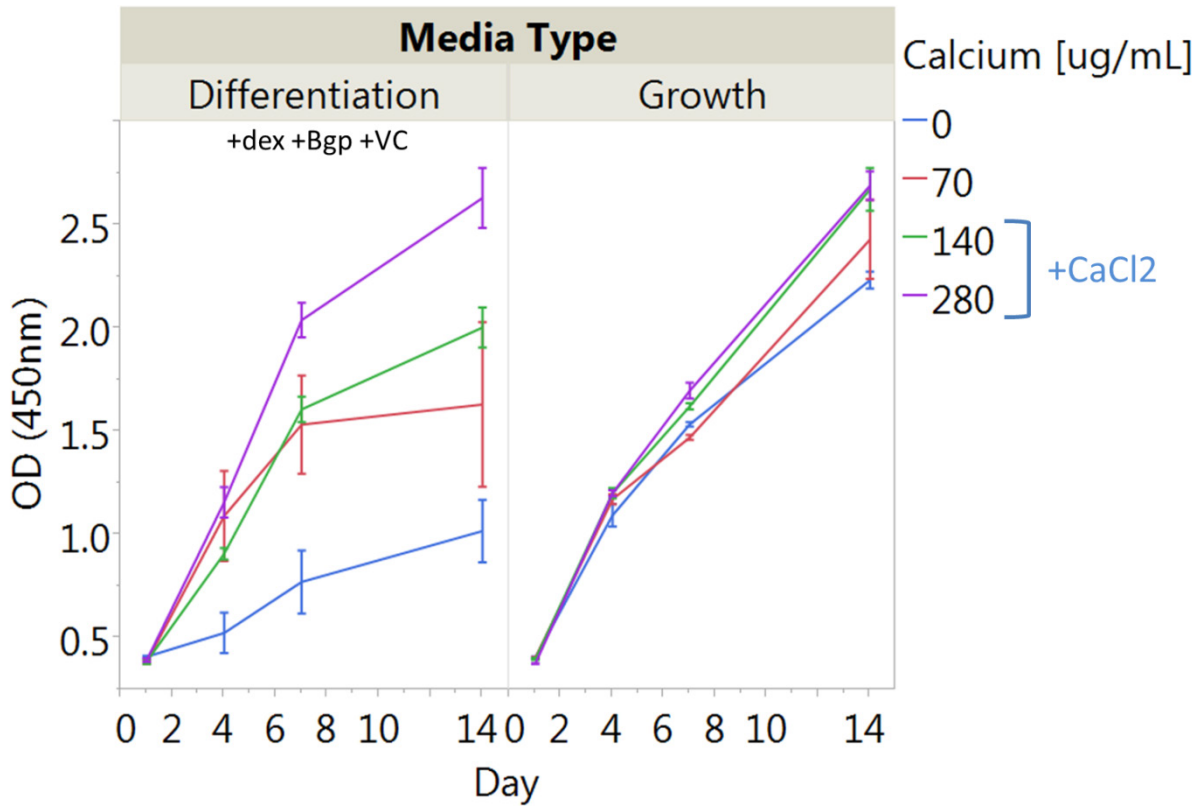
Figure 5.6 Proliferation of rabbit BMSCs cultured on tissue culture plastic over 14 days in osteogenic differentiation media (on left) or growth media (on right) for calcium concentrations of 0, 70, 140, or 280 µg/ml. Error bars represent standard error.
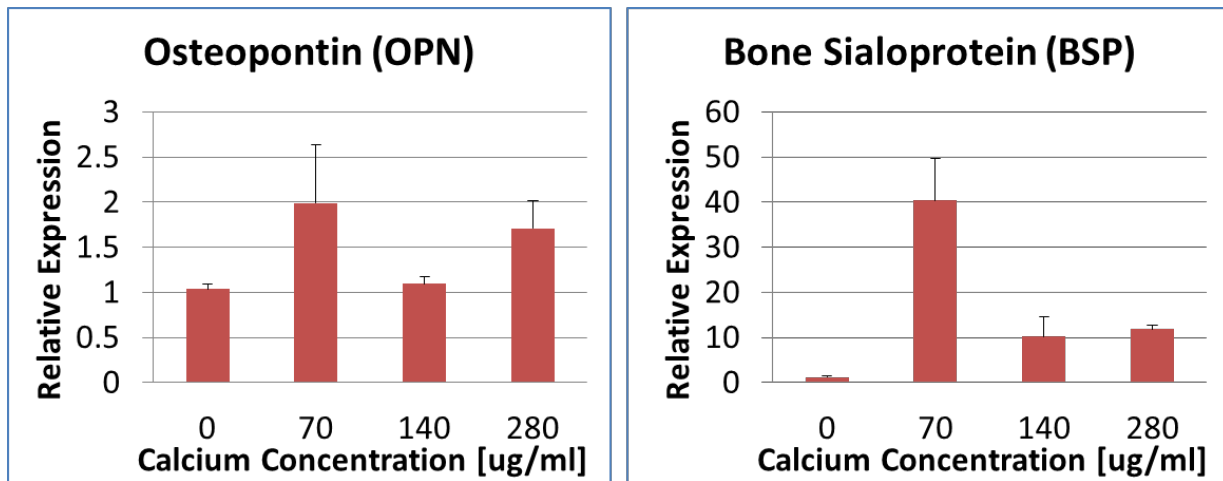
Figure 5.7 Relative osteopontin (left) and bone sialoprotein (right) gene expression of rabbit BMSCs cultured on tissue culture plastic over 14 days in osteogenic differentiation media with exogenous calcium concentrations of 0, 70, 140, or 280 µg/ml. Error bars represent standard deviation.

REFERENCES

1.   Blaker JJ, Nazhat SN, Maquet V, Boccaccini AR. Long-term in vitro degradation of PDLLA/Bioglass bone scaffolds in acellular simulated body fluid. Acta Biomaterialia. 2011;7:829-40.

2.   Francis L, Meng D, Knowles JC, Roy I, Boccaccini AR. Multi-functional P(3HB) microsphere/45S5 Bioglass-based composite scaffolds for bone tissue engineering. Acta Biomaterialia. 2010;6:2773-86.

3.   Hajiali H, Karbasi S, Hosseinalipour M, Rezaie HR. Preparation of a novel biodegradable nanocomposite scaffold based on poly (3-hydroxybutyrate)/bioglass nanoparticles for bone tissue engineering. J Mater Sci: Mater Med. 2010;21:2125-32.

4.   Hench LL. Bioceramics. J Am Ceram Soc. 1998;81(7):1705-28.

5.   Kundu B, Soundrapandian C, Nandi SK, Mukherjee P, Dandapat N, Roy S, et al. Development of New Localized Drug Delivery System Based on Ceftriaxone-Sulbactam Composite Drug Impregnated Porous Hydroxyapatite: A Systematic Approach for In Vitro and In Vivo Animal Trial. Pharm Res. 2010;27:1659-76.

6.   Milan J, Planell JA, Lacroix D. Computational modelling of the mechanical environment of osteogenesis within a polylactic acid–calcium phosphate glass scaffold. Biomaterials. 2009;30(25):4219-26.

7.   Misra SK, Ansari TI, Valappil SP, Mohn D, Philip SE, Stark WJ, et al. Poly(3-hydroxybutyrate) multifunctional composite scaffolds for tissue engineering applications. Biomaterials. 2010;31:2806-15.

8.   Xu C, Su P, Wang Y, Chen X, Meng Y, Liu C, et al. A novel biomimetic composite scaffold hybridized with mesenchymal stem cells in repair of rat bone defects models. J Biomed Mater Res. 2010;95A(2):495-503.

9.   Xu C, Su P, Chen X, Meng Y, Yu W, Xiangc AP, et al. Biocompatibility and osteogenesis of biomimetic Bioglass-Collagen- Phosphatidylserine composite scaffolds for bone tissue engineering. Biomaterials. 2011;32:1051-8.

10.   Hing KA, Wilson LF, Buckland T. Comparative performance of three ceramic bone graft substitutes. The Spine Journal. 2007;7:475-90.

11.   Douglas T, Pamula E, Hauk D, Wiltfang J, Sivananthan S, Sherry E, et al. Porous polymer/hydroxyapatite scaffolds: characterization and biocompatibility investigations. J Mater Sci: Mater Med. 2009;20:1909-15.

12.   Henriksen SS, Ding M, Vinther Juhl M, Theilgaard N, Overgaard S. Mechanical strength of ceramic scaffolds reinforced with biopolymers is comparable to that of human bone. J Mater Sci: Mater Med. 2011;22:1111-8.

13.   Khan Y, El-Amin SF, Laurencin CT, editors. In Vitro and In Vivo Evaluation of a Novel Polymer-Ceramic Composite Scaffold for Bone Tissue Engineering. 28th IEEE EMBS Annual International Conference; 2006; New York.

14.   Kim S, Ahn KM, Park MS, Lee JH, Choi CH, Kim BS. A poly(lactide-co-glycolide)/hydroxyapatite composite scaffold with enhanced osteoconductivity. J Biomed Mater Res. 2007;80A:206-15.

15.   Kim S-S, Park MS, Gwak S-J, Choi CY, Kim B-S. Accelerated Bonelike Apatite Growth on Porous Polymer/Ceramic Composite Scaffolds in Vitro. Tissue Engineering. 2006;12(10):2997-3006.

16.   Kim S, Park MS, Jeon O, Choi CY, Kim B-S. Poly(lactide-co-glycolide)/hydroxyapatite composite scaffolds for bone tissue engineering. Biomaterials. 2006;27:1399-409.

17. Leong NL, Jiang J, Lu HH, editors. Polymer-Ceramic Composite Scaffold Induces Osteogenic Differentiation of Human Mesenchymal Stem Cells. 28th IEEE EMBS Annual International Conference; 2006; New York City.

18. Lv Q, Nair L, Laurencin CT. Fabrication, characterization, and in vitro evaluation of poly(lactic acid glycolic acid)/nano-hydroxyapatite composite microsphere-based scaffolds for bone tissue engineering in rotating bioreactors. J Biomed Mater Res. 2008;91A:679-91.

19. Qiu X, Hong Z, Hu J, Chen L, Chen X, Jing X. Hydroxyapatite Surface Modified by L-Lactic Acid and Its Subsequent Grafting Polymerization of L-Lactide. Biomacromolecules. 2005;6:1193-9.

20. Scaglione S, Lazzarini E, Ilengo C, Quarto R. A composite material model for improved bone formation. J Tissue Eng Regen Med. 2010;4:505-13.

21. Zhang R, Ma P. Poly(alpha-hydroxyl acids) hydroxyapatite porous composites for bone-tissue engineering. I. Preparation and morphology. Journal of biomedical materials research. 1999;44(4):446-55.

22. Zhang RY, Ma PX. Porous poly(L-lactic acid)/apatite composites created by biomimetic process. Journal of biomedical materials research. 1999 Jun 15;45(4):285-93.

23. He C, Xiao G, Jin X, Sun C, Ma PX. Electrodeposition on Nanofibrous Polymer Scaffolds: Rapid Mineralization, Tunable Calcium Phosphate Composition and Topography. Advanced Functional Materials. 2010 Oct 22;20(20):3568-76.

24. He C, Zhang F, Cao L, Feng W, Qiu K, Zhang Y, et al. Rapid mineralization of porous gelatin scaffolds by electrodeposition for bone tissue engineering. Journal of Materials Chemistry. 2012 2012;22(5):2111-9.

25. Vijayaraghavan TV, Bvensalem A. Hydroxyapatite (HA) coating by electrodeposition on Alpha-Ti and Alpha-Beta-Ti alloys. Journal of Dental Research. 1995;74:474.

26. Eyckmans J, Roberts SJ, Schrooten J, Luyten FP. A clinically relevant model of osteoinduction: a process requiring calcium phosphate and BMP/Wnt signalling. Journal of Cellular and Molecular Medicine. 2010;14(6b):1845-56.

27. Hu J, Liu X, Ma PX. Induction of osteoblast differentiation phenotype on poly(L-lactic acid) nanofibrous matrix. Biomaterials. 2008;29(28):3815-21.

28. Li XR, Xie JW, Yuan XY, Xia YN. Coating Electrospun Poly(epsilon-caprolactone) Fibers with Gelatin and Calcium Phosphate and Their Use as Biomimetic Scaffolds for Bone Tissue Engineering. Langmuir. 2008 Dec;24(24):14145-50.

29. Garreta E, Gasset D, Semino C, Borrós S. Fabrication of a three-dimensional nanostructured biomaterial for tissue engineering of bone. Biomolecular Engineering. 2007;24(1):75-80.

30. D'Angelo F, Armentano I, Cacciotti I, Tiribuzi R, Quattrocelli M, Del Gaudio C, et al. Tuning Multi/Pluri-Potent Stem Cell Fate by Electrospun Poly(l-lactic acid)-Calcium-Deficient Hydroxyapatite Nanocomposite Mats. Biomacromolecules. 2012;13(5):1350-60.

31. Lao L, Zhu Y, Zhang Y, Gao Z, Zhou F, Chen L, et al. Mineralization of Collagen-Coated Electrospun Poly(lactide-co-glycolide) Nanofibrous Mesh to Enhance Growth and Differentiation of Osteoblasts and Bone Marrow Mesenchymal Stem Cells. Advanced Engineering Materials. 2012 Apr;14(4):B123-B37.

32.   Polini A, Pisignano D, Parodi M, Quarto R, Scaglione S. Osteoinduction of Human Mesenchymal Stem Cells by Bioactive Composite Scaffolds without Supplemental Osteogenic Growth Factors. PLoS ONE. 2011;6(10):e26211.

33.   Liu X, Smith LA, Hu J, Ma PX. Biomimetic nanofibrous gelatin/apatite composite scaffolds for bone tissue engineering. Biomaterials. 2009;30:2252-8.

34.   Ngiam M, Liao S, Patil AJ, Cheng Z, Chan CK, Ramakrishna S. The fabrication of nano-hydroxyapatite on PLGA and PLGA/collagen nanofibrous composite scaffolds and their effects in osteoblastic behavior for bone tissue engineering. Bone. 2009;45(1):4-16.

35.   Smith L, Liu X, Hu J, Wang P, Ma PX. Enhancing Osteogenic Differentiation of Mouse Embryonic Stem Cells by Nanofibers. Tissue Engineering: Part A. 2009;15(7):1855-64.

36.   Woo KM, Chen VJ, Ma PX. Nano-fibrous scaffolding architecture selectively enhances protein adsorption contributing to cell attachment. Journal of Biomedical Materials Research Part A. 2003;67A(2):531-7.

37.   Nur-E-Kamal A, Ahmed I, Kamal J, Schindler M, Meiners S. Three-dimensional nanofibrillar surfaces promote self-renewal in mouse embryonic stem cells. Stem cells. 2006;24(2):426-33.

38.   Woo K, Jun J, Chen V, Seo J, Baek J, Ryoo H, et al. Nano-fibrous scaffolding promotes osteoblast differentiation and biomineralization. Biomaterials. 2007;28(2):335-43.

39.   Woo K, Seo J, Zhang R, Ma P. Suppression of apoptosis by enhanced protein adsorption on polymer/hydroxyapatite composite scaffolds. Biomaterials. 2007;28(16):2622-30.

40.   Song JH, Kim JH, Park S, Kang W, Kim HW, Kim HE, et al. Signaling responses of osteoblast cells to hydroxyapatite: the activation of ERK and SOX9. J Bone Miner Metab. 2008 Mar;26(2):138-42.

41.   Wei GB, Ma PX. Macroporous and nanofibrous polymer scaffolds and polymer/bone-like apatite composite scaffolds generated by sugar spheres. Journal of Biomedical Materials Research Part A. [Article]. 2006 Aug;78A(2):306-15.

42.   He C, Jin X, Ma PX. Calcium phosphate deposition rate, structure and osteoconductivity on electrospun poly(L-lactic acid) matrix using electrodeposition or simulated body fluid incubation. Acta Biomaterialia. 2014 Jan;10(1):419-27.

CHAPTER 6

CONCLUSION

SUMMARY

To overcome the significant drawbacks of current treatments, in this dissertation, we have combined a trifecta of material science, engineering, and biology to design tissue-engineered cartilage and bone grafts as an alternate therapy for small defect repair. Previously, our group has made significant progress in developing novel nanofibrous, porous polymer scaffolds for tissue regeneration. Using a 3D nanofibrous poly(L-lactic acid) (PLLA) scaffold seeded with bone marrow-derived mesenchymal stem cells (BMSCs), three specific aims were investigated.

Aim 1 studied the scaffold pore size effect on cartilage formation in vitro and in vivo. In this study, we compared the chondrogenic differentiation of hMSCs on three-dimensional nanofibrous (NF) PLLA scaffolds with small pore size (125-250 µm) or large pore size (425-600 µm) both *in vitro* and *in vivo*. Following 4 wk in vitro chondrogenic culture and 8 wk subcutaneous implantation in nude mice, small-pore scaffolds supported avascular cartilage formation, but large-pore scaffolds contained only fibrous tissue. Therefore, small-pore scaffolds enhanced chondrogenic differentiation *in vitro* and cartilage formation *in vivo* compared to large-pore scaffolds.

In Aim 2, we took the previous study one step further and systematically studied four different pore sizes ranges instead of just two. Additionally, we removed the initial in vitro induction

85

culture and implanted scaffolds 24 hours after cell seeding in order to investigate how pore size affected endochondral ossification with integral interaction with host vasculature from day 1. Using this setup, in a highly interconnected porous, nanofibrous PLLA scaffold seeded with rabbit BMSCs and implanted subcutaneously for 8 weeks, a small pore size of 125-250μm, even less than 300 μm often required, could still promote capillary ingrowth for mature bone formation, while the very small pore size scaffold (60-125 μm) prevented endochondral ossification for cartilage formation. Furthermore, a medium pore scaffold (250-425μm) and large pore scaffold (425-600μm) supported high bone volume due to ingrowth of large blood vessels, shown by CD31 staining, through the interconnected pore network. Therefore, scaffold pore size can be a useful tool for controlling endochondral ossification in vivo.

In Aim 3, using the same ectopic in vivo model for bone regeneration used in Aim 2, we explored whether an electrodeposited calcium phosphate (CaP) coating on a medium pore size, nanofibrous PLLA scaffold could promote the scaffold's osteoconductivity. Beneficially, electrodepositing of the calcium phosphate is two to three orders of magnitude faster than the standard simulated body fluid incubation but had not yet been studied in a 3D scaffold model. This study showed that the electrodeposited calcium phosphate (CaP) on a nanofibrous PLLA scaffold seeded with rabbit bone marrow-derived mesenchymal stem cells (BMSCs) enhanced mature, mineralized bone formation compared to a blank scaffold without CaP, shown by MicroCT and histological analysis. Furthermore, the calcium in the beneficial flower-shaped CaP coating promoted rabbit BMSC proliferation, shown by an in vitro model.

By combining the knowledge gained from this dissertation, a novel biphasic scaffold with two unique pore size ranges could be fabricated to regenerate the entire osteochondral (cartilage-

bone) interface. A preliminary study is described below that reveals initial results indicating successful regeneration of this challenging tissue interface using one continuous, biphasic material with biphasic growth factor delivery.

PRELIMINARY RAT KNEE DEFECT STUDY WITH TGF-β1-LOADED SCAFFOLD

TGF-β1 delivery has previously been used for cartilage regeneration in vivo; however, dosages widely vary between the few studies reported in literature. Therefore, prior to using biphasic delivery of TGF-β1 and BMP-2 for osteochondral repair (Figure 1.1), we determined the effect of TGF-β1 delivered throughout the medium pore, nanofibrous PLLA scaffold in a rat knee defect model to ensure its bioactivity.

A defect (2mm diameter, 3mm deep) was made in the patellar groove of the distal rat femur. A scaffold with controlled release of 1µg TGF-β1 loaded in PLGA microspheres was implanted into the defect (n=8). Two other control groups included the scaffold alone without TGF-β1 (n=2) and a sham control where no material was implanted into the defect (n=2). After 8 weeks, the sham control exhibited minimal repair with white abnormal fibrous tissue or fibrocartilage on the joint surface (**Figure 6.1**, left). In the 'scaffold only' group, the defect and implanted scaffold were still visible with apparent damage to the surrounding cartilage (**Figure 6.1**, middle). Impressively, the TGF-β1-loaded scaffold supported excellent repair of the joint surface such that the defect in no longer visible after 8w (**Figure 6.1**, right). Furthermore, Safranin O staining revealed that the 1 µg TGF-β1-loaded scaffold promoted a thick layer of strongly stained GAG-rich cartilage with typical rounded chondrocytes in hollow lacunae with columnar organization, indicating successful knee defect repair (**Figure 6.2**). As expected, the scaffold alone had

minimal Safranin O-positive cartilage repair, and the sham control had negative staining with no repair.

Therefore, TGF-β1 encapsulated in PLGA microspheres and loaded on the PLLA scaffold remained bioactive and promoted successful knee defect repair in rat model. In the next preliminary study, BMP-2 will be added along with TGF-β1 in a novel biphasic scaffold with two unique pore size ranges to determine if the important interface between cartilage and bone can be further enhanced.
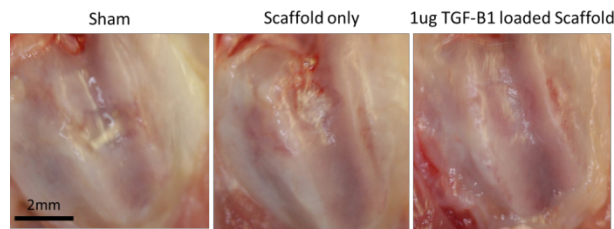

Figure 6.1 Gross appearance of 8w rat knee defect repaired with sham control, medium pore scaffold implanted, or scaffold with 1μg of TGF-β1 loaded scaffold. Defect in patellar groove is still visible in sham and scaffold-only groups but is minimally visible with scaffold loaded with 1μg of TGF-β1, indicating repair to joint surface.
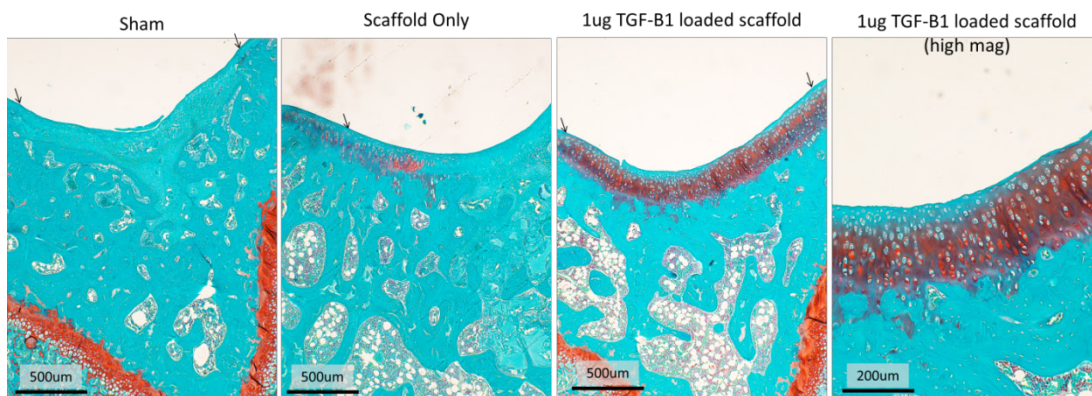
Figure 6.2 Safranin O staining of cross-section of patellar groove in distal femoral head after 8w rat knee defect repaired with sham control, medium pore scaffold implanted, or scaffold with 1μg of TGF-β1 loaded scaffold. 1μg TGF-β1-loaded scaffold had significant Safranin O staining on joint surface with typical rounded chondrocytes in lacunae with columnar organization. Scaffold only had minimal repair, and sham control exhibited no repair. Arrows show defect boundaries.

PRELIMINARY BIPHASIC SCAFFOLD STUDY

Based on the results described in Aim 2, a very small pore size (60-125μm) can prevent blood vessel ingrowth for cartilage regeneration. Oppositely, a medium pore size (250-425μm) can allow blood vessel invasion for significant mature bone formation. Using these two pore size ranges, a biphasic scaffold with an upper cartilage layer of very small pores and a lower bone layer with medium pores was fabricated for osteochondral regeneration (**Figure 6.3**). This biphasic continuous material could not only support both unique tissues but also their interface, which adhering two different materials together could not achieve.
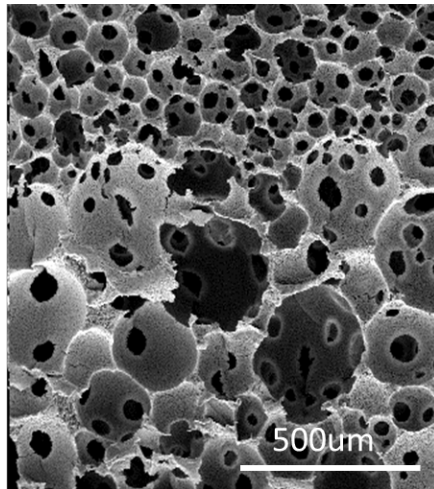
Figure 6.3 SEM of biphasic scaffold for osteochondral regeneration with top cartilage layer with 60-125μm and bottom bone layer with 250-425μm pores.

In order to direct stem cell differentiation, biphasic growth factor delivery of TGF-β1 and BMP-2 was used to drive cartilage and bone regeneration in their individual layers. The growth factors were loaded into PLGA microspheres and immobilized onto either the upper or lower layer of the scaffold. Three groups were compared as described in **Table 1** below: 1) biphasic delivery of both TGF-β1 and BMP-2 (n=4), 2) BSA delivery as generic protein control (n=2), and 3) single delivery of TGF-β1 in both layers (n=2). We hypothesized that the biphasic delivery of both

growth factors could regenerate both cartilage and bone simultaneously on the biphasic pore size scaffold (**Figure 6.3**) when seeded with rabbit BMSCs and implanted subcutaneously in nude mice for 2w or 6w. (A rat knee defect model was not used because two distinct layers of 1ug TGF and 1ug BMP could not be achieved in a tiny 2mm scaffold at this time.)

Table 1 Biphasic pore size and growth factor delivery scaffold study design for osteochondral regeneration, describing upper cartilage layer and lower bone layer.

|	Pore Size (um)	Cells	Group 1: Dual Delivery	Group 2: BSA control	Group 3: TGF only
Upper Cartilage Layer	60-125	BMSC	1ug TGF-B1	1ug BSA	1ug TGF-B1
Lower Bone Layer	250-425	BMSC	1ug BMP2	1ug BSA	1ug TGF-B1

After 2w and 6w subcutaneous implantation, gross appearance reveals that the biphasic pore size scaffold with biphasic delivery of bioactive TGF-β1 and BMP-2 (**Figure 6.4**, left) appears to have an upper cartilage phase and a highly vascularized lower bone phase. Scaffolds with BSA (**Figure 6.4,** middle) and TGF-β1 delivery (**Figure 6.4,** right) appear as glossy cartilage with minimal vascularization after 6w.

Based on further evaluation using MicroCT reconstructions and histological analysis with Safranin O staining, after two weeks, the BSA loaded scaffold best exhibited a clear interface of cartilage and bone tissue at the interface of the very small and medium pores (**Figure 6.5**). The TGF-β1 and TGF-β1/BMP2 groups contained some positive Safranin O staining inside the

scaffold with mineralization on the easily vascularized outer layer of the scaffold after 2w (**Figure 6.5**).

After 6w subcutaneous implantation, all three groups underwent significant endochondral ossification throughout the entire scaffold (**Figure 6.6**) due to the limitation of the ectopic subcutaneous implantation model, which does not provide the native microenvironment of a knee defect repair model. Interestingly, the TGF-β1 group did prevent endochondral ossification in the center of the scaffold, where positive Safranin O-stained cartilage tissue remained.

Therefore, based on this preliminary data, this biphasic material combining multiple technologies may be a promising foundation for osteochondral defect repair, though more studies are required, as detailed below in future work.
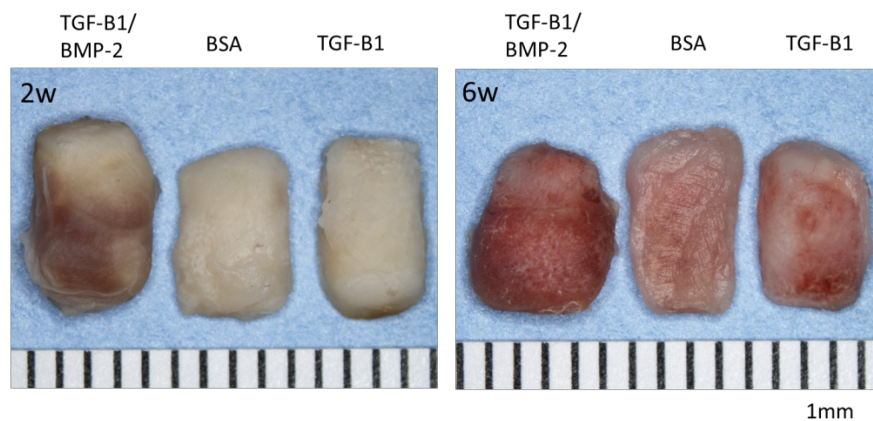
Figure 6.4 Gross appearance of cell-scaffold constructs after 2w or 6w mouse subcutaneous implantation. Biphasic pore size scaffold with biphasic delivery of TGF-β1 and BMP-2 (left) appears to have an upper cartilage phase and a highly vascularized lower bone phase after 2w and 6w. After 6w, scaffolds with BSA (middle, control) and TGF-β1 delivery (right) appear as glossy cartilage with minimal vascularization.
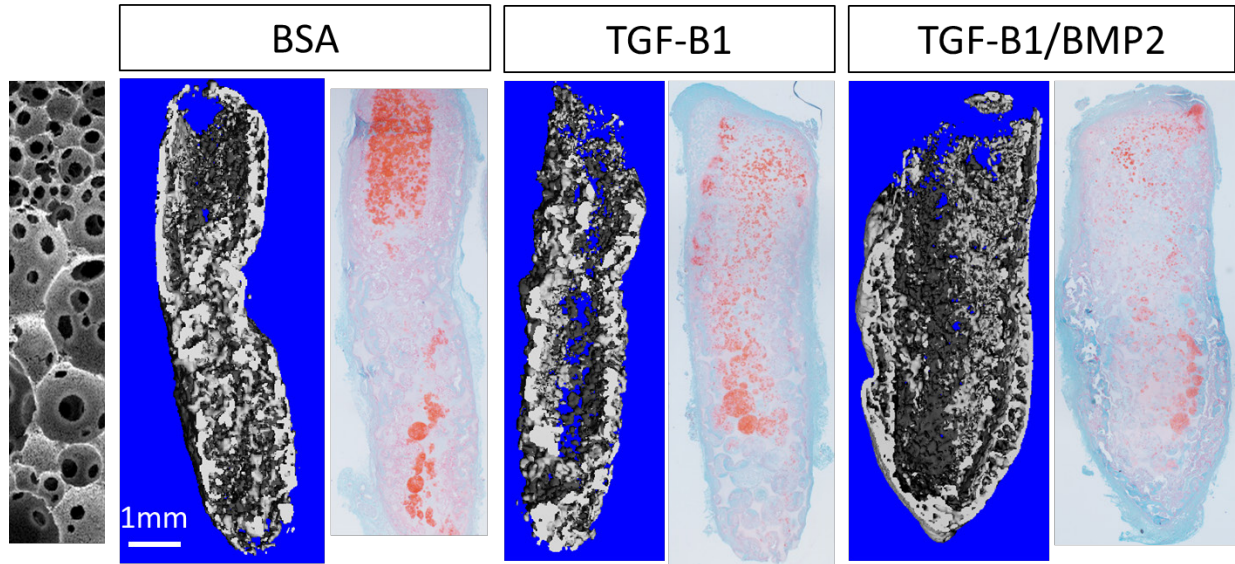
Figure 6.5 MicroCT reconstruction and Safranin O staining of cross-section of BSA, TGF-β1, or TGF-β1/BMP2 loaded on biphasic pore scaffold after 2w mouse subcutaneous implantation.
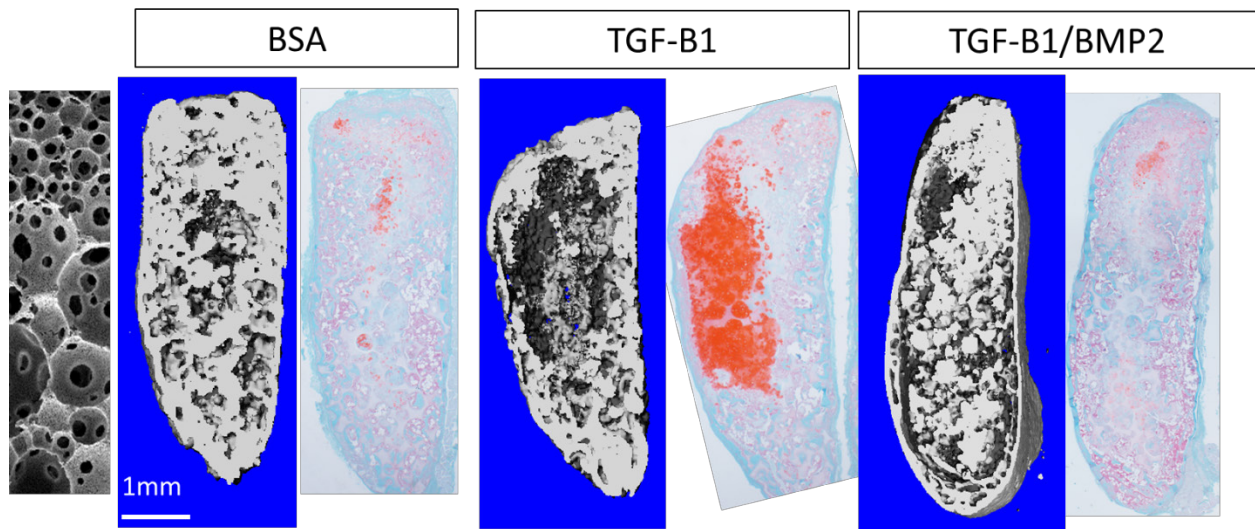
Figure 6.6 MicroCT reconstruction and Safranin O staining of cross-section of BSA, TGF-β1, or TGF-β1/BMP2 loaded on biphasic pore scaffold after 6w mouse subcutaneous implantation, showing significant calcification in all three groups.

FUTURE WORK

Each of the studies presented as Aims 1-3, in Chapters 3-5 respectively, could serve as the foundation for further studies to provide a deeper understanding of how the material properties affect biological processes.

In Aim 1 described in Chapter 3, a deeper mechanistic study can be performed in order to elucidate why the small pore scaffold enhances chondrogenic differentiation in vitro, compared to the large pore scaffold. The roles that Yap (a transcription factor involved in mechanotransduction) and Smad2/3 (the effector of the TGF-β signaling pathway) play in mesenchymal condensation, an important step in chondrogenic commitment, can be compared in both pore size scaffolds. We hypothesize that in the small pore scaffold, Yap is downregulated while p-Smad2/3 is upregulated as a result of increased mesenchymal condensation, enhancing chondrogenic differentiation after 1 day of TGF-β1 induction in vitro, compared to the large pore scaffold using Western blot. To show a causal effect, we further hypothesize that an siRNA knockdown of Yap will promote chondrogenic differentiation in the large pore scaffold. Through these deep biological studies, we can determine *why* the small pore scaffold enhances chondrogenic differentiation.

To further study Aim 2 (Chapter 4), we can go beyond pore size to study the effect of pore interconnection size on endochondral ossification in an ectopic model. This is important because how pore interconnection size of a polymer scaffold affects bone formation has not been studied previously, to our knowledge. This is likely because most researchers do not have the technology to finely control interconnection size without using a different fabrication method, resulting in more pore architecture variance than just interconnection size. Preliminary data (not shown)

reveals that when pore interconnection size in the small pore scaffold is decreased from 85μm to 40μm, the 40μm interconnections still allow blood vessel ingrowth for bone formation. We hypothesize that an even smaller interconnection size with an average of 30μm will prevent vessel invasion for cartilage formation, while still allowing cell penetration. This interconnection size study, which most researchers do not have the technology to control, would further characterize how pore architecture can control blood vessel invasion and therefore endochondral ossification.

For Aim 3, this promising CaP/polymer composite scaffold that enhanced ectopic bone regeneration could be used to enhance femoral bone defect repair without any implanted cells by encouraging host stem cell proliferation. In this defect model, the CaP effect can be seen more clearly without the reliance on implanted cells but solely host cells. Lastly, the CaP effect on osteogenic differentiation can be further characterized with a time course study with several bone markers.

Overall, the future of this tissue-regenerative work is to push toward a solution for osteochondral defect repair. The same biphasic material study described in Table 1 above should be repeated in a rabbit osteochondral defect model, which is the accepted animal model for this type of repair. The only difference from the preliminary ectopic study described above would be that stem cells would not need to be implanted because host chondrocytes and stem cells will migrate into the scaffold, which will be promoted by the growth factor delivery and facilitated by the pore structure. However, the main challenges in fabricating this complex material are achieving 1) a high enough dosage of each growth factor that 2) still remains localized to only one layer of the scaffold in a small scaffold that fits in the knee defect (5mm diameter, 3mm deep). To solve

these challenges, instead of pipetting, a higher technology method may be required to load the PLGA microspheres onto the biphasic scaffold. Alternatively, silica nanoparticles could be used as the drug delivery vehicle which can load a 5-fold higher dose of the growth factors than the PLGA microspheres. Thus, a smaller amount of vehicle would be loaded onto the scaffold, which would be easier to localize in a single layer of the scaffold. Based on preliminary data, once this material fabrication hurdle is overcome, **this complex biphasic scaffold with unique pore sizes and biphasic growth factor delivery could simultaneously guide host stem cell fate toward the chondrogenic and osteogenic lineages for osteochondral defect repair. In the future, this tissue-engineered osteochondral knee graft could aid in developing therapies for other articulating joints, as well as other joint pathologies like osteoarthritis. This cell-instructive, biomimetic composite material could even serve as a platform to engineer various complex tissues and organ systems.**